THE MECHANICS OF CELLULAR ABSCISSION AND BODY AXIS LENGTHENING

by

Kay Larkin

A DISSERTATION

Presented to the Department of Cell and Developmental Biology and the Oregon Health Sciences University School of Medicine in partial fulfillment of the requirements for the degree of Doctor of Philosophy

September 1999

School of Medicine

Oregon Health Sciences University

CERTIFICATE OF APPROVAL

This is to certify that the Ph.D. thesis of

Kay Larkin

has been approved.

[redacted]

Professor in charge of thesis

[redacted]

Member

[redacted]

Member

[redacted]

Member

[redacted]

Member

[redacted]

Associate Dean for Graduate Studies

TABLE OF CONTENTS

Acknowledgments

I would like to thank: my advisor, Dr. Mike Danilchik, for giving me the freedom to follow my own interests in his lab; Drs. Jerry Adey, Steve Black, Jan Christian, Duane Compton, Frank Gwilliam, Bob Kayton, Steve Matsumoto, Joanne Otto, and Tom Schroeder for providing equipment, expert advice, and general encouragement; Marc Carey, Laura Wilson, and everyone else on the upper floors of the dental school for providing camaraderie; CharEll Melfi, Phyllis Stewart, and Elaine Offield for shepherding me through the bureaucracy; and of course, my friends and family for everything.

Abstract

We have described a new array of microtubules (MTs) in the cleavage furrows of dividing sea urchin and frog eggs. Analysis of MT function during division indicates that MTs are required for completion of division, abscission, in sea urchin embryos and in furrow deepening in frog embryos. Additionally, in frog eggs, the furrow MT array, FMA, appears to be formed in the midzone and bundled with a minus end-directed kinesin. Another set of MTs present in the egg is required for addition of the large amount of membrane added to the furrow region during division since disruption of the FMA does not inhibit membrane addition whereas disruption of all MTs does.

Following the period of rapid cell divisions, rearrangements of cells have been shown to be a major morphogenetic force in embryogenesis. Analyses of gastrulation found that rearrangements of dorsal cells accounts for lengthening of the anterior-posterior axis during gastrulation (reviewed in Keller, 1991). Although ventral tissues are generally thought to be morphogenetically passive, here we show that mediolateral cell rearrangements of ventral mesodermal cells contribute to the doubling in length of the anterior-posterior axis between the neurula and tailbud stages.

Introduction

The development of an animal egg into a multicellular adult can be thought of as a series of events, which together give the animal its size, shape, and organs. Each of these events can be studied at a variety of levels -- from molecular interactions within cells to the behaviors of cells to changes in body shape. This thesis investigates three problems at several levels: first, the role of microtubules (MT) in the terminal events of cleavage of sea urchin embryos; second, the functions of different MT populations in furrow deepening and membrane addition in frog embryos; and finally, the behaviors of cells during the transition from the spherical shape of the frog embryo into the elongate shape of the tadpole.

Roles of the cytoskeleton in cytokinesis

Before entering into details of cytoskeletal organization during cytokinesis, the phases of cell division will be presented and then the structures will be introduced. The phases of mitotic cell division are based upon the positions of chromosomes, as chromosomes are the most readily visible features of a dividing cell (Figure 1.1). During prophase, prometaphase, and metaphase chromosomes are paired and centered in the cell by the the MT-based mitotic spindle and asters. During anaphase, as the paired chromosomes separate, a cleavage furrow is stimulated to form in a belt surrounding the midpoint of the spindle. The cleavage furrow is the result of formation and contraction of the actin-myosin based contractile ring (CR). During telophase the CR constricts the cell and the MT-based midbody forms in the cytoplasmic bridge connecting the presumptive daughter cells. Cytokinesis culminates in the separation of daughter cells, a process we call

abscission.

The cytoskeletal machinery present during mitosis consists of the MT-based mitotic apparatus that separates the chromosomes and positions the cleavage furrow, the actin-myosin-based CR that constricts the cell by deforming the cell membrane, the MT-based midbody, and the newly identified MT structures near the cleavage furrow that will be described in Chapters 2 and 3. For many years the mitotic apparatus was the only known population of MTs present in a cell during cytokinesis. However, our reinvestigation of the roles of MTs in dividing embryos of both the frog, *Xenopus laevis* and the sea urchin, *Strongylocentrotus purpuratus*, led us to the discovery of novel MT structures in each of these embryos (Danilchik *et al.*, 1998; Larkin and Danilchik, submitted). MTs are polymers of α- and β-tubulin dimers, which appear to grow from sites containing γ-tubulin, another isoform originally identified as an essential component of centrosomes, which resides at the centers of mitotic asters (Oakley *et al.*, 1990; Oakley and Oakley, 1989). MTs are dynamic and directional, having the γ-tubulin isoform associated with the minus end, at which more αβ-tubulin dimers would be lost than added without the influence of the associated γ-tubulin. The plus ends of MTs have a higher rate of dimer addition than loss; therefore, MTs extend from the plus end. Aside from their role in the separation of chromosomes, MTs have also been shown to be involved in CR stimulation (Beams and Evans, 1940; Swann and Mitchison, 1953; Hiramoto, 1956; Rappaport, 1961; Hiramoto, 1971). The dependence of CR stimulation on MTs highlights the integration of cytoskeletal functions in cytokinesis.

How MT- and actin-based events are temporally and spatially coordinated during cytokinesis has been an area of fruitful research. There are

two major hypotheses concerning furrow stimulation. One hypothesis states that during anaphase astral MTs interact with the cell cortex such that the CR forms as a narrow belt perpendicular to the long axis of the spindle. Chromosomes are not required for CR formation, since cytokinesis continues normally when they are removed during metaphase (Zhang and Nicklas, 1996). Spindle MTs are not required, since removal of the spindle does not hinder furrowing (Hiramoto, 1971). Although removal of the entire mitotic apparatus at the end of anaphase has no effect on furrowing, removal of the asters prior to anaphase does prevent furrowing (Hiramoto, 1956). Additionally, disruption of all MTs with colchicine prior to anaphase also prevents furrowing (Beams and Evans, 1940; Swann and Mitchison, 1953). Displacement of the asters with needles has demonstrated that a CR can form where the cortex comes under the influence of two asters that need not be connected by spindle MTs (Rappaport, 1961). Therefore, the interaction of more than one aster with the cell cortex at the beginning of anaphase is necessary for stimulation of CR formation.

The polar relaxation hypothesis of furrow stimulation states that a increase in cytoplasmic stiffness in conjunction with a decrease in cell surface tension at the points farthest from the region of furrowing acts in the establishment of the CR. Sea urchin embryos can be cultured in colchicine such that the presumed source of cytoplasmic stiffness, the mitotic apparatus, never forms; however, these embryos still undergo the normal exponential increase in stiffness culminating in anaphase, indicating that the hypothesis of MT-cortex interaction discussed above is not the only event taking place prior to CR formation (Hiramoto, 1968; Schroeder, 1981; Schroeder, 1990).Although there is evidence that polar relaxation occurs prior to CR

formation, the hypothesis that polar relaxation is necessary for CR formation has not been tested.

The CR consists primarily of actin and myosin, which together can exhibit contractile behaviors (Schroeder, 1968; Schroeder, 1969; Schroeder, 1972; Schroeder, 1973; Schroeder, 1975; Schroeder, 1990). The CR, unlike the actin-myosin fibers of muscle, does not normally relax and does not increase in width or thickness, and thus becomes smaller in volume as it contracts (Schroeder, 1972). When the CR becomes approximately six percent of its original diameter, it becomes undetectable ultrastructurally (Schroeder, 1972). Although many proteins that interact with actin have been identified, few have been shown to be involved in cytokinesis (Mabuchi, 1990). Of those that do, Rho GTPase and its substrates appear to be involved in regulation of CR function, but their influence on furrow formation is still unclear (Drechsel *et al.*, 1997; Kishi *et al.*, 1993; Mabuchi *et al.*, 1993). On the other hand, septin, an actin cross-linking protein, is present with the CR in active cleavage furrows, and its disruption halts cleavage. suggesting that microfilament cross-linking is necessary during furrowing (Fares *et al.*, 1995; Kinoshita *et al.*, 1997). Even though actin cross-linking appears to be important during contraction, it remains uncertain whether the CR is formed by bundling of existing filaments or by polymerization of new ones.

The cytoplasmic bridge that results from constriction of a cell by the CR can persist such that another division cycle will commence without the previous cycle achieving complete separation of cells, as occurs in large, yolky embryos such as *X. laevis*. However, in many cells, including echinoderm embryos, cleavage does appear to be completed prior to initiation of the next division cycle as determined both by electrophysiology and by dye injection (Cameron *et al.*, 1989; McCain and McClay, 1996; Pochapin *et al.*, 1983;

Sanger *et al.*, 1985; Summers *et al.*, 1996; Larkin and Danilchik, in press; Chapter 2 of this thesis). However, under conditions that may destabilize MTs, such as low temperatures, high pressure, and hypertonicity, a connection can persist even in sea urchin embryos, leading us to investigate the role of MTs in abscission in these embryos (Schroeder, 1972; Scott, 1946; Vacquier, 1968). Regardless of how long the cytoplasmic bridge persists, complete separation of the daughter cells requires the membrane at the cytoplasmic bridge to break and reseal around each cell.

As the CR reaches maximal constriction, but before cleavage is completed, the midbody, a MT-containing structure, forms in the cytoplasmic bridge connecting the two presumptive daughter cells (See Figure 1.1). The midbody is composed of bundles of short MTs that interlace at the cleavage plane (Longo, 1972). Although the function of midbody MTs is still uncertain, recent experiments have shown that they may be involved in abscission. For example, disruption of MTs with nocodazole in telophase mammalian tissue culture cells results in failure of those cells to undergo abscission (Wheatley and Wang, 1996). Additionally, intracellular injection of antibodies or antisense RNA to γ-tubulin prevents formation of a normal midbody, as well as any other newly nucleating MT structures, and also prevents complete separation of daughter cells (Julian *et al.*, 1993; Shu *et al.*, 1995). Therefore, the midbody and/or other newly nucleated MT structures are required for abscission

Although many proteins accumulate in the region of the midbody, only a few appear to be necessary for abscission and these have a microfilament- or MT-binding domain. For example, disruption of Nedd5, a mammalian septin, by injection of a monoclonal antibody, prevents

abscission even though furrowing appears normal up to that point (Kinoshita *et al.*, 1997). Also, when CYK-1, a *Caenorhabditis elegans* formin, is inactivated by mutation, abscission is prevented (Swan *et al.*, 1998). And finally, when the MT-binding domain of INCENP, a chromosomal passenger protein with a MT-binding domain, is mutated, the protein no longer associates with the midbody and the cells are prevented from undergoing abscission (Mackay *et al.*, 1998). Together, these findings suggest that abscission utilizes MTs, microfilaments, and their binding proteins. As yet, specific MT-actin linking proteins have not been identified, although a dependence of MT organization on microfilament organization in the cortex of sea star embryos has been documented (Otto and Schroeder, 1984).

Even though most of the early studies of the cytoskeletal machinery of cytokinesis were carried out with sea urchin embryos, a furrow MT structure was never described in echinoderms. In Chapter 2 we describe a population of MTs that is distinct from the mitotic apparatus and midbody, and is present in the furrows of dividing sea urchin embryos (Larkin and Danilchik, submitted). Further we show that MTs are required for abscission in dividing sea urchin embryos (Larkin and Danilchik, in press).

Chapter 3 investigates the function of the furrow MT array (FMA) that we described in *X. laevis* embryos (Danilchik *et al.*, 1998). The FMA first becomes detectable by indirect immunofluorescence at the base of the deepening cleavage furrow during late anaphase. The FMA consists of bundles of short MTs (15-20 μm) with a gap in antibody staining at the plane of cleavage (Figure 1.2 A and B). Despite the descriptive similarity to midbodies of other cells, *i.e.* interlaced short MT bundles surrounded by the constricting furrow, the FMA does not appear to be a definitive midbody. A

midbody-like structure, composed of short MT bundles is also present in these cells, but does not become localized to the cytoplasmic bridge. Since furrow MTs and the midbody-like structure have complementary features of a typical midbody, it is possible that the extreme size of the *X. laevis* embryo has facilitated the separate identification of these two distinct structures that are too close together to resolve in smaller cells, such as tissue culture cells.

To address the functions of MTs in frog embryo cleavage, MTs were disrupted with nocodazole, which causes depolymerization of all MTs. MT-disruption during second cleavage blocked addition of new membrane in the second cleavage furrow and prevented that furrow from deepening (Figure 1.2 C, arrowheads) without altering the first cleavage furrow (Danilchik *et al.*, 1998). Because all MTs were disrupted in these experiments, we could not conclude that FMA MTs were involved in either process. Disruption of the CR with cytochalasin prevented furrowing but not membrane addition, which was evident as the unpigmented band surrounding the regressed furrow (Figure 1.2 D, arrowheads). The experiments presented in Chapter 3 experimentally separate FMA MTs from other MTs and shows that FMA MTs are involved in furrow deepening but not membrane addition. The dependence of membrane delivery on MTs thus remains an interesting, unresolved problem.

Membrane addition is an important part of cell division because a dramatic increase in surface area must occur when a cell divides. Recognition of this fact has led to numerous investigations of how cells accommodate this change. Membrane addition appears to be the primary means of increasing surface area; sea urchin embryos, for example, undergo enormous fluctuations in surface area prior to cleavage (Burgess and Schroeder, 1977;

Schroeder, 1978; Schroeder, 1979). Upon fertilization, embryos secrete the contents of many thousands of cortical granules by fusion of these vesicles with the surface, nearly doubling the surface area; however, much of this membrane is subsequently endocytosed (Schroeder, 1979). Sea urchin embryos accommodate this extra membrane by projecting numerous microvilli from the surface. Microvilli of sea urchin embryos undergo two rounds of elongation, one of which coincides with cortical granule exocytosis, and the other occurring approximately one third of the way through first cleavage (Burgess and Schroeder, 1977; Schroeder, 1978; Schroeder, 1979). The extra surface area available in microvilli is sufficient to cover the two prospective daughter cells, but since microvilli decrease in neither dimension nor number at cleavage, new membrane may still be added to the embryo surface during division.

Membrane addition in dividing frog embryos occurs in the cleavage furrow, as evidenced both by ultrastructural studies and studies of live embryos (Bluemink *et al.*, 1976; Byers and Armstrong, 1986; Sawai, 1987; Sawai, 1992; Selman and Perry, 1970). New membrane is easily distinguished from old membrane by its lack of underlying pigment granules (Figure 1.2 D). New membrane is thought to be stored in the embryo as a large cytoplasmic pool of Golgi-derived vesicles. Sawai (1992) provided the first evidence for a MT-dependent mechanism of membrane addition when he found that disruption of all MTs with colchicine halted furrowing and membrane addition. We confirmed those findings using a different MT inhibitor, nocodazole, which has many fewer side effects, and now interpret them to indicate a specific blockage of both membrane addition and furrow deepening (Danilchik *et al.*, 1998).

As mentioned previously, some MT-binding proteins have been

implicated in division. We have looked at another class of MT-binding proteins, the MT motors. There are two MT motor families: dyneins and kinesins, both of which have similarities to myosins, the actin motors. In general cytoskeletal motor proteins have a heavy chain with motor and cytoskeletal-association domains at one end, a cargo domain at the other, and a coiled coil dimerization domain in the middle. We will focus on the minus-end directed kinesins, also called the non-claret disjunction (NCD) protein family (McDonald and Goldstein, 1990; McDonald *et al.*, 1990). The NCDs have heavy chains with a carboxyl terminal motor, and MT-association domains at both ends, in addition to a central dimerization region (McDonald and Goldstein, 1990 and Chandra *et al.*, 1993). The motor is a Mg^{2+}-dependent ATPase that arrests on MTs in the presence of an ATP analog, AMP-PNP *in vitro* (Brady, 1985; Scholey *et al.*, 1985; Vale *et al.*, 1985a; Vale *et al.*, 1985b; Cohn *et al.*, 1987; Foster *et al.*, 1998). Although these proteins are able to transport cargo toward MT minus ends *in vitro* at the rate of 6 μm per minute (McDonald *et al.*, 1990), the presence of MT-association domains at both ends explains their apparent role in MT-bundling observed *in vivo* (Chandra *et al.*, 1993). NCD was originally identified in *Drosophila melanogaster* because of its role in chromosomal disjunction (McDonald and Goldstein, 1990; McDonald *et al.*, 1990). Further investigation of the *in vivo* function of NCD revealed it as a MT bundling protein essential for formation of the meiotic spindle (Endow and Komma, 1996; Endow and Komma, 1997; Karabay and Walker, 1999; Matthies *et al.*, 1996). Chapter 3 presents evidence that NCD is present with the FMA and is necessary for FMA organization and furrow deepening.

Morphogenesis in late frog embryos

Following the cleavage stages in *X. laevis* embryos, there is a period of global morphogenetic movements beginning with gastrulation (stages 10 to 12), continuing through neurulation (stages 12 to 16), and culminating in the neurula-to-tailbud transition (stages 16 to 27) (Nieuwkoop and Faber, 1994). In this last phase, between the neurula (stage 16) and tailbud stages (stage 27), *X. laevis* embryos more than double in length (Nieuwkoop and Faber, 1994). The physical mechanism of this event is unknown, and we find that active mediolateral intercalation of ventral mesodermal cells contributes to body axis lengthening.

Mediolateral intercalation of dorsal mesodermal cells is the primary cell behavior that results in the near doubling of the dorsal side of the embryo during gastrulation (Keller *et al.*, 1985a; Keller *et al.*, 1985b; Keller and Danilchik, 1988; Keller and Tibbetts, 1989; Wilson and Keller, 1991; Keller and Shih, 1992; Keller *et al.*, 1992; Keller and Jansa, 1992; Keller and Winklbauer, 1992; Shih and Keller, 1992). Dorsal mesodermal cells undergo some radial intercalation, thinning the mesoderm in the dorso-ventral (D-V) dimension and lengthening it in the anterior-posterior (A-P) dimension, as demonstrated by SEM (Keller, 1980).

Later, during neurulation, the notochord and somites form from the dorsal mesoderm. Notochordal cell differentiation does not require contact with any other tissue, but isolated notochordal cells do not make a rigid structure (Mookerjee *et al.*, 1953). The notochord has an extracellular proteinacous sheath that is induced by the notochord but secreted by neighboring cells (Mookerjee, 1953). Adams *et al.* (1990) found that normal lengthening and rigidity of the notochord is dependent upon constraint of

notochordal cells by the notochordal sheath. Microsurgical disruption of a portion of the notochord does not inhibit A-P axis lengthening, suggesting that the notochord is not required for A-P axis lengthening during neurula stages (Malacinski and Youn, 1981). SEM studies of somitogenesis reveal that there are movements of individual cells within somite blocks preceding rotation of the entire somite (Youn *et al.*, 1980). Somite rotation was partially inhibited in U.V.-irradiated embryos and was interpreted to result from lack of association with the notochord (Youn and Malacinski, 1981). However, Wilson *et al.* (1989) followed up those observations using notochordless dorsal explants and found that segmentation and rotation of somites did occur and was capable of lengthening the A-P axis of dorsal pieces by 45% during and after neurulation (stages 12.5 to 21). Therefore, somite rotation can occur in the absence of notochord and can account fully for the degree of lengthening observed during the stages studied.

Because of the lack of information regarding the doubling in length of the embryo following neurulation, we examined the possible roles of cell shape change, cell division, and cell rearrangement in X. *laevis* during these later stages. Chapter 4 of this thesis investigates potential cellular mechanisms of A-P axis lengthening, and shows that mediolateral intercalation of ventral cells is involved in the doubling in A-P axis length during the neurula-to-tailbud transition (Larkin and Danilchik, in press).

Figures

Figure 1.1. Phases of cell division. Spindle and aster formation and chromosome separation take place during prophase, prometaphase, and metaphase. During anaphase the furrow is stimulated by astral MTs. During telophase, the furrow deepens and finally, during abscission, the daughter cells are separated.

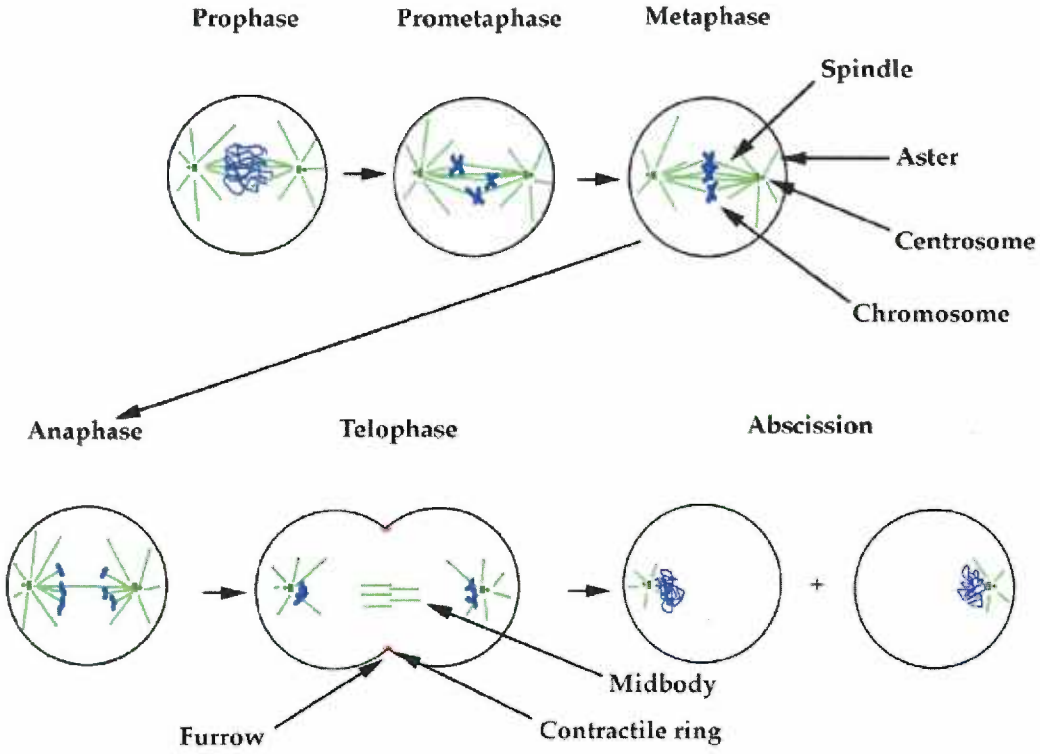
Prophase
Prometaphase
Metaphase
Spindle
Aster
Centrosome
Chromosome
Anaphase
Telophase
Abscission
Midbody
Furrow
Contractile ring

Figure 1.2. FMA MTs are present at the furrow base from five minutes after furrow formation until the end of division, and MTs are correlated with furrow deepening and membrane addition. Nine minutes after furrow formation the FMA is visible as short MT bundles interlacing at the furrow base in the finely granular animal cytoplasm (A). 25 minutes after furrow formation, the FMA is still at the furrow base which has cut down into the center of the embryo where large yolk platelets are visible (B). Disruption of all MTs with nocodazole during second cleavage blocks furrow deepening and membrane addition in the second furrow, evidenced by the lack of dimpling at the furrow and by the lack of new, unpigmented membrane (arrowheads, C). Disruption of the CR with cytochalasin prevents furrowing and new membrane continues to be added (arrowheads, D). From Danilchik *et al.*, 1998.

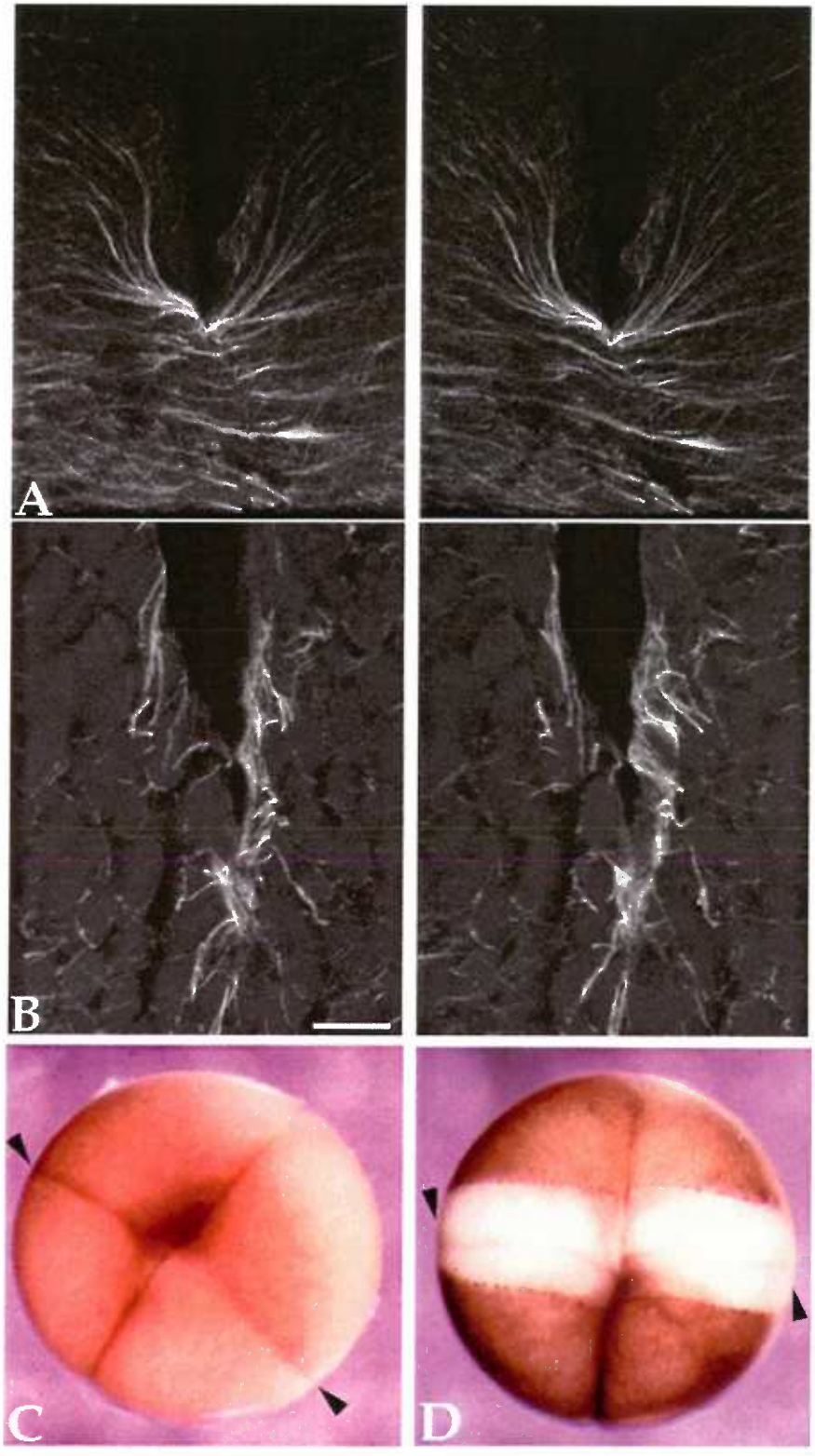
A
B
C
D

Materials and Methods

S. purpuratus *gamete collection and fertilization.*

S. purpuratus were collected from the Oregon coast (Oregon Department of Fish and Wildlife permit #8-1291) and maintained in chilled salt water tanks. Animals were spawned by injection of 0.5 M KCl (2 to 5 mL); sperm were collected by inverting males over dry petri dishes and eggs were collected by inverting females over small beakers full of artificial sea water (ASW). Eggs were separated from detritus by filtering through 250 μm Nitex mesh, rinsed twice with ASW, then once with para-aminobenzoic acid in ASW (PABA-ASW) to prevent hardening of the fertilization membrane. Sperm were activated by 1:500 dilution in ASW, and synchronous fertilization was accomplished by mixing eggs in a minimal volume of PABA-ASW and sperm at a 1:5 ratio. One minute after addition of sperm, the eggs were flooded with PABA-ASW, allowed to sit for 15 minutes, then filtered 8 times through 73 μm Nitex mesh to remove the fertilization membranes. For experiments requiring removal of the hyaline layer, eggs were fertilized in a minimal volume of ASW, within 1 minute flooded with Ca^{2+} Mg^{2+}-free ASW, rinsed twice with Ca^{2+} Mg^{2+}-free ASW, filtered 8 times through 73 μm Nitex mesh to remove both the fertilization membrane and hyaline layer, and then rinsed twice and incubated in Ca^{2+}-free ASW to prevent reformation of the hyaline layer (Strathmann, 1992). As a control for the effects of development without the hyaline layer, some eggs were treated with 1 M urea in deionized water for 2.5 minutes, then fertilized with dilute sperm as above, and after one minute were rinsed twice with ASW (Moore, 1930).

S. purpuratus *Pharmacological treatments*

Embryos were transferred to 10 μg/mL nocodazole, 10 μg/mL cytochalasin D, or 0.1% DMSO at several time points prior to furrowing. Embryos determined retrospectively to have been treated with nocodazole 15 +/- 3 minutes before furrowing had the highest incidence of embryos that initiated furrowing but were unable to finish dividing. Embryos were photographed at 25 X on T-Max or TechPan film (Kodak) with a Leitz compound microscope and camera.

S. purpuratus *Fixation and microscopy*

Embryos were fixed in Gard's fixative (modified as in Danilchik *et al.*, 1998) for 2-4 hours at 4-10°C, then post-fixed in ethanol or methanol indefinitely at -20°C. Alternatively, embryos were fixed in -20°C methanol for a minimum of 16 hours or in Otto's fixative (4% paraformaldehyde, 0.1% Triton X-100, 0.9 M glycerol, 5 mM EDTA, 0.1 M PIPES, 1 mM DTT, pH 7.15 (J. Otto, personal communication)). Fixed embryos were pelleted by centrifugation between washes. Embryos were centrifuged at a low speed on a clinical centrifuge (IEC) for 2-3 minutes or at a high speed on a microcentrifuge (Taylor) for 2-3 seconds. Background fluorescence due to fixative was reduced by treatment with 100 mM $NaBH_4$ in PBS overnight. Embryos were rinsed three times in NTBS (155 mM NaCl, 10 mM tris pH 7.4, 0.1% NP-40) after reduction and antibody treatments. MTs were stained with a monoclonal antibody directed against *S. purpuratus* α-tubulin (B-5-1-2, diluted 1:1000, Sigma) for one hour with agitation, and visualized with TRITC-conjugated goat anti-mouse secondary antibody (diluted 1:1000, Sigma) also incubated for one hour with agitation. After washing in NTBS, stained

embryos were dehydrated in ethanol or methanol and cleared in 2:1 benzyl benzoate: benzyl alcohol. Embryos were imaged on a confocal microscope (BioRad MRC500) with a high/low pass filter (KronHite) using Kalman averaging and a 63 X Planapo oil immersion lens (n.a. 1.2, Zeiss). Stacks of images were analyzed and projected using NIH Image (version 1.61) on a Macintosh computer. NIH Image was developed at the U.S. National Institutes of Health and is available on the Internet at http://rsb.info.nih.gov/nih-image.

S. purpuratus *Electrophysiology*

Embryos raised for electrical recordings were fertilized and treated with nocodazole or DMSO as described above. One mm glass capillaries, with filament, were pulled into 20-30 MΩ electrodes with an electrode puller (Narishige), filled with 4 M potassium acetate, and mounted in electrode holders filled with ASW. Cover glass was coated with 10 mg/mL poly-l-lysine (Sigma), then rinsed 10 times in water and allowed to dry. Treated embryos were placed on coated coverslips and the coverslips were placed in a grounded plastic recording chamber. After initiation of furrowing, each of the incipient daughter cells was impaled with an electrode. Hyper- and depolarizing pulses were then introduced in one cell while recording from both cells, following which the other cell was pulsed. Data were passed through an analog/digital converter and saved *via* a video tape recorder (Sony). For analysis, recordings were passed back through the digital/analog converter, through a computer interface (Instrutech) onto a Macintosh computer using Acquire (Bruxton) and Igor (WaveMetrics) software.

X. laevis *egg collection and fertilization.*

Eggs were collected in a dry dish from *X. laevis* females injected 15 to 18 hours previously with 600 units of human chorionic gonadotropin (Sigma or Organon). Testes were removed from anesthetized, pithed male frogs for *in vitro* fertilization. A small piece of testis was homogenized in 1 mL of 1/3 X MMR and poured onto the eggs (1 X MMR: 100 mM NaCl, 2 mM KCl, 2 mM $CaCl_2$, 1 mM $MgCl_2$, 5 mM HEPES, pH 7.4). When approximately half of the eggs showed constriction of the pigmented animal hemisphere, eggs were dejellied with 2% cysteine in water, pH 8. Once eggs were able to touch each other, indicating that the jelly was gone, the cysteine was washed out with 5 changes of 1/5 X MMR. Embryos were then cultured in 1/5 X MMR at temperatures between 15 and 24°C in an incubator (Forma) or on a channeled aluminum plate with a circulating water bath (VWR).

X. laevis *Embryo Fixation and Immunostaining*

Embryos were fixed in Gard's for 2-4 hours at room temperature with agitation (80 mM K-PIPES, pH 6.8, 5 mM EGTA, 1 mM $MgCl_2$, 3.7% formaldehyde, 0.25% glutaraldehyde, 0.2% Triton x-100), followed by post-fixation in methanol at -20°C for at least 16 hours. Pigmented embryos were then bleached in 10% H_2O_2 in methanol on a light table until the pigment was sufficiently lightened (1 to 2 hours, depending on the original degree of pigmentation of the embryos). After bleaching, embryos were rinsed three times in PBS (128 mM NaCl, 2 mM KCl, 8 mM NaH_2PO_4, 2 mM KH_2PO_4, pH 7.2) for a total of 1.5 hours, then reduced in 100 mM $NaBH_4$ in PBS overnight at room temperature with agitation. Treatment with $NaBH_4$ decreases the background fluorescence caused by unreacted aldehydes and to some extent

autofluorescence of yolk. $NaBH_4$ was removed by rinsing in NTBS three times for 1.5 hours, following which embryos were bisected parallel or perpendicular to the first cleavage plane with a razor blade fragment. Bisection of embryos was done to aid antibody penetration and allow imaging of the middle of embryos with a short-working distance high resolution objective. Bisected embryos were then incubated with antibodies diluted in NTBS with 10% fetal bovine serum and 5% DMSO at room temperature for 2 hours with 3 one hour washes with NTBS after each antibody incubation. Mouse monoclonal antibodies against αβ-tubulin (Charles River; 1:1000), and γ-tubulin (GTU-88, Sigma; 1:100), were used in conjunction with goat anti-mouse TRITC for single label or FITC for double label of αβ-tubulin and NCD (Sigma 1:1000). Polyclonal antibodies against actin (Sigma; 1:100) and NCD (provided by D. Compton; 1:100) were followed by sheep anti-rabbit TRITC secondary (Sigma; 1:1000). After immunostaining, embryos were dehydrated fully in methanol, then cleared in two rinses of Murray's (2:1 benzyl benzoate:benzyl alcohol).

X. laevis *Pharmacological treatments and microinjections*

MTs were stabilized by incubation in 50% D_2O in 1/5 X MMR at various times relative to first cleavage, or by injection of 0.5 nL paclitaxel (10 mg/mL in DMSO; Sigma) at the animal pole just prior to furrowing. MT motors were disrupted by injection of embryos just under the furrow at the time membrane addition began, with motor-specific antibodies or chemical inhibitors of motor function. Injectate volumes ranged from 0.5 to 12 nL and were calculated to result in cytoplasmic concentrations of injectate in their active range. Most of the embryo cytoplasm is in the animal hemisphere and constitutes about 1/3 of the embryo volume, the rest being yolk, therefore

cytoplasmic volume was taken to be approximately 300 nL. Antibodies were injected to final protein concentrations between 200 and 300 μg/mL. Stocks of pharmacological inhibitors were injected so that final concentrations were 5 mM for AMP-PNP and NEM to inhibit kinesins, and 2 mM for NEM and 1 mM for EHNA to inhibit dyneins. Data was only collected from embryos which cleaved normally, or in the case of treated embryos, those which did not appear dead (perforated and oozing yolk) and which had untreated siblings with a high percentage of normal cleavage.

X. laevis *Dissections*

Embryos were dissected and cultured in 1/2 X NAM (1 X NAM: 110 mM NaCl, 2 mM KCl, 1 mM $Ca(NO_3)_2$, 1 mM $MgSO_4$, 0.1 mM EDTA, 2 mM Na_2HPO_4/NaH_2PO_4, pH 7.5, 1 mM $NaHCO_3$, 25 μg/mL gentamycin). The vitelline envelope was removed with sharpened watchmakers forceps and the embryos dissected with an eyelash attached with wax to the end of a pasteur pipette. Embryo fragments were generated by cutting through the blastopore, the lateral body wall, and the prospective mouth region, ventral to the anterior neural folds (Figure 4.1 A). Since the archenteron is an epithelial layer that lines the internal surface of the dorsal and ventral sides at this stage, isolated sides had epithelium on both surfaces, which helped maintain the integrity of embryo fragments. Isolated dorsal and ventral pieces, and the dorsal and ventral sides of intact embryos, were measured at mid-neurula and tailbud stages (stages 16 and 27, respectively) to determine the change in length of the A-P axis. Measurements were made following the external contour of each piece or embryo for the full extent of the A-P axis, from cement gland to blastopore (Figure 4.1 B).

X. laevis *Post-Neurula Fixation and Confocal Microscopy*

Embryos were anesthetized by adding several drops of 0.15% tricaine to the culture medium to relax the embryos into a straight posture to aid microscopic analysis, then fixed in Dent's (4:1 MeOH:DMSO) overnight at -20°C, followed by indefinite post-fixation in MeOH, also at -20°C. Alternatively, for analysis of cell division, embryos were fixed in Dent's containing 5 μg/mL propidium iodide. Embryos were dehydrated fully in MeOH before clearing in two rinses of Murray's (2:1 benzyl benzoate:benzyl alcohol). After clearing, optical sections of embryos were made on a confocal microscope using low magnification (5 X and 10 X objectives, Zeiss). For cell division analysis, higher magnification was used (40 X objective, Zeiss) and image slices 1 μm apart were taken from the anterior, middle, and posterior regions that were 211 μm tall by 317 μm wide by 20 μm deep. Image stacks were analyzed with NIH Image, as described above.

X. laevis *Scanning Electron Microscopy*

Embryos were anesthetized as described in the previous section, then fixed in 2.5% glutaraldehyde, 0.1 M Na cacodylate, pH 7.5 overnight at 4°C, after which they were transferred into 0.1 M Na cacodylate, pH 7.5 and held at 4°C. Embryos were cut transversely with a razor blade fragment, or were peeled of ectoderm with forceps to expose the ventral mesoderm. Then, embryos were dehydrated through an ethanol series (50, 75, 95, 100% X 3) and held in the final rinse of 100% overnight. Embryos were transferred to mesh baskets and dried by infiltrating with 1:1 ethanol:Peldri (Ted Pella) for 1 hour, then two rinses in 100% Peldri above 26°C for 1 hour each. The embryos were

then cooled below 23°C by placing the basket on a piece of cooled aluminum. Peldri was removed by sublimation under vacuum for 3 hours below 23°C. SEM stub tops were coated with silver paste and dried embryos were transferred to the stubs with forceps. Once the silver paste was dry, stubs were sputter coated with platinum to 25 nm at 50% power (Anatech). Photographs were taken with a 4 X 5 camera (JEOL) on PolaPan 55 film (Polaroid) using a JEOL JXA6400 SEM with a Link Analytical eXL computer for making length and width measurements.

X. laevis *Lineage labeling*

Four-cell embryos were labeled by injected the equatorial region of each cell with 0.5 nL of 5% tetramethylrhodamine isothiocyanate-conjugated dextran in water (mw 10,000, TRITC-dex, Sigma). Glass needles were pulled from 0.75 mm o.d. filament glass capillary tubes, back-filled, and attached to a picospritzer II (General Valve). Embryos were placed in 6% Ficoll in 1/5 X MMR to collapse the vitelline envelope onto the embryo surface to aid injection. Embryos were held in place using a piece of fiberglass screen and forceps.

X. laevis *Transplants*

After removal of the vitelline envelope with forceps, a strip of ectoderm and mesoderm was removed from the ventro-lateral region of unlabeled host embryos. A similar strip was removed from labeled donors and placed onto the graft site of the unlabeled host. The strips were longer in the A-P dimension than in the D-V dimension to aid visualization of cell rearrangements. Transplants were secured by placing the embryos in clay

wells under fragments of cover glass. Hosts were cultured in 1/2 X NAM at temperatures between 15 and 18°C.

X. laevis *Time-lapse recordings*

For time-lapse recordings of mesoderm cells, ectoderm was carefully cut and peeled away from the ventral sides of embryos (stage 20-24) with eyelash knives and forceps. Cells were vitally stained with 1% Nile blue sulfate in 1/5 X MMR, then transferred to 1 X NAM for recording. The primary contaminant of Nile blue is Nile red, which can be visualized with fluorescence optics using a rhodamine filter set (GHS). Time-lapse recordings were made on a confocal microscope using low magnification.

Chapter 2

Microtubules are required for completion of cytokinesis in sea urchin embryos.

Abstract

Completion of cytokinesis, abscission, has been studied surprisingly little despite the intensive studies of the onset and contractile mechanism of the earlier phases of division. It has been well documented that MT-disruption before furrow stimulation prevents furrowing, while MT-disruption after furrow stimulation allows division to proceed. We have confirmed those findings using the MT inhibitors, nocodazole and demecolcine. In addition, we have found that MT-disruption after furrow stimulation but before completion of division, prevents abscission as evidenced by the observation that prospective daughter cells in MT-disrupted embryos maintain electrical continuity. Continued observation of MT-disrupted embryos revealed that the furrows did not result in abscission, but rather persisted until the time when controls underwent second cleavage, at which point the furrows regressed. These findings extend the recent reports that MTs are required for completion of division in mammalian tissue culture cells and frog embryos, to invertebrates, suggesting a common mechanism of abscission for animal cells.

Introduction

Although cytokinesis has been studied intensively, the physical separation of daughter cells, which we call abscission, has received comparatively little attention. The cytoskeletal machinery present during mitosis consists of the microtubule (MT)-based mitotic apparatus that separates the chromosomes and positions the division furrow, and the actin-myosin-based contractile ring (CR) that constricts the cell by deforming the cell membrane. The mitotic apparatus begins disassembling as the CR forms; then, just before the incipient daughter cells separate, the CR becomes undetectable ultrastructurally. The midbody, visible in living cells because of the MT component, is the remaining cytoskeletal element present in the vicinity of the cytoplasmic bridge. Do MTs mediate abscission? Our recent discovery that MTs are required for division in frog embryos (Danilchik *et al.*, 1998), led us to examine the distribution and function of MTs during abscission in sea urchin embryos, a classical model for studying cell division.

Although this chapter addresses the role of MTs at the end of cytokinesis, it is instructive to begin with a description of the more familiar role of MTs in stimulating furrowing, since this is a necessary step before abscission can occur. The majority of studies of the mechanism of furrow stimulation in sea urchin embryos support the hypothesis that astral microtubules interact with the cell cortex during anaphase such that the CR forms as a narrow belt perpendicular to the long axis of the spindle. Chromosomes are evidently not required for CR formation, as their removal, following alignment at the metaphase plate, does not hinder cytokinesis (Zhang and Nicklas, 1996). Microsurgical removal of spindle MTs, leaving astral MTs intact, does not inhibit division (Hiramoto, 1971), showing that spindle MTs are also not necessary for CR stimulation. MT disruption with colchicine, prior to anaphase, does prevent furrowing, suggesting that astral

MTs are necessary for furrow stimulation (Beams and Evans, 1940; Swann and Mitchison, 1953). The most compelling evidence that astral MTs, but not spindle MTs or chromosomes, are involved in furrow stimulation is from an experiment displacing the first mitotic apparatus with a glass rod, which generates a torus shaped, binucleate embryo. The rod was kept in place through second cleavage, at which point the embryo was able to generate a furrow between the two asters that were not connected by a spindle, as well as at the mid-points of the two spindles, showing that the influence of two asters on responsive cortex is sufficient for cleavage initiation (Rappaport, 1961). Although furrowing can be initiated experimentally from well before anaphase to well after furrowing is normally complete (Rappaport and Rappaport, 1993), microsurgical removal of asters at the end of anaphase does not hinder division (Hiramoto, 1956). Taken together, these experiments indicate that the asters normally trigger CR formation during anaphase, after which they are unnecessary for furrowing. Furrowing requires intact microfilaments, and at a minimum, the actin-regulating proteins, Rho, MAD-1, citron, and AIM-1 (Mabuchi *et al.*, 1993; Drechsel *et al.*, 1997; Jin *et al.*, 1998; Madaule *et al.*, 1998; Terada *et al.*, 1998).

Once the CR has formed, it begins constricting the cell in a way that was for a time compared to the contractile activities of muscle fibers (for example Schroeder, 1968). However, unlike skeletal muscle fibers, the CR does not normally relax after contraction, and it maintains a constant width and thickness such that it becomes smaller volumetrically as it contracts (Goodenough *et al.*, 1968; Schroeder, 1972). When the CR is approximately six percent of its original diameter, it becomes undetectable and is presumed to be completely disassembled, after which the daughter cells separate completely (Schroeder, 1970; Schroeder, 1972). The resulting cytoplasmic bridge is present normally only briefly as demonstrated by both electrophysiological (Ashman *et al.*, 1964; Tupper *et al.*, 1970; Dale *et al.*,

1982) and dye injection techniques (Pochapin *et al.*, 1983; Sanger *et al.*, 1985; Cameron *et al.*, 1989; McCain and McClay, 1996; Summers *et al.*, 1996). However, under a variety of conditions that may destabilize MTs, the cytoplasmic bridge can persist long into the next division cycle before abscission is accomplished, suggesting that MTs may function in abscission (Scott, 1946; Vacquier, 1968; Schroeder, 1972).

During constriction of the cell by the CR, the midbody, a MT-containing structure, forms in the cytoplasmic bridge connecting the two presumptive daughter cells. The midbody is composed of bundles of short MTs that interlace at the cleavage plane. This region of MT overlap is also a site where many proteins congregate during telophase. Of these proteins, the ones that have been shown experimentally to be necessary for abscission, but not furrowing, have a microfilament- or MT-binding domain. For example, Nedd5, a mammalian septin family member, associates with actin and is found in the midbodies of dividing cells. Nedd5 can be disrupted functionally by injection of a monoclonal antibody, after which cells begin furrowing but are unable to undergo abscission (Kinoshita *et al.*, 1997). INCENP, a chromosomal passenger protein with a MT-binding domain also localizes to the center of the midbody at the end of division. When the MT-binding domain is mutated, INCENP no longer associates with the midbody and the cells suffer a failure of abscission (Mackay *et al.*, 1998).

Although the function of midbody MTs is still uncertain, recent experiments have shown that pharmacological disruption of midbodies in mammalian tissue culture cells results in failure of abscission (Julian *et al.*, 1993). Intracellular injection of antibodies to γ-tubulin prevents formation of a normal midbody, and presumably any other MT structures nucleated after anaphase, and also prevents separation of daughter cells, suggesting that newly nucleated MTs are required for abscission (Shu *et al.*, 1995). Together,

these findings suggest that abscission utilizes both microfilaments and MTs in mammalian cells.

Naturally occurring pseudofurrows, as well as some experimentally induced ones, fail to cause abscission and also lack MTs in the cytoplasmic bridge. For example, the polar lobe furrow in the embryo of the mollusc, *Ilyanassa obsoleta* constricts so tightly that it appears to have completely separated the polar lobe from the rest of the embryo. However, the polar lobe constriction does not surround MTs, and it relaxes prior to the next cleavage (Conrad *et al.*, 1992; Conrad *et al.*, 1994). Some substrate-adherent *Dictyostelium discoideum* myosin II mutant cells are able to form furrows, presumably through traction. However, these furrows rarely lead to complete division and the MTs are in an interphase-like arrangement, *i.e.* the cytoplasmic bridge does not contain a division-related MT structure, although some unidirectional MTs may pass through (DeLozanne and Spudich, 1987; Knecht and Loomis, 1987). In mammalian tissue culture cells a direct correlation was found between presence of MTs, but only in a midbody-like structure, and ability of experimentally induced furrows to complete division (Savoian *et al.*, 1999). And finally, in sand dollar embryos, experimental repositioning of the mitotic apparatus after furrow initiation causes regression of the furrow, but only if the spindle portion of the mitotic apparatus is moved completely out of the constriction (Rappaport and Rappaport, 1993). Since it has been shown that the spindle is not required for furrow stimulation, it appears that MTs in the cleavage plane act at a point later in division -- presumably abscission. The similar requirements for MTs in abscission of substrate-adherent and spherical cells suggests that the mechanism of abscission in both cell types is also similar. Here we reexamine the end of cytokinesis in sea urchin embryos and present evidence that MTs are required for abscission and that a spatially distinct population of MTs is present in the cleavage furrows of these embryos.

Results

Timing of MT disruption.

Because there is known to be a delay between the time of colchicine application and the time of MT disruption (Beams and Evans, 1940; Swann and Mitchison, 1953), the length of delay in action of nocodazole and demecolcine was determined by applying the drugs at different times relative to fixation, then staining for MTs. Nocodazole treatment of 15 or more minutes resulted in elimination of MT staining (Figure 2.1 A), whereas treatment times of 10 or fewer minutes had no discernible effects on MT staining (Figure 2.1 B). DMSO, the solvent for nocodazole, had no effect on MT staining (Figure 2.1 C). An array of MTs at the furrow is present that is similar to the furrow array seen in frog embryos.

Demecolcine was also used to disrupt MTs because it can be inactivated with ultra-violet (U.V.) light. The external coats of sea urchin embryos are the proteinacious fertilization membrane and hyaline layer. Embryos for demecolcine treatments were not stripped of their fertilization membrane. Although this resulted in a slightly longer delay in action of demecolcine, the length of the delay was more consistent than that observed for embryos stripped of their fertilization membrane. Embryos in their fertilization membrane were fixed in -20°C methanol for antibody staining because penetration of the aldehyde-containing Gard's fixative through the fertilization membrane was insufficient for antibody staining. Treatment with demecolcine for more than 25 minutes completely disrupted MTs (Figure 2.2 A), while treatment with U.V.-inactivated demecolcine for 25 to 40 minutes had no apparent effect on MTs (Figure 2.2 B).

Because there is some variability in the length of time to first cleavage ,

for this and subsequent experiments, groups of embryos were treated at multiple time points prior to the anticipated time of first cleavage. The time of first cleavage was then recorded and the actual time of treatment, relative to furrowing, was determined. To simplify the presentation of results, estimated times of MT disruption (*i.e.* retrospectively determined treatment times plus 15 minutes) are reported. Demecolcine was found to act more slowly and more variably than nocodazole, making interpretations of the results much less certain. Higher concentrations of demecolcine, which should disrupt MTs more quickly, show effects unrelated to MT disruption, as revealed by similarly high concentrations of U.V.-inactivated demecolcine (Sluder, 1976; Sluder, 1979) and were not used in this study. Therefore, the results from nocodazole disruption of MTs are more conclusive, but parallel demecolcine experiments were run because, together with the U.V.-inactivated form, they provide assurance that MT-disruption rather than side effects is responsible for the observed effects on abscission.

Disruption of MTs during early to mid-anaphase prevents furrowing.

The necessity of MTs for furrow stimulation was confirmed by MT disruption five minutes before furrowing. Embryos were treated with nocodazole 20 to 25 minutes before furrowing or with demecolcine 30 to 40 minutes before furrowing and furrowing was blocked in all embryos (Figure 2.3 A and B). Embryos were in early to mid-anaphase at that time. Therefore, MTs were disrupted at the expected time of furrow stimulation, thus the lack of furrowing. Not surprisingly, MT disruption five minutes after first cleavage resulted in 98% of embryos dividing normally when treated with nocodazole zero to 10 minutes before first cleavage and 88.6% when treated

with demecolcine four to 11 minutes before first cleavage. In these cases the MTs were not disrupted until after abscission, thus abscission occurred normally (Figure 2.3 D and E). These results are consistent with the timing of furrow stimulation, early to mid-anaphase, that has been established by many others using a variety of techniques (Beams and Evans, 1940; Swann and Mitchison, 1953; Hiramoto, 1956; Schroeder, 1990; Rappaport, 1996). All embryos treated with DMSO or U.V.-inactivated demecolcine completed division normally(Figure 2.3 C and F).

MT disruption just before abscission arrested cleavage.

A novel result was obtained when MTs were disrupted during division. Disruption of MTs after the furrow was stimulated, but before division was complete, resulted in furrow initiation followed by failed abscission (Figure 2.4 A). Nocodazole treatment 13 to 17 minutes before furrowing resulted in 45% of embryos failing to divide, 18% dividing completely, and 37% arresting at abscission (results were pooled from 3 batches of embryos, n=152). For the purpose of visualizing the presence or absence of cytoplasmic bridges, embryos were freed of the hyaline layer as follows, which did not alter timing or effectiveness of nocodazole treatment (see Figure 2.1). Embryos without a hyaline layer were generated by incubation in Ca^{2+} Mg^{2+}-free ASW shortly after fertilization, filtering through 73 μm mesh, then culturing in Ca^{2+}-free ASW to prevent reformation of the hyaline layer (see methods for details). Embryos raised in this way had normal cleavages and MT structures, but were fragile. Alternatively, embryos lacking both the fertilization membrane and hyaline layer were generated by urea treatment prior to fertilization, as this method

has been shown to result in the appearance of a hyaline substance between blastomeres (Moore, 1930 and Figure 2.4 C). However, the appearance of the hyaline substance seen in urea-treated embryos is unlike the connection visible between blastomeres in Figure 2.4 A, therefore removal of the fertilization membrane and hyaline layer does not result in a connecting stalk. Demecolcine treatment 16 to 20 minutes before cleavage resulted in 17% failing to divide, 36% dividing completely, and 47% arresting at abscission (results were pooled from seven batches of embryos, n=497). Because the connecting stalk is only visible in embryos stripped of their fertilization membrane, demecolcine-treated embryos are not shown here, but are shown in Figure 2.6.

Prospective daughter cells of embryos that arrested at abscission maintain electrical continuity.

Electrical coupling of prospective daughter cells was tested to confirm that what we identified as a cytoplasmic bridge in nocodazole-treated embryos was truly a cytoplasmic connection. Both daughter cells were impaled with microelectrodes, following which one cell was alternately hyper- and depolarized while recordings were made from both cells (Figure 2.5 A). Impaling of the membrane was assured by measuring membrane potential before and after hyper- and depolarizing pulses. Membrane potentials ranged between -30 to -60 mV (not shown), which is consistent with that described in other echinoderms (Ashman *et al.*, 1964; Tupper *et al.*, 1970; Dale *et al.*, 1982). Embryos treated with nocodazole 15 minutes before first cleavage so that MTs were disrupted during cleavage, maintained electrical continuity even 40 minutes after furrow initiation (3 of 3); *i.e.* the daughter cells remained ionically, and therefore, cytoplasmically, coupled (Figure 2.5 B).

DMSO-treated control embryos lacked electrical continuity (5 of 5) showing that division had completed 20 minutes after furrow formation (Figure 2.5 C). These results confirm that normal embryos separate shortly after constriction by the contractile ring, while embryos with MTs disrupted just before abscission fail to sever the connection between daughter cells. The completion of division in control embryos within 20 minutes of furrowing is consistent with findings in other echinoderms both by electrical recordings (Ashman *et al.*, 1964; Tupper *et al.*, 1970; Dale *et al.*, 1982) and by dye injection (Pochapin *et al.*, 1983; Sanger *et al.*, 1985; Cameron *et al.*, 1989; McCain and McClay, 1996; Summers *et al.*, 1996).

Failure of abscission resulted in recession of the first furrow at the time control embryos underwent second cleavage.

Cleavage arrested embryos were followed to the time that sibling controls underwent second cleavage to observe later effects of MT disruption. Embryos from several batches were photographed at multiple times between first and second cleavage. Large numbers of embryos were scored by photographing through a dissecting microscope, but for the purpose of Figure 2.6, individual embryos were followed through the first two divisions in depression slides and photographed through a compound microscope with a 50 X water immersion lens. First cleavage was initiated in embryos with MTs disrupted just before abscission, as described above. Nocodazole-treatment 13-17 minutes before furrowing, allowed formation of a furrow (Figure 2.6 A). However, at the time of second cleavage of the DMSO-treated embryo (Figure 2.6 F), the first furrow of the nocodazole-treated embryo regressed and no new furrow formed (Figure 2.6 B). Treatment with demecolcine 16-20 minutes

before furrowing also allowed formation of a furrow (Figure 2.6 C) that then receded at the time of second cleavage (Figure 2.6 D).

Furrow MTs are present in cleavage furrows of sea urchin embryos during the final two-thirds of cytokinesis.

Since MTs are required for completion of division in sea urchin embryos, what MT structures are present during cytokinesis? Confocal microscopy revealed immunofluorescently stained MTs in the cleavage furrows of sea urchin embryos that we call furrow MTs. Furrow MTs are short (8-24 μm) bundles of MTs visible on either side of the cleavage furrow once it has cut approximately one third of the way through the embryo (Figure 2.7 B, arrow). Furrow MTs are arranged perpendicularly to the astral MTs (Figure 2.7 B, arrowheads) that they come closest to, and obliquely to the midbody/spindle axis. The length of furrow MTs changes little as the CR progresses, while the angle relative to the spindle axis increases (Figure 2.7 C and D). Furrow MTs persisted to the end of cleavage (Figure 2.7 D).

Furrow MTs are discontinuous with the mitotic poles.

To analyze the relationship of furrow and astral MTs, image stacks of early and late furrows with the highest possible resolution were used. Optical sections were made on the confocal microscope with the aperture stopped down fully, to take the thinnest sections possible. Additionally, the focus motor was set to advance 0.1 μm per section, the closest spacing possible. Image stacks were reconstructed in NIH Image and MT bundles were traced through the stack, frame-by-frame, and highlighted so that upon projection they could be easily distinguished from the many other MTs present nearby.

Because we were analyzing the relationships of furrow and astral MT bundles, the MTs selected for analysis were MTs beneath the furrow that appeared, upon flat projection, to connect with astral bundles. When stacks were animated to rotate about the X- or Y-axis, it became clear that furrow MTs were not continuous with astral MTs. This is can also be seen statically in projections of stereo pairs and in projections at various angles (Figure 2.8). Individual MTs stained fluorescently are at the limit of resolution of light microscopes, so although furrow MT bundles are not continuous with astral MT bundles, it is possible that individual MTs may extend between the two. Furrow MT bundles appear to form *de novo*, but may arise from bundling of individual MTs emanating from astral bundles or from polar spindle fibers on either side of the cleavage plane.

Early in cleavage, before furrow MTs are apparent (slightly later than the embryo in Figure 2.7 A), astral MTs abut and occasionally intersect at the furrow base (Figure 2.8 A, green). A different set of MT bundles were identified that crossed the cleavage plane just under the shallow furrow, and could not be traced to either spindle pole (Figure 2.8 A, red). In the stack of images in Figure 2.8 A, which grazed the shallow furrow, the short furrow MT bundles (red) are closer to the viewer than the intersecting astral MT bundles (green). When the stack is projected at 90°, the separation of the red and green highlighted MTs is evident (Figure 2.8 B). Once furrow MTs are distinct, most appear to cross the cleavage plane and extend four to 16 μm on either side. Some furrow MTs curve toward the cell center on one or both sides, but could not be traced to the spindle poles unlike nearby astral MTs. In Figure 2.8 C, the astral MTs (green) in the upper part of the embryo extend primarily towards the viewer, while the seemingly adjacent furrow MTs (red)

fall in the plane of the page. The lower, furrow MTs (red) lie in a plane above the astral MT bundle (green). Projection of the same stack at 75° and 100° aids visualization of the distance between furrow and astral MTs (Figure 2.8 D and E).

Discussion

The necessity of MTs for completion of division in sea urchin embryos is consistent with recent findings in frog embryos (Sawai, 1992; Danilchik *et al.*, 1998) and mammalian tissue culture cells (Julian *et al.*, 1993; Shu *et al.*, 1995; Wheatley and Wang, 1996), as well as with some older studies in other echinoderms (Scott, 1946; Vacquier, 1968; Schroeder, 1972). As expected, MTs are required during anaphase to stimulate formation of the CR. In addition, we have shown with two pharmacological agents that disruption of MTs immediately after furrow stimulation does not prevent furrowing, as slightly earlier treatments do, but does block abscission of the prospective daughter cells.

In embryos devoid of both fertilization membrane and hyaline layer, when MTs are disrupted during cleavage a persistent cytoplasmic bridge forms. The connecting stalk formed in nocodazole-treated embryos is distinctly different from the substance that appears between the clearly divided blastomeres of embryos denuded with urea. In addition, electrical continuity of daughter blastomeres was maintained only in embryos with MTs disrupted during division, whereas normal embryos completed division within 20 minutes of furrow formation. Although batches of embryos are not completely synchronous, the analysis of hundreds of embryos can correct for such small differences. Hamaguchi (1975) used half embryos to avoid the slight differences in timing between embryos to investigate the timing of furrow stimulation by MTs. Hamaguchi (1975) confirmed that furrow stimulation occurs in early anaphase and mentioned in passing that at some timepoints of MT-disruption furrows formed and later regressed, but he did not further investigate the this effect on abscission. The phenomenon of

abscission failure following MT disruption was most likely not noticed previously due to the narrow window in which MT disruption results in abscission failure, as well as the delay between drug treatment and MT disruption, and the difficulty of determining if cleavage is complete without removing the hyaline layer, making electrical recordings, or waiting until the time of the next cleavage.

MTs have now been found to be essential for abscission in sea urchin embryos, frog embryos, and mammalian tissue culture cells, so it is possible that MTs may mediate abscission generally in animal cells. Which MTs are necessary for cell separation remains unclear, although there is evidence in frog embryos that midbody MTs are not essential for completion of division (Danilchik *et al.*, 1998). Another study in which MTs were disrupted in dividing mammalian cells suggested that newly nucleated MTs are required for abscission (Shu *et al.*, 1995).

Although the presence of furrow MTs in sea urchin embryos is somewhat contradictory to the dogma of cytoskeletal structure during division, *i.e.* that the only MTs present in the cell are part of the mitotic apparatus, it is consistent with experimental evidence that MTs are required for completion of division (Danilchik *et al.*, 1998; Julian *et al.*, 1993; Sawai, 1992; Shu *et al.*, 1995). The disparity between our observations of MT organization and those of the older sea urchin literature at least partly due to our application of computer-aided, three-dimensional analysis of confocal microscope optical sections.

MTs in sea urchin embryos have been studied using polarized light, immunofluorescence, and electron microscopy. Birefringence studies of dividing sea urchin embryos were helpful in determining that the mitotic

apparatus is composed largely of MTs (Rebhun and Sander, 1967; Sato *et al.*, 1975) and in monitoring the effects of MT-disrupting agents in live embryos (Aronson and Inoué, 1970; Sluder, 1976; Sluder, 1979; Sluder *et al.*, 1986). The most detailed structural studies utilizing birefringence, however, used isolated spindles. The absence of furrow MT structures in isolated spindles is not surprising since the two MT populations appear to be distinct.

There have been many immunofluorescence and transmission electron microscopic studies of MTs prior to and during initiation of furrowing (Harris, 1970; Harris *et al.*, 1980b; Schroeder and Battaglia, 1985; Gross *et al.*, 1958; Tilney and Marsland, 1969; Asnes and Schroeder, 1979), but few have investigated MT structure during the period when furrow MTs would be present (Longo, 1972; Schmekel, 1975). Furrow MTs have not been visible in immunofluorescence images published possibly due to fixation but more likely due to the dimness of furrow MTs relative to the brightly stained mitotic apparatus (Harris *et al.*, 1980a; Schroeder, 1987). Without the aid of computers for three dimensional reconstruction of sections, it would be extremely difficult to appreciate that MTs in the furrow are not continuous with astral MTs or the spindle poles. Furrow or midbody MTs may function by transporting vesicles to the cytoplasmic bridge, as has been hypothesized for both frog and fish embryos (Danilchik *et al.*, 1998; Jesuthasan, 1998). MTs may also interact with microfilaments, possibly of the contractile ring, near the end of division to aid completion of division.

A variety of proteins have been found to colocalize with midbody MTs, some of which appear to be necessary for cytokinesis. Disruption of many of the midbody-associated proteins prevents furrowing altogether, for example MAD1 and AIM-1, but these shed little light on abscission (Jin *et al.*, 1998;

Terada *et al.*, 1998). However, disruption of a small number of other midbody-associated proteins causes furrowing to halt after constricting by as much as 50%, then relax, allowing the cells to return to spherical, but binucleate cells. When the Ras related protein, IQGAP, of *D. discoideum* is inactivated by mutation, cells fail cytokinesis at abscission (Adachi *et al.*, 1997). Nedd5 is an actin-associating protein of the septin family. Injection of antibody to Nedd5 increases its GTPase activity, causes it to dissociate from actin filaments, and ultimately results in furrow relaxation (Kinoshita *et al.*, 1997). The recently described *C. elegans* formin family protein, CYK-1, also has a microfilament binding region, is found in the cytoplasmic bridge, and when mutated prevents complete division of the cells (Swan *et al.*, 1998). INCENP, a chromosomal passenger protein, has chromatin and MT-association domains. When the MT-association domain is deleted from INCENP in mammalian tissue culture cells, it no longer colocalizes with the midbody and abscission is prevented (Mackay *et al.*, 1998). In addition, ectopic furrows in mammalian tissue culture cells that result in abscission have midbody-like MTs as well as INCENP, while ectopic furrows that do not complete may have MTs, but not in a midbody-like arrangement, and also lack INCENP protein (Savoian *et al.*, 1999). Additionally, actin-myosin based traction has been found to be sufficient for furrowing in *D. discoideum*, but abscission does not occur and MTs are not organized as they would be in a normal furrow (DeLozanne and Spudich, 1987; Knecht and Loomis, 1987). In summary, there is now considerable functional evidence that MTs, in addition to microfilaments and several of their binding proteins, are involved in separation of animal cells, thereby providing the first clues to the nature of the machinery of abscission.

Figures

Figure 2.1. Treatment with nocodazole for at least 15 minutes (in this case 21 minutes) completely dissolved MTs (A). Nocodazole treatment for 10 minutes did not disrupt MTs perceptibly (B). DMSO, the solvent for nocodazole, had no effect on MTs (C). Embryos were stripped of their hyaline layer after fertilization. Length of treatment also reflects time prior to cleavage that treatment began.

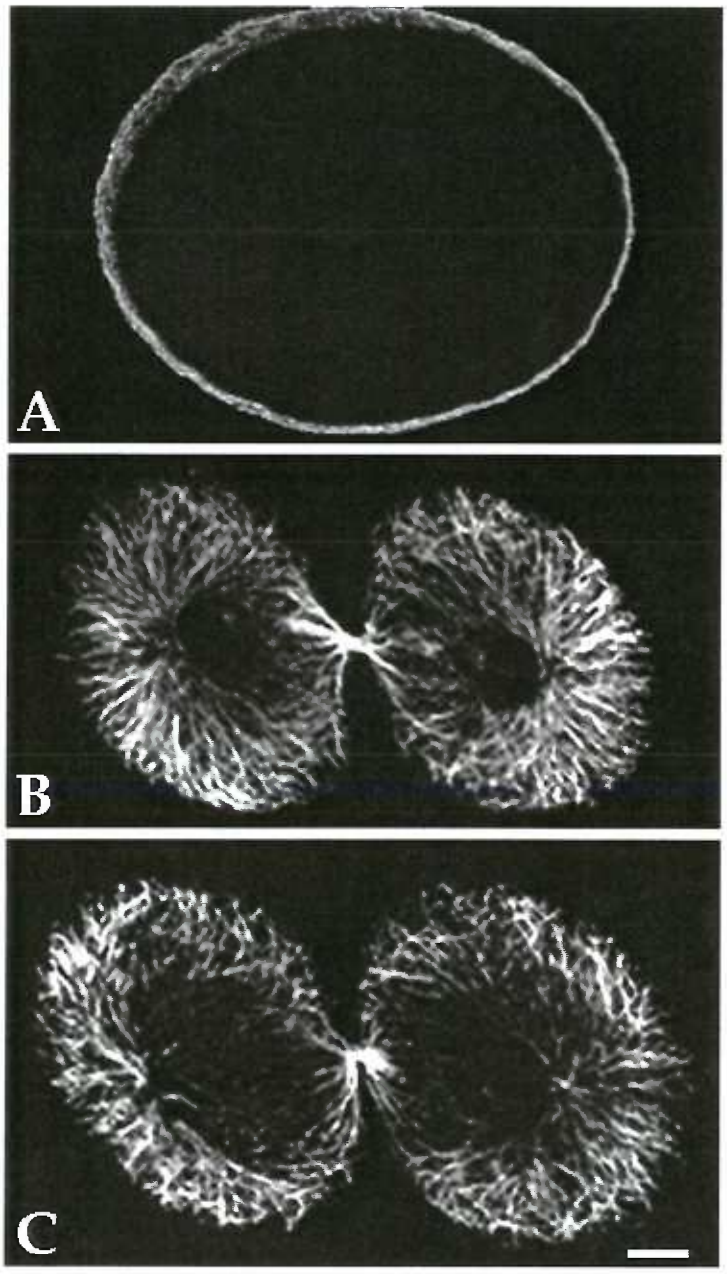
A
B
C

Figure 2.2. Demecolcine acts similarly to nocodazole, but more slowly. Treatment with demecolcine for 30 minutes completely dissolved MTs (A), while treatment for 35 minutes with U.V.-inactivated demecolcine did not disrupt MTs (B). DMSO-treatment did not affect MTs (C). Fertilization membranes were not removed, and embryos were fixed in -20°C methanol.

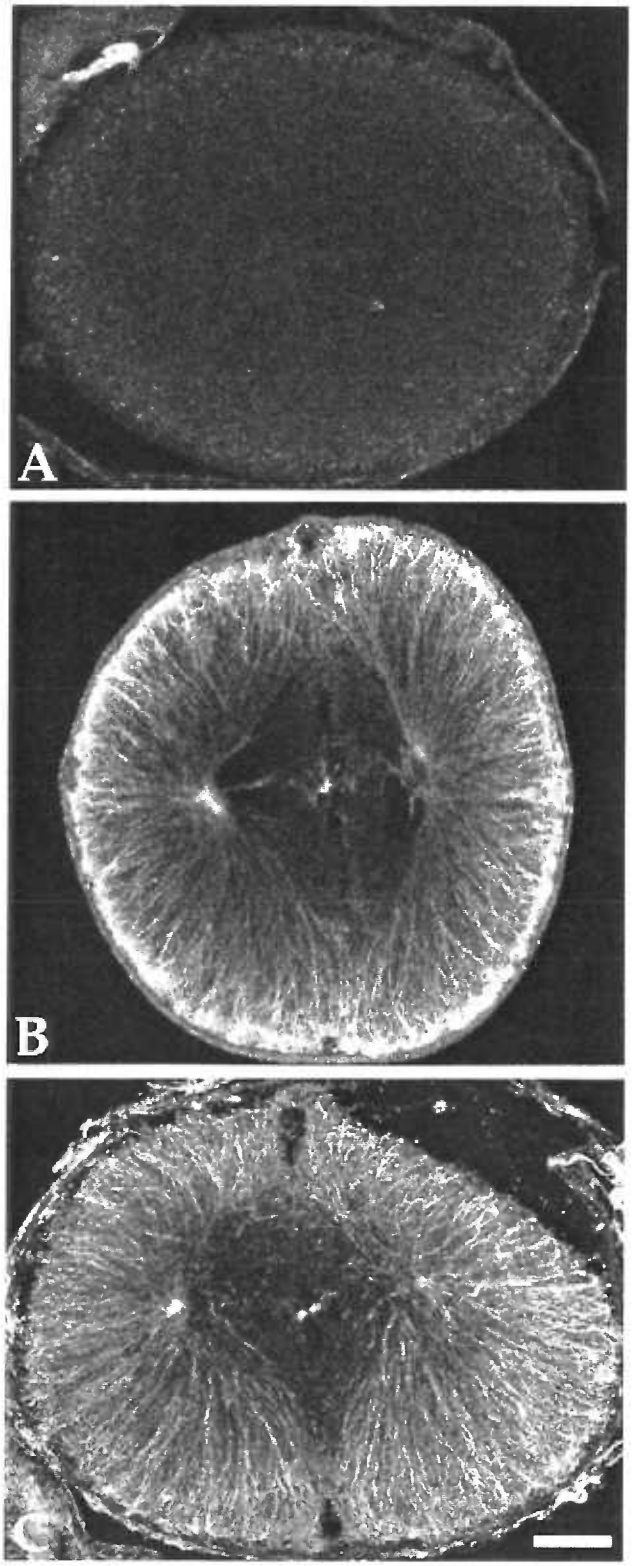
A
B
C

Figure 2.3. MT disruption before furrow stimulation prevented furrowing, while MT disruption after abscission had no effect on the completed cleavage. An embryo treated with nocodazole 21 minutes before first cleavage (A) and an embryo treated with demecolcine 35 minutes before first cleavage did not form a furrow (D). An embryo treated with nocodazole at the time of furrow formation (B) and an embryo treated with demecolcine 9 minutes before first cleavage (E) completed division. Treatment with DMSO (C) or U.V.-inactivated demecolcine for 35 minutes (F) had no effect on division. Embryos in A-C were freed of their fertilization membrane. Embryos in D-F retained their fertilization membrane.

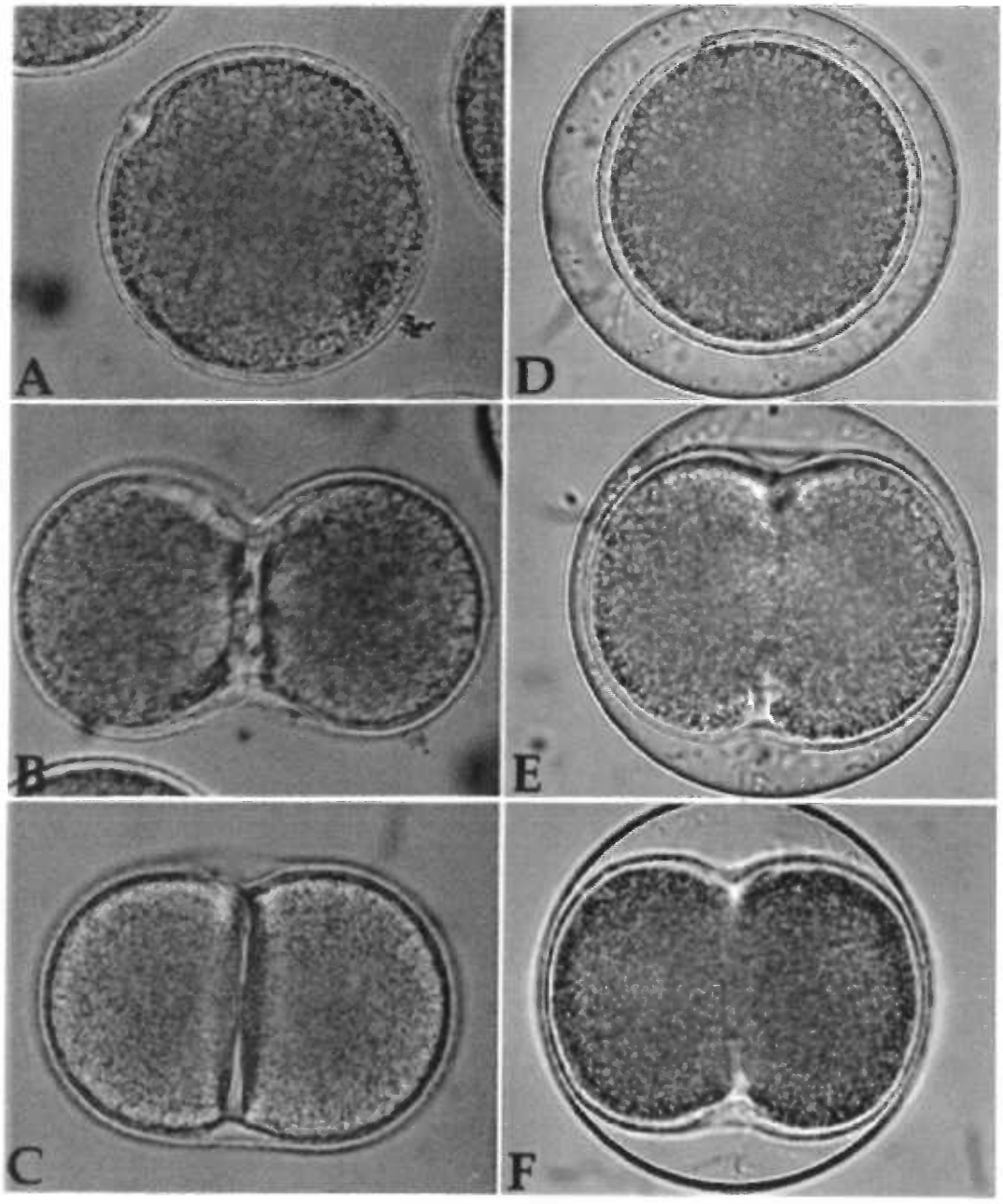
A
D
B
E
C
F

Figure 2.4. MT disruption after furrow stimulation, but before abscission, arrested division. Nocodazole-treatment 13 minutes before first cleavage resulted in the lasting presence of a cytoplasmic bridge (A, arrow). DMSO-treated embryos divided normally (B). Embryos in A and B were stripped of the hyaline layer with Ca^{2+} Mg^{2+}-free ASW to aid visualization of the cytoplasmic bridge. Urea-treatment to prevent the fertilization membrane and hyaline layer from forming did not result in a connecting stalk (C). The clear substance that appears between blastomeres of many embryos thus treated is unlike the connection caused by MT disruption (compare C and A) and no such substance is seen between blastomeres of embryos fertilization membranes were removed with Ca^{2+} Mg^{2+}-free ASW (B).

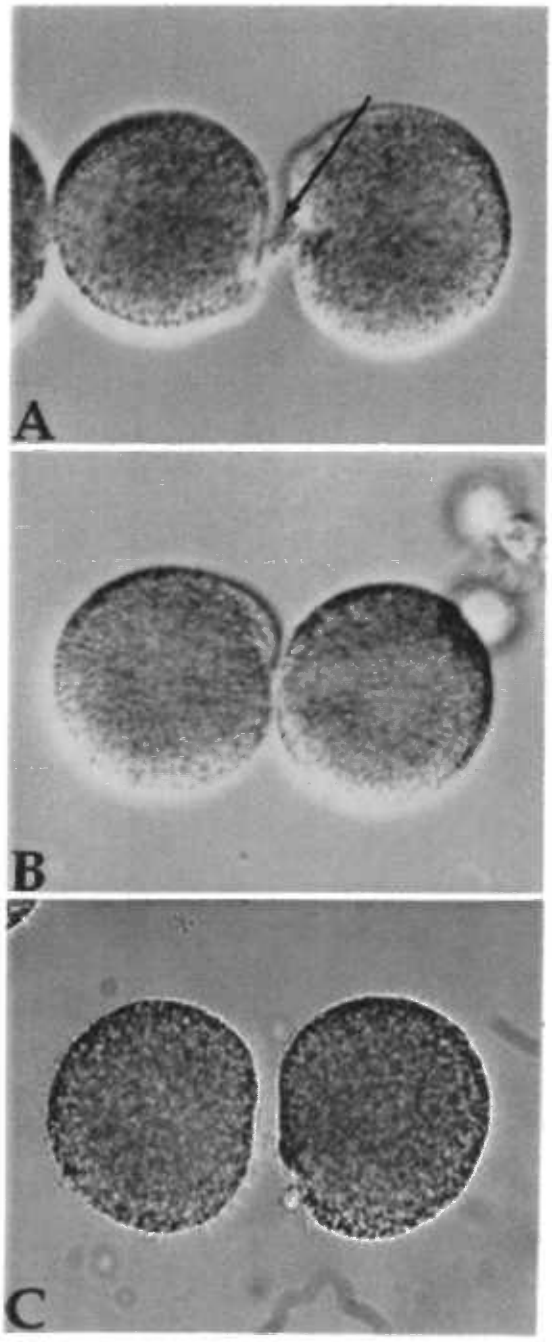
A
B
C

Figure 2.5. Electrical continuity of prospective daughter cells was maintained in embryos that were prevented from undergoing abscission by MT-disruption. Both incipient daughter cells were impaled with microelectrodes and recordings were made from both as each was hyper- then depolarized (A). Cleavage-arrested embryos failed to complete division as evidenced by electrical continuity of the cells 40 minutes after initiation of furrowing (B, arrows). Control embryos treated with 0.1% DMSO divided completely within 20 minutes of initiation of furrowing as can be seen by the lack of electrical coupling (C, arrows). The top two traces indicate voltage in the two cells and the bottom line diagrams the current pulses.

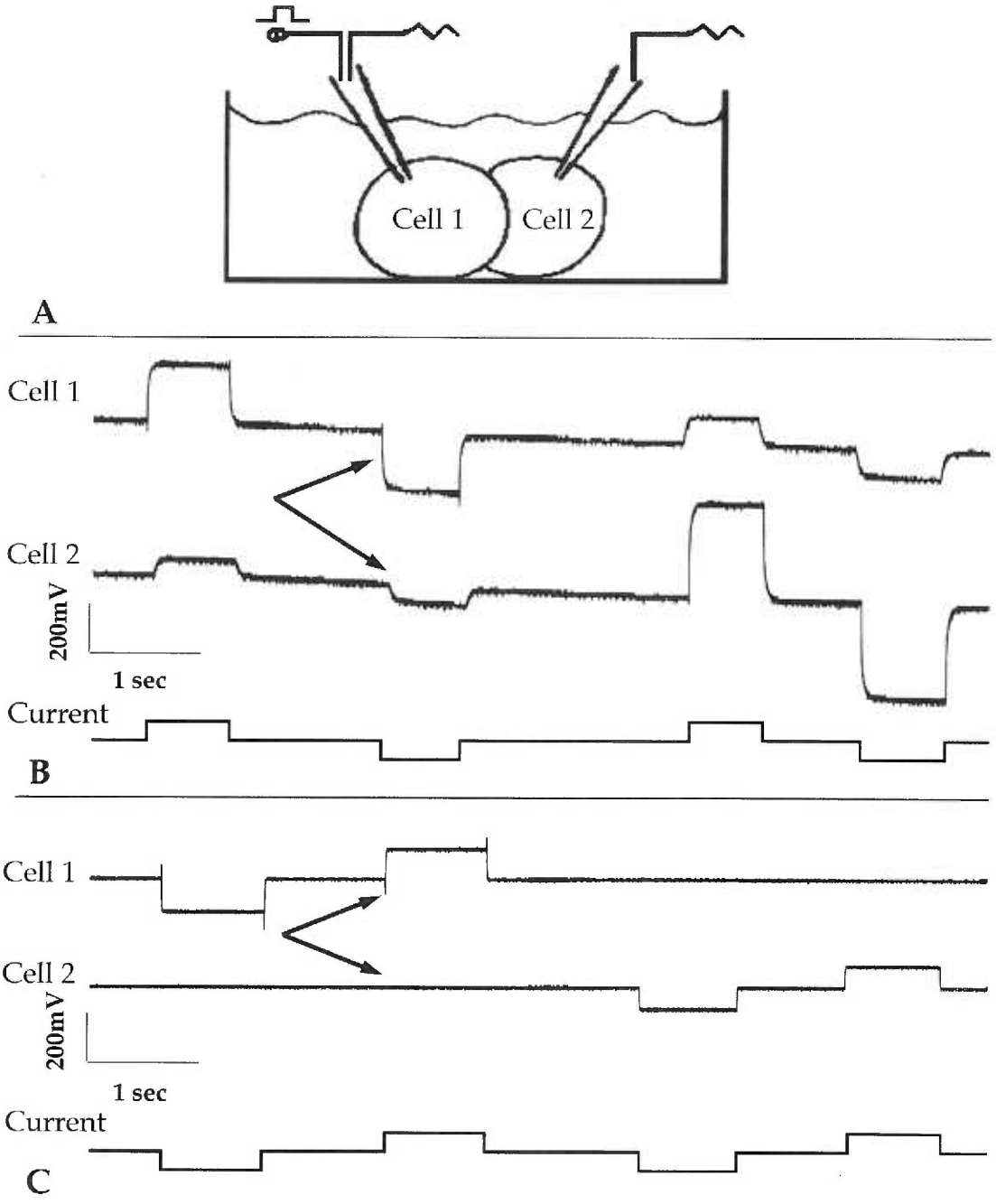
Cell 1
Cell 2
A
Cell 1
Cell 2
200mV
1 sec
Current
B
Cell 1
Cell 2
200mV
1 sec
Current
C

Figure 2.6. The arrested first furrow of MT-disrupted embryos regressed at the time of second cleavage. An embryo with MTs disrupted just before abscission by nocodazole-treatment 15 minutes before furrowing, initiated a furrow, although it was slightly later than controls (A). In the same embryo, at the time of second cleavage, the first furrow relaxed and no new furrow formed (B). An embryo treated with demecolcine 17 minutes before furrowing, at first cleavage (C), and seconds after the furrow receded, at the time of second cleavage of control embryos (D). A DMSO-treated embryo at first (E) and second (F) cleavages divided normally.

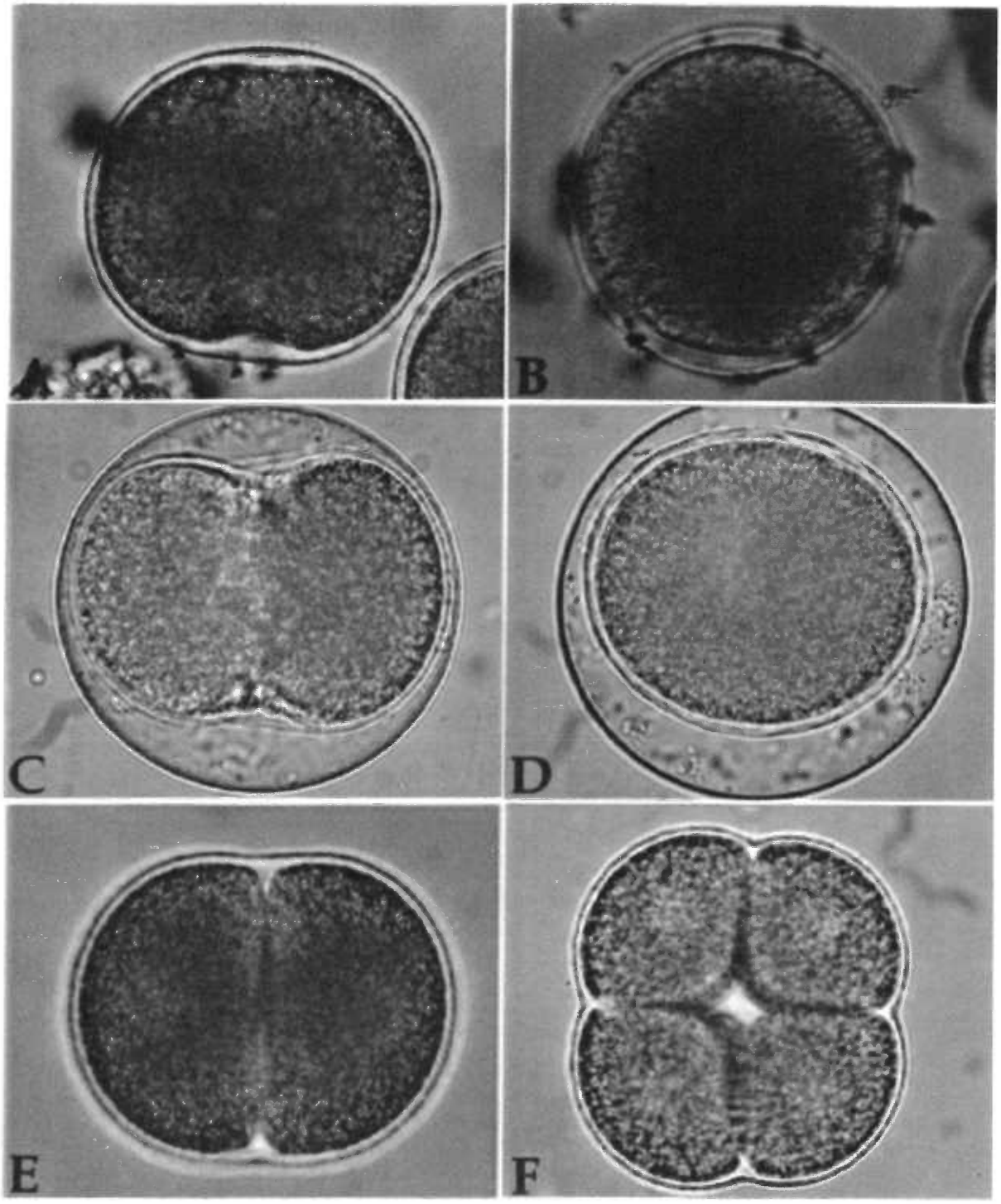
B
C
D
E
F

Figure 2.7. Ontogeny of furrow MTs in embryos of *S. purpuratus*. Stereo pair images of a series of embryos fixed at progressively later points in cleavage, stained with an anti-α-tubulin antibody. At the beginning of furrowing, furrow MTs are not present (A). Several minutes into furrowing, furrow MTs appear (arrow) and are roughly perpendicular to astral MTs (arrowhead) (B). Five to seven minutes into furrowing, furrow MTs are even more apparent and slightly longer (C). Just before abscission furrow MTs are still present and full length, while astral MTs are diminished (D). Scale bar is 10 μm.

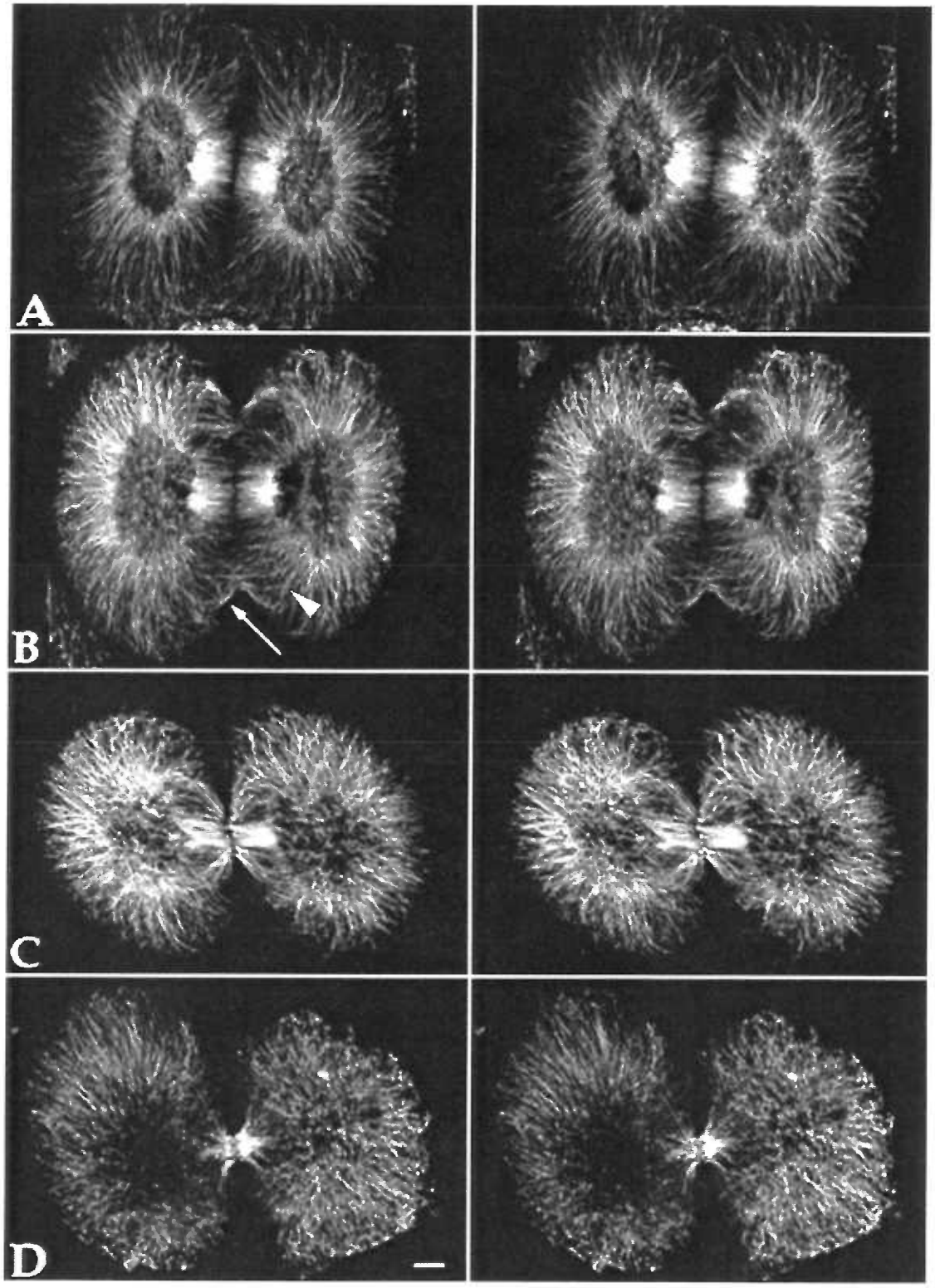
A
B
C
D

Figure 2.8. Three-dimensional analysis of confocal images revealed that furrow MTs were spatially distinct from astral MT bundles. In an early furrow, at a slightly later stage than the embryo in Figure 2.7 A, some astral MTs intersect at the cleavage plane (green) and a few furrow MTs (red) span the shallow furrow and are not continuous with astral bundles (A). Projection of the stack in A at 90° (B) clarifies the relationship an distance (arrows) between the two groups of MTs. Later in cleavage, at a slightly later stage than the embryo in Figure 2.7 B, astral MTs (green) do not reach as close to the cleavage plane, but often intersect furrow MTs (red) (C). Projection of the stack in C at 75° (D) and 100° (E) reveals the distance between the groups of MTs (arrows). Scale bar is 10 μm.

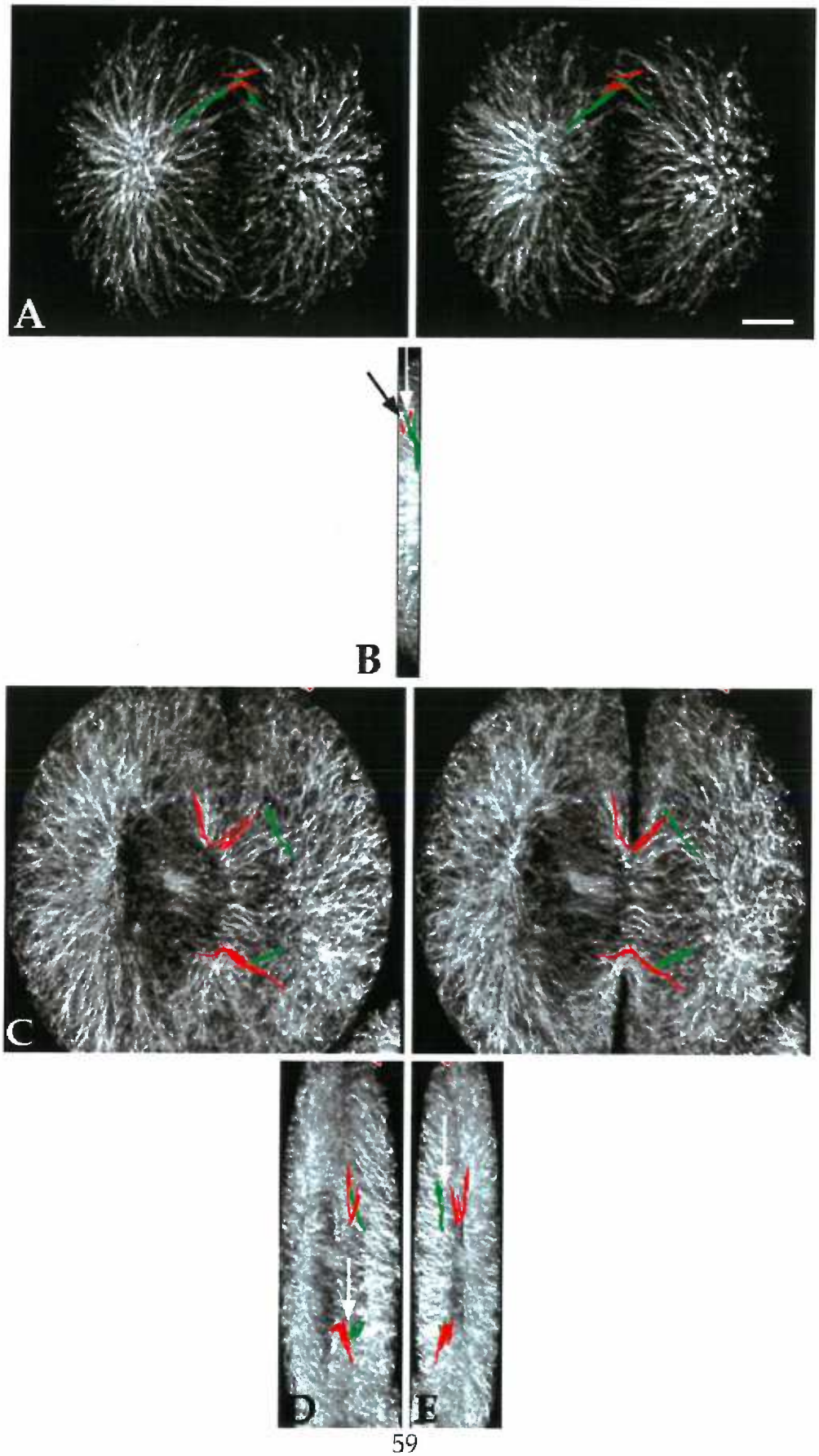
A
B
C
D
E

Chapter 3

The furrow microtubule array functions in deepening of cleavage furrows and not in membrane addition in dividing *X. laevis* embryos.

Abstract

It has been demonstrated previously that microtubules (MTs) are required for membrane addition and furrow deepening in dividing *X. laevis* embryos. Here we identify two characteristics of the furrow MT array (FMA) that distinguishes it from other MT populations in dividing embryos and utilize these differences to specifically disrupt the FMA. We find that the FMA is nucleated by γ-tubulin at the furrow and is bundled by an nonclaret disjunction (NCD)-family kinesin. Disruption of FMA nucleation and bundling prevents furrow deepening but not membrane addition.

Introduction

The cytoskeletal machinery present during mitosis consists of the microtubule (MT)-based mitotic apparatus that separates the chromosomes and positions the division furrow, and the actin-myosin-based contractile ring (CR) that constricts the cell by deforming the cell membrane. In many cells the mitotic apparatus appears to be the only population of MTs present in a cell early in division, with midbody MTs arising near the end of division. However, we have discovered and characterized novel MT structures in the division furrows of embryos of both the frog, *X. laevis* and the sea urchin, *S. purpuratus* (Danilchik *et al.*, 1998; Larkin and Danilchik, submitted, see Chapter 2).

The CR is stimulated by astral MTs such that it forms a narrow belt perpendicular to the long axis of the spindle. Chromosomes are not required for CR formation, as their removal upon aligning at the metaphase plate does not hinder cytokinesis (Zhang and Nicklas, 1996), although some chromosomal passenger proteins are necessary for abscission (Mackay *et al.*, 1998).

The CR is composed primarily of actin and myosin and is a ring with constant width and thickness, *i.e.* it becomes smaller volumetrically as it contracts (Schroeder, 1968, 1969, 1972). Although many proteins that interact with actin have been identified, few have been shown to be involved in cytokinesis (Mabuchi, 1990). Of those that do, Rho GTPase and its substrates appear to be involved in regulation of CR function, but its influence on furrow formation is still unclear (Drechsel *et al.*, 1997; Kishi *et al.*, 1993; Mabuchi *et al.*, 1993). Septin, an actin cross-linking protein, is present with the CR in active cleavage furrows, and its disruption halts cleavage (Fares *et*

al., 1995; Kinoshita *et al.*, 1997). It also remains uncertain whether the CR is formed by polymerization of new microfilaments or by alignment and bundling of existing ones.

The CR in many cells is initially present as a ring and constricts the cell. In *X. laevis* embryos, however, cleavage is unipolar, which means that the CR begins as an arc at the animal pole of the embryo and propagates around the embryo meridian until the ends meet at the vegetal pole forming an actual ring (Figure 3.1). Deepening of the furrow is presumed to be solely dependent on the contractile activity of the CR. However, global disruption of MTs prevents furrow deepening, while disruption of actin after cleavage onset, with cytochalasin B, completely abolishes the furrow and membrane addition proceeds normally (Danilchik *et al.*, 1998).

In frog embryos a large amount of new membrane is added at the cleavage furrow, as evidenced both by ultrastructural studies and studies of live embryos in which new membrane is recognizable by its lack of pigment and by movement of labeled membrane (Bluemink *et al.*, 1976; Byers and Armstrong, 1986; Sawai, 1987; Sawai, 1992; Selman and Perry, 1970). The storage form of the membrane is thought to be a large cytoplasmic pool of Golgi-derived vesicles. The first evidence for a MT-dependent mechanism for membrane addition was provided by Sawai (1992), who found that disruption of MTs with colchicine halted membrane growth and furrow advance. We confirmed those findings using a different MT inhibitor that has many fewer side effects, nocodazole, and now interpret them to indlicate a specific blocking of membrane addition and furrow deepening. Temporary disruption of MTs by 4°C cold shock resulted in dissolution of almost all detectable MTs within the embryo, and upon return to 20°C only FMA MTs reformed

(Danilchik *et al.*, 1998). Therefore, FMA MTs can form *de novo* at the furrow and, thus, are unlikely to be formed entirely by gathering of spindle MTs. The additional observation was made that MT disruption prevents furrow deepening. Further, we described a novel MT structure at the furrow, the FMA, but were unable to specifically disrupt it (Danilchik *et al.*, 1998).

The FMA of *X. laevis* embryos (see Figure 1.2) consists of bundles of MT 15 to 40 μm long on either side of the furrow that abut at the cleavage plane and appears at about the time that membrane begins to be added (Danilchik *et al.*, 1998). Despite some descriptive similarities to midbodies of other cells, the FMA does not appear to be a definitive midbody. A midbody-like structure, composed of short, presumably spindle derived MT bundles, is also present in these cells, but does not become localized to the cytoplasmic bridge. Since furrow MTs and the midbody-like structure have complementary features of a typical midbody, it is possible that the large size of the *X. laevis* embryo has facilitated the separate identification of these two distinct structures that are too close together to resolve in smaller cells, such as tissue culture cells.

As the CR reaches maximal constriction, but before cleavage is completed, the midbody, a MT-containing structure, forms in the cytoplasmic bridge connecting the two presumptive daughter cells. The midbody is composed of bundles of short MTs that interlace at the cleavage plane (Longo, 1972). Although the function of midbody MTs is still uncertain, recent experiments have shown that disruption of MT in mammalian tissue culture cells with nocodazole results in failure of those cells to divide completely (Wheatley and Wang, 1996). Intracellular injection of antibodies or antisense RNA to γ-tubulin prevents formation of a normal midbody, and potentially

other MT structures, and prevents complete separation of daughter cells, suggesting that newly nucleated MTs are required for completion of division (Julian *et al.*, 1993; Shu *et al.*, 1995). The initial interpretation of the γ-tubulin disruption experiments was that the midbody is required for completion of furrowing, although disruption of other MTs could account for the observed effects. Here we show that in frog embryos FMA MT formation requires γ-tubulin, the nucleating isoform of tubulin, and that the FMA is necessary for furrow deepening but not membrane addition.

There are two classes of kinesins, named plus end-directed and minus end-directed based on their motility *in vitro*. Most kinesins are of the plus end-directed type and have an amino terminal MT-association and motor domain, a carboxyl terminal cargo-association domain, and a central dimerization region, and as their name suggests, they progress along MTs toward the plus end. The kinesin motor is a Mg^{2+}-dependent ATPase that arrests on MTs in the presence of a non-hydrolyzable ATP analog, AMP-PNP, *in vitro* (Brady, 1985; Scholey *et al.*, 1985; Vale *et al.*, 1985a; Vale *et al.*, 1985b).

Minus end-directed kinesins have heavy chains with a carboxyl terminal motor, and MT-association domains at both ends, in addition to the central dimerization region (McDonald and Goldstein, 1990 and Chandra *et al.*, 1993). Although these proteins are able to transport cargo toward MT minus ends *in vitro* at the rate of 6 μm per minute (McDonald *et al.*, 1990), the presence of MT-association domains at both ends explains their apparent role in MT-bundling observed *in vivo* (Chandra *et al.*, 1993). The original member of this class, NCD, was identified in *D. melanogaster* as a gene involved in chromosomal disjunction (McDonald and Goldstein, 1990; McDonald *et al.*, 1990). It was identified as a member of the kinesin family by

sequence comparison (McDonald and Goldstein, 1990; McDonald *et al.*, 1990) and further investigation of its *in vivo* function revealed it as a MT bundling protein essential for formation of the meiotic spindle (Endow and Komma, 1996; Endow and Komma, 1997; Karabay and Walker, 1999; Matthies *et al.*, 1996). NCD can be inhibited by AMP-PNP *in vitro* (Foster *et al.*, 1998), because although it is structurally and behaviorally different from plus end-directed kinesins, the motor domains are highly conserved (McDonald and Goldstein, 1990).

Following the discovery that ncd encodes a kinesin, related genes were identified in a variety of other organisms. The human analog, HSET, is also involved in meiotic, but not mitotic spindles where its bundling function is apparently crucial for meiotic spindle formation in the absence of centrosomes. An antibody generated against the central dimerization region of HSET recognizes an 80 kD protein from *X. laevis* oocyte extract (Mountain and Compton, 1998). With this antibody we find that the 80 kD protein is associated with the FMA and its disruption results disorganized MT bundles and prevention of furrow deepening.

Results

Paclitaxel-induced tubulin sheets block membrane addition and furrow deepening.

Are MTs necessary functionally for membrane addition and furrow deepening? MT function has been shown to be dependent upon normal tubule morphology (Hamm-Alvarez *et al.*, 1993). Paclitaxel, formerly known as taxol, stabilizes microtubules by enabling side-to-side association of tubules, resulting in sheets rather tubes (Hamm-Alvarez *et al.*, 1993). Injection of paclitaxel to 17 μM into the animal hemisphere of embryos 80 to 90% of the way through the first cell cycle, blocked both furrowing and membrane delivery (27 of 29 cases, Figure 3.2 A). DMSO injection, at a similar site and time, allowed normal cleavage in most cases (15 of 18 cases, Figure 3.2 C). Determination of final concentrations of injected substances as well as the details of timing and method of injection are discussed in the Methods section. Induction of tubulin sheets in taxol-injected embryos was confirmed by αβ-tubulin staining (Figure 3.2 B). Membrane delivery was blocked, possibly, by the inability of tubulin sheets to engage in transport of vesicles to the surface. Furrowing may have been blocked by tubulin sheets physically obstructing the contractile ring or by blocking formation of normal MTs that stabilize furrows -- a possibility supported by later experiments.

MTs stabilization by D_2O does not block membrane addition or furrow deepening.

To show that inhibition of membrane addition and furrow deepening in paclitaxel-injected embryos did not result from MT-stabilization, D_2O was also used as a stabilizing agent. MTs within *X. laevis* embryos were stabilized

by treatment with D_2O. D_2O alters αβ-tubulin dimer on/off rates, without altering MT morphology (Rowning *et al.*, 1997). Treatment of embryos with 50% D_2O in 1/5 X MMR starting 60 to 82% of the way through the first cell cycle, resulted in the appearance of circular patches of unpigmented membrane across the entire animal surface (Figure 3.3 A). The unpigmented patches appear to be areas of new membrane addition, and arose at the time when untreated siblings were cleaving. In normally dividing embryos the new membrane added in the furrow is unpigmented (Byers and Armstrong, 1986). Although D_2O treatment prior to cleavage allowed membrane addition, it blocked formation of the first cleavage furrow in 19 of 19 embryos (Figure 3.3 A). Therefore, furrowing is not a prerequisite for membrane addition, although it does normally precede membrane growth. Furrow deepening cannot be addressed in embryos treated with D_2O early because furrow formation is prevented, but can be addressed by later D_2O treatment (see below). The appearance of new membrane in D_2O-treated embryos indicates that MT stabilization, in and of itself, does not inhibit delivery of new membrane. Indirect immunofluorescence of αβ-tubulin in embryos treated with D_2O before cleavage revealed large numbers of monasters throughout the cytoplasm, many of which were subcortical (Figure 3.3 D). The nucleation of microtubules virtually anywhere within the embryo supports our hypothesis that furrow MTs are nucleated at the furrow, rather than deriving from spindle MTs. Sea urchin embryos have also been found to form numerous monasters in response to D_2O treatment (Kuriyama and Borisy, 1983).

When D_2O was applied within ten minutes of furrow formation, normal furrowing occurred in 81% of 54 embryos, while the other 19%

arrested shortly after furrow formation. All of the embryos, regardless of furrowing activity delivered new membrane only to the active cleavage furrow (Figure 3.3 B and C). Confocal images of fixed embryos stained with αβ-tubulin antibody, revealed a denser than normal network of microtubules in the cytoplasm of embryos treated with D_2O during cleavage (Figure 3.3 E). Because embryos treated with D_2O at the time of cleavage continued to cleave without disrupting furrow deepening, one can conclude that stabilized MTs do not inhibit membrane addition or furrow deepening. Therefore, the disruption of both processes following paclitaxel-treatment must result from some other effect, such as the abnormal morphology of the MTs.

γ-tubulin is present around the furrow and injection of antibody to γ-tubulin blocks furrowing locally while membrane growth continues.

If FMA MTs do arise at the furrow, then nucleating sites must be present there. Indirect immunofluorescence revealed that γ-tubulin, the nucleating isoform of the tubulin family, was present in the vicinity of FMA MTs. A large amount of γ-tubulin was found in the cytoplasm of the animal hemisphere and, presumably due to the action of the CR, became more concentrated at and along the advancing cleavage furrow (Figure 3.4 A). The amount and location of γ-tubulin staining in the embryo is consistent with that found in oocytes, *i.e.* diffuse staining throughout the animal cytoplasm (Gard, 1994; Gard *et al.*, 1995). Injection of antibody to γ-tubulin at the onset of furrowing prevented furrow deepening locally without inhibiting membrane delivery (Figure 3.5 A). Embryos did recover from the local loss of nucleating sites after 20 to 25 minutes. αβ-Tubulin staining of γ-tubulin antibody-injected embryos, fixed during recovery, revealed very few MTs in the FMA near the

site of injection (Figure 3.5 C, arrow). These results corroborate the findings with D_2O and cold shock experiments that at least some furrow MTs nucleate at the furrow. The inability of the furrow to deepen in the absence of newly nucleated FMA MTs suggests that the FMA is involved in furrow deepening, while the continuation of membrane growth in the absence of the FMA indicates that other MTs are involved in membrane addition.

A minus end-directed kinesin colocalizes with the FMA.

Most kinesins are plus end-directed MT motors but there is a subset that is minus end-directed. The minus end-directed motors are involved in organizing MT structures that do not arise from centrosomes. Antibody to a human minus-end directed kinesin, related to the NCD protein of *D. melanogaster*, recognizes an 80 kD protein in *X. laevis* oocyte extracts (Mountain and Compton, 1998). When used for double-label immunolocalization in dividing embryos, it stained in a fibrous pattern overlapping with that of the αβ-tubulin antibody (Figure 3.6 E and F, arrow). Very low background was observed for the secondary antibodies (Figure 3.6 B and C) although there was considerable bleed-through of TRITC staining into the FITC channel (C). The colocalization of some of NCD protein with FMA MTs suggests that it may function with MTs in cleavage.

Pharmacologic disruption of ATPases suggests a role for kinesins in furrow deepening.

To investigate the possibility that a kinesin is involved in furrow deepening or membrane addition, ATPase inhibitors that are know to halt kinesins were injected into dividing embryos. Injection of AMP-PNP or NEM to 5 mM prevented furrow deepening. AMP-PNP prevented membrane

addition and furrow deepening (24 of 29 from three batches, Figure 3.7 A), much like nocodazole (compare with Figure 1.2 C). MT-staining of AMP-PNP-injected embryos revealed short thick bundles of MTs not organized as an FMA with a normal complement of thin MT bundles (Figure 3.7 D). Injection of NEM to 5 mM resulted in inhibition of furrow deepening, while membrane addition appeared to be unaffected (24 of 30 from three batches, Figure 3.7 B), much like the response to injection of antibody to γ-tubulin (compare with Figure 3.5 A). MTs in 5 mM NEM-treated embryos also appeared to be short thick bundles that did not organize into an FMA and normal appearing thin MT bundles (Figure 3.7 E, arrow).

To see if ATPase activity *per se* is necessary, or if only kinesin-like ATPase activity is necessary for furrow deepening, ATPase inhibitors that do not halt kinesins were also injected into dividing embryos. Two mM NEM and 1 mM erythro-9-[3-(2-hydroxynonyl)]adenine (EHNA) had no noticeable effects on cleavage (each 20 of 20 from two batches, Figure 3.8 A and B) or on MT organization (Figure 3.8 D and E). Embryos were observed to continue dividing normally through several more rounds of cleavage. Two mM NEM inhibits dyneins in *X. laevis* egg extracts, therefore the lack of effects on membrane addition and furrow deepening suggest that dyneins are not involved in either process. Additionally, EHNA concentrations over 1 mM halt actin-myosin contraction and dynein motility (Pennigroth, 1972), but since furrowing was uninhibited by 1 mM EHNA, the CR must have been functioning normally. The most potent known effect of EHNA is on adenosine deaminase, which also appears not to be required for cleavage (Pennigroth, 1972). Prevention of membrane addition only by AMP-PNP suggests that an ATPase is involved in that process, but apparently not a

known MT motor since membrane addition was not halted by 5 mM NEM. The sensitivity of furrow deepening and MT organization to various ATPase inhibitors suggests involvement of a kinesin in these processes, leading us to further investigate the functional significance of the colocalization of an NCD-type kinesin with the FMA.

X. laevis NCD protein is required for FMA organization and function in furrow deepening.

Because of the broad effects of the pharmacological agents used to inhibit ATPases, the results of the previous experiments do not conclusively demonstrate a requirement for kinesin in furrow deepening. Therefore a more specific method of disrupting NCD was sought. Injection of antibody to NCD was used to specifically block activity of NCD. The anti-NCD antibody is directed against a region spanning the junction between the carboxyl terminal MT-association domain and the central dimerization region (Mountain and Compton, 1998). The disruption of NCD function by the antibody may result from prevention of association of the carboxyl-terminal MT-association domain with MTs thereby preventing MT bundling. Injection of anti-NCD antibody was found to prevent furrow deepening without inhibiting membrane addition (16 of 20 from two batches, Figure 3.9 A), much like injection of the γ-tubulin antibody and 5 mM NEM (compare with Figures 3.5 A and 3.7 B). MTs in anti-NCD injected embryos were found to be short bundles deep to the surface that did not organize into an FMA, with normally distributed thin MT bundles (Figure 3.9 C). Injection of a rabbit antibody to a protein that is not present in the embryo cytoplasm, fibronectin, had no effect on cleavage (20 of 20 from two batches, Figure 3.9 B) and the MT staining pattern was also normal (Figure 3.9 D). The 80 kD minus end-directed kinesin recognized by the anti-NCD antibody, therefore, appears to function in furrow deepening by organizing FMA MTs.

Discussion

Although the traditional model of cell division does not assign a function to MTs after furrow stimulation and separation of chromosomes, there is mounting evidence that MTs are required for the terminal events of cytokinesis in a variety of cell types. For example, general disruption of MTs, *i.e.* with cold shock, nocodazole, or colchicine, blocks cytokinesis cell types as diverse as mammalian tissue culture cells, sea urchin embryos, and *X. laevis* embryos (Julian *et al.*, 1993; Shu *et al.*, 1995; Larkin and Danilchik, in press; Danilchik *et al.*, 1998). We have utilized *X. laevis* embryos because their large size offers advantages for the study of cytoskeletal structures. In cleavage stage *X. laevis* embryos these cytoskeletal structures tend to be spatially distinct from neighboring structures making structural analyses relatively easy. The large size of these embryonic cells also puts demands on the mitotic cytokinetic machinery that may not arise in smaller cells, and therefore, *X. laevis* embryos offer the opportunity to study the specialized mechanism for the addition of a large amount of membrane in the cleavage furrow.

Using MT stabilizing, and disrupting agents, as well as ATPase inhibitors and antibodies that specifically disrupt FMA MTs, we have shown that FMA MT organization is required for furrow deepening and not for membrane addition. The requirement of MTs for furrow deepening suggests some dependence of the contractile ring (CR) on MTs in *X. laevis* cleavage stage embryos. The CR in *X. laevis* early embryos begins as a wide band which narrows during the same period in which the FMA organizes, *i.e.* five to seven minutes after furrow initiation (Danilchik, personal communication). Based on this coincidence of timing and on the preliminary observation that CRs do not narrow in embryos which have been treated such

that the FMA does not organize, we speculate that CR narrowing is dependent upon FMA organization. In other, smaller cells, the CR has only been found as a narrow band and so, once again, the large size of *X. laevis* embryos may provide an advantage in the study of CR formation. The possibility that the CR might be narrowed by FMA MTs suggests involvement of a MT-microfilament cross-linking protein. As yet no such proteins have been found, but the abundance of microfilaments and MTs in *X. laevis* early embryos and the ease with which embryos can be generated, makes them a good choice for a biochemical search.

Our finding that FMA MTs are nucleated by the γ-tubulin isoform at the furrow is consistent with many other reports in the past five years that MTs can be nucleated at sites other than centrosomes and that these sites contain γ-tubulin (Akashi *et al.*, 1997; Karabay and Walker, 1999; Matthies *et al.*, 1996; Zheng *et al.*, 1995). Additionally, the necessity of NCD for FMA organization is also consistent with the originally defined function of NCD in organizing non-centrosomal MT structures (Endow and Komma, 1996; Endow and Komma, 1997; Karabay and Walker, 1999; Matthies *et al.*, 1996).

The sensitivity of FMA organization and furrow deepening to ATPase inhibitors known to inhibit kinesins and insensitivity to those that do not inhibit kinesins, in addition to sensitivity to anti-NCD antibody, confirms that *X. laevis* NCD is similar functionally to other NCDs. The inhibition of membrane addition by the ATP analog AMP-PNP but not by the high dose of NEM (5 mM) is puzzling since AMP-PNP is much more specific for ATPase. However, because NEM can only alkylate exposed sulfhydryl groups, it is possible that AMP-PNP affects an ATPase that does not have functionally relevant surface sulfhydryls. Since sulfhydryls are reactive groups that are

readily converted to disulfide bonds, which are insensitive to NEM, it is not unreasonable that a di- or multimeric ATPase would be insensitive to NEM while still being sensitive to AMP-PNP.

The following model can be synthesized from the available functional and structural evidence (Figure 3.10): membranous vesicles fuse to the furrow walls especially near the furrow base and are not dependent on FMA organization; furrow deepening is mechanically dependent on FMA MTs that are newly nucleated by γ-tubulin and bundled by the 80 kD minus end-directed kinesin recognized by the anti-NCD antibody.

Figures

Figure 3.1. The geometry of *X. laevis* cleavage differs from that of smaller, less yolky embryos such as those of the sea urchin. Sea urchin embryos initiate and constrict a furrow circumferenltially as diagrammed in cross-section and sagittal section (A). *X. laevis* embryos initiate a furrow at the animal pole and the furrow deepens from the top while the ends of the furrow wrap around the embryo eventually forming a ring that lies below the embryo center and does not surround the original spindle axis(B).

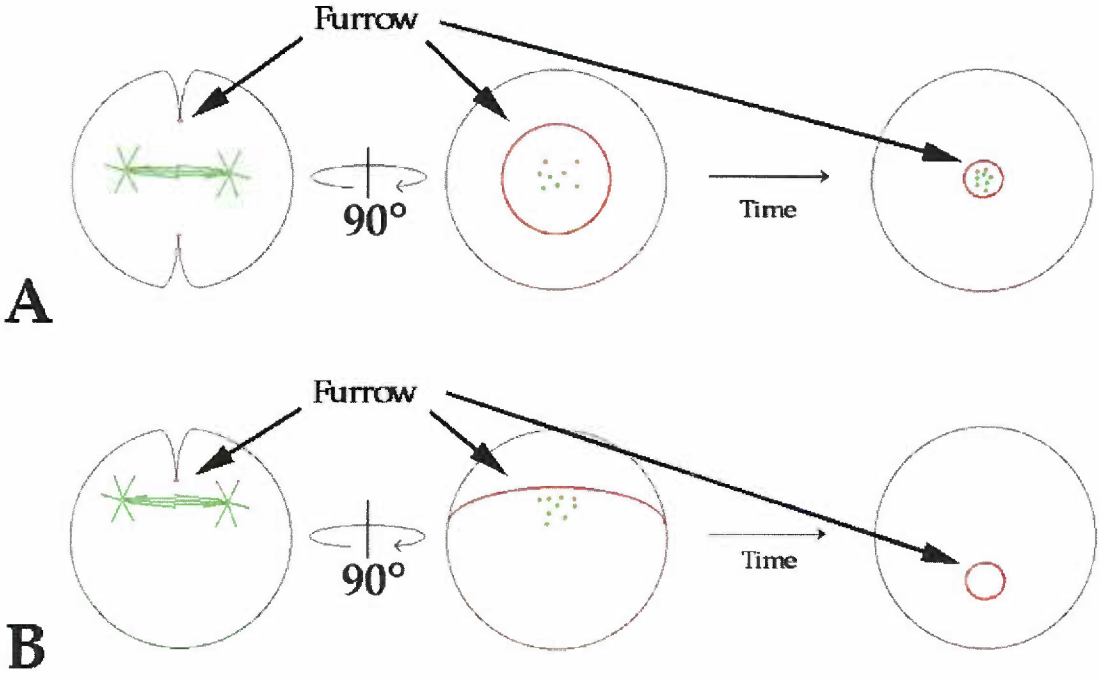
Furrow
90°
Time
A
Furrow
90°
Time
B

Figure 3.2. Injection of paclitaxel, a drug that disrupts MT morphology, blocked membrane addition and furrow deepening. Injection of 0.5 nL paclitaxel (10 mg/mL in DMSO) at the animal pole (asterisk) just prior to furrowing prevented the furrow form forming and new membrane from being deposited (A). Optical section in the plane of the furrow of αβ-tubulin staining in a taxol injected embryo shows the sheet-like nature of taxol-stabilized MTs (B). Injection of 0.5 nL DMSO had no effect on cleavage (C). Scale bar for B is 10 μm.

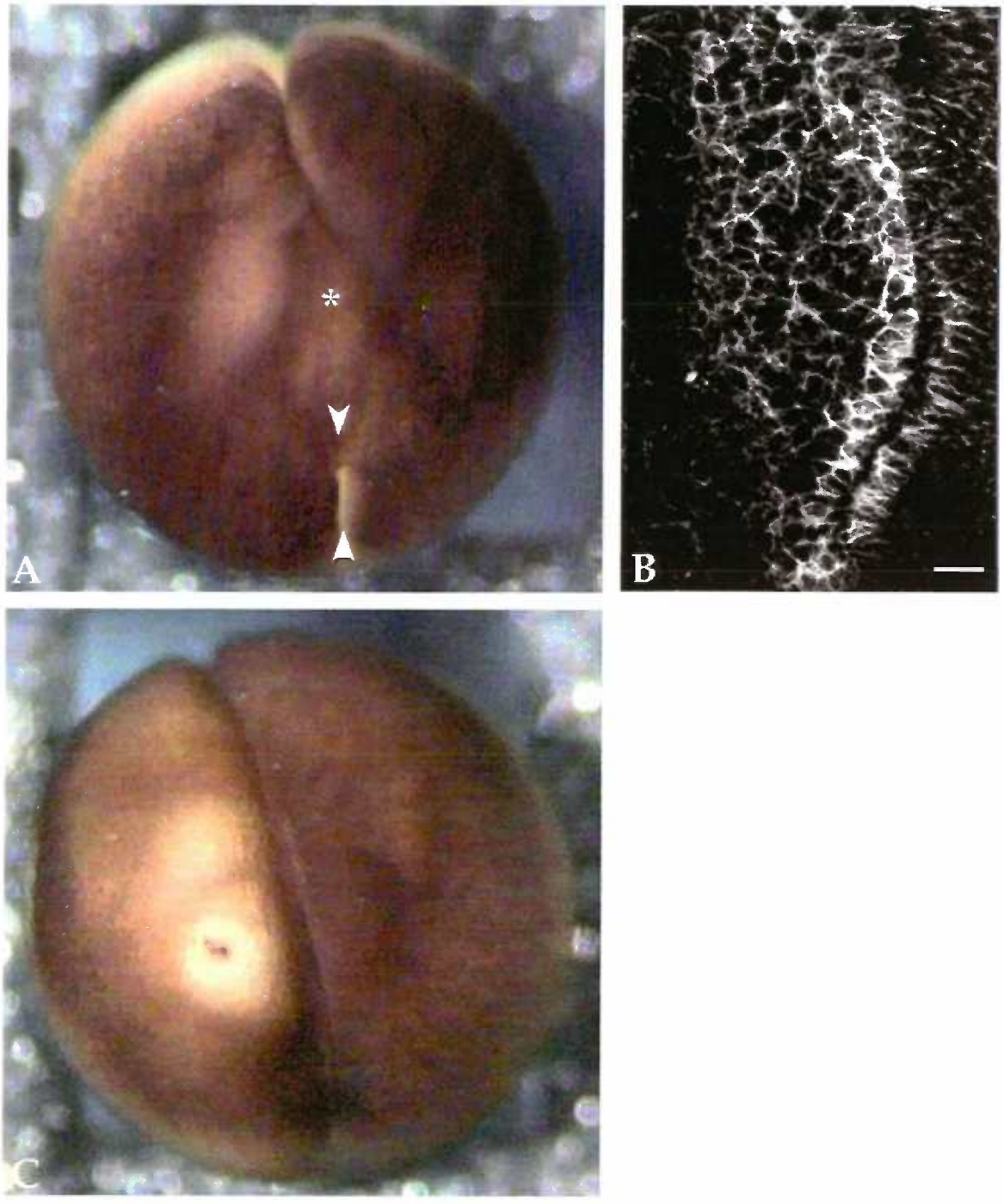
A
B
C

Figure 3.3. Treatment of embryos with D_2O prior to cleavage allowed membrane addition in the absence of furrowing, while late treatment allowed membrane addition and furrow deepening. Application of 50% D_2O before first cleavage prevented furrow initiation but did not inhibit delivery of new membrane, which occurred in spots across the surface at the time that untreated embryos cleaved (A). D_2O-treatment at the time of cleavage allowed membrane growth and furrow deepening to proceed. D_2O treatment after first (B) or second (C) cleavage resulted in the growth of the new membrane domain at the subsequent furrow. Confocal image of αβ-tubulin staining revealed multiple monasters when embryos were treated with D_2O before first cleavage (D), while αβ-tubulin staining revealed a denser than usual MT network at the furrow when embryos were treated with D_2O during cleavage (E).

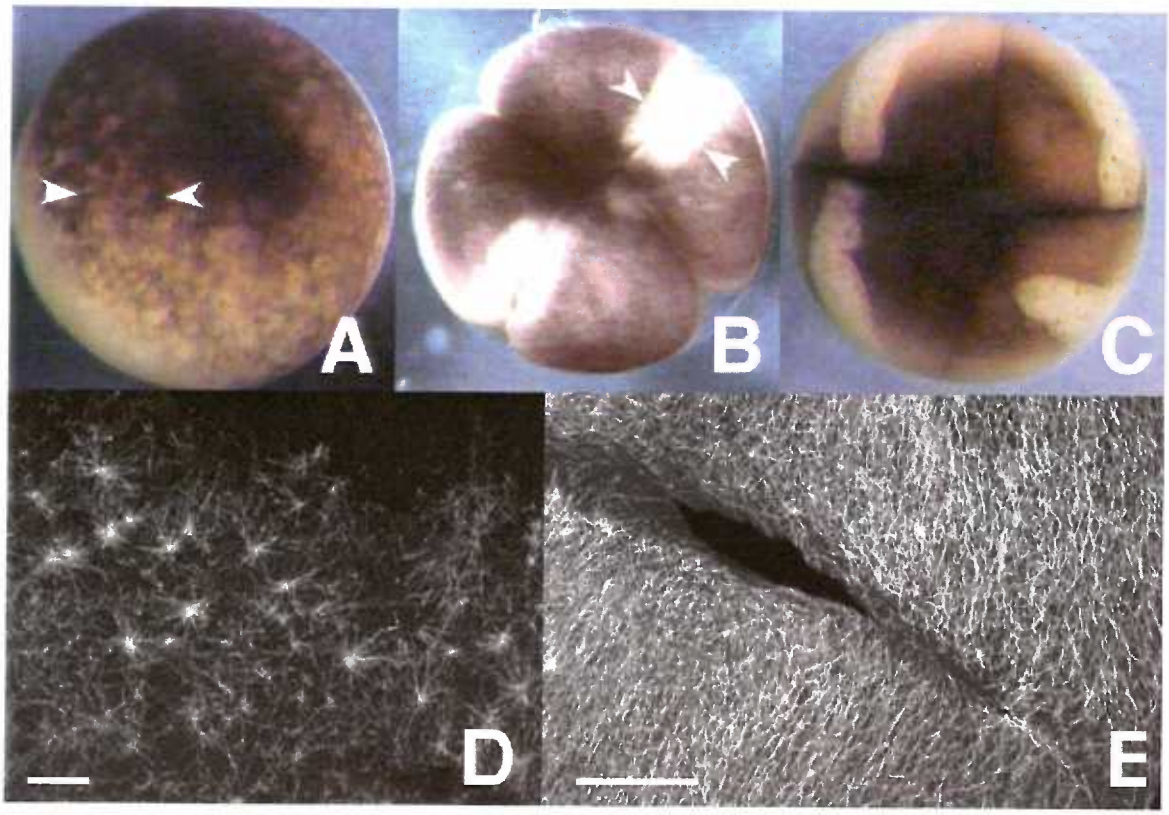
A
B
C
D
E

Figure 3.4. γ-tubulin is present at the base of the furrow. Confocal cross-section of an embryo stained with anti-γ-tubulin revealed much staining in the cortical cytoplasm and particularly around the furrow (A). The background level of staining by anti-mouse-TRITC was very low (B). Scale bar is 10 μm.

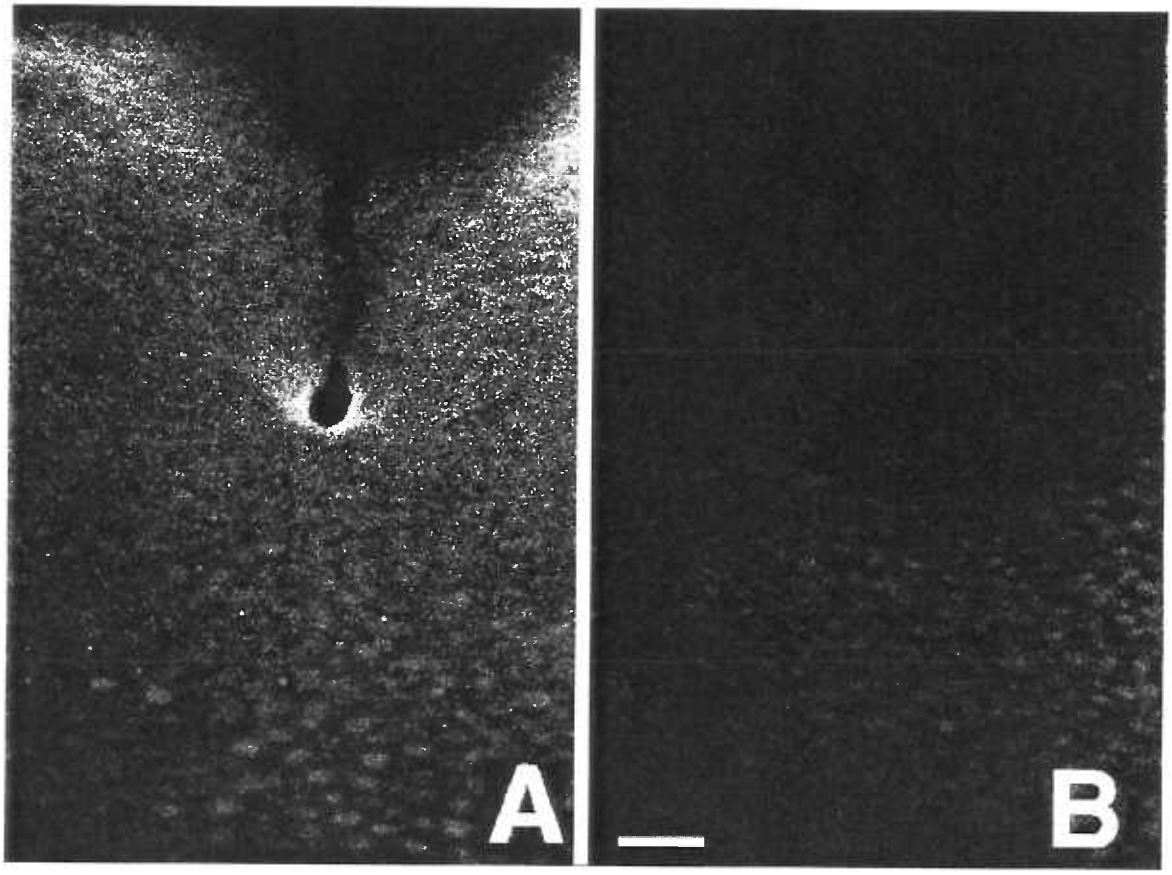
A
B

Figure 3.5. Newly nucleated MTs are involved in furrow deepening. Injection of antibody to γ-tubulin at the onset of cleavage relaxed the furrow without disrupting membrane addition (A, arrow). Injection of an equivalent volume of secondary antibody had no effect on cleavage (B). αβ-Tubulin staining of embryos injected with antibody to γ-tubulin and fixed 20 minutes later revealed very few MT bundles at the injection site (C, arrow). Arrowheads indicate approximate plane of confocal sections. Scale bar for C is 20 μm.

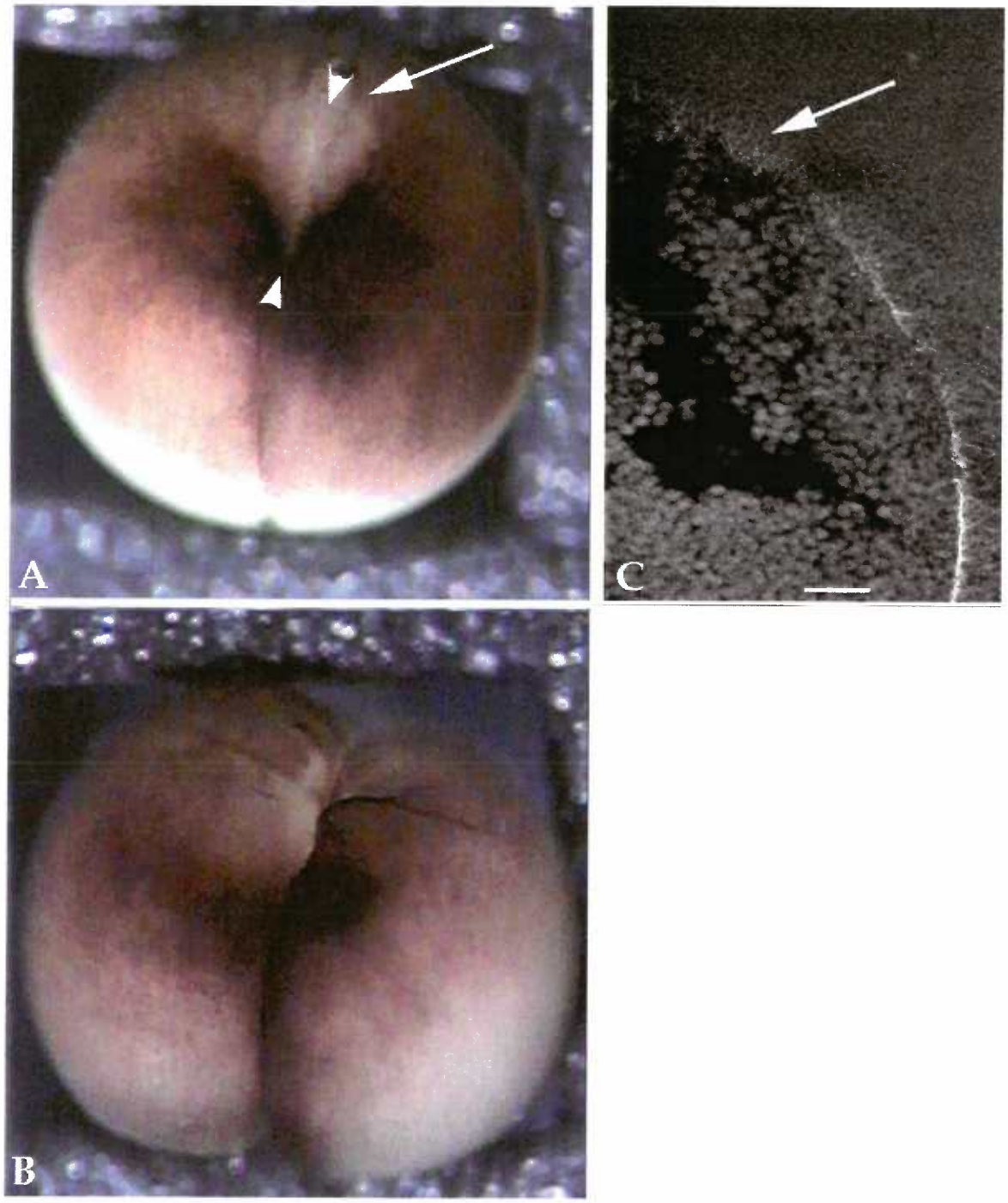
A
B
C

Figure 3.6. A minus end-directed kinesin is present with furrow MTs as shown by double-labelling of kinesin and MTs. MT staining followed by both secondary antibodies revealed typical FMA and thin MT bundles in the FITC channel (A) and not in the TRITC channel (B). Anti-NCD followed by both secondary antibodies stained fibrous structures in the area where furrow MTs would be (D, arrow) with some bleed-through in the FITC channel (C). Embryo stained with both primary antibodies showing MTs (E) and NCD (F). Although NCD-stained fibers are also MT-positive (E and F, arrow), some MTs have no NCD staining (E and F, arrowhead).

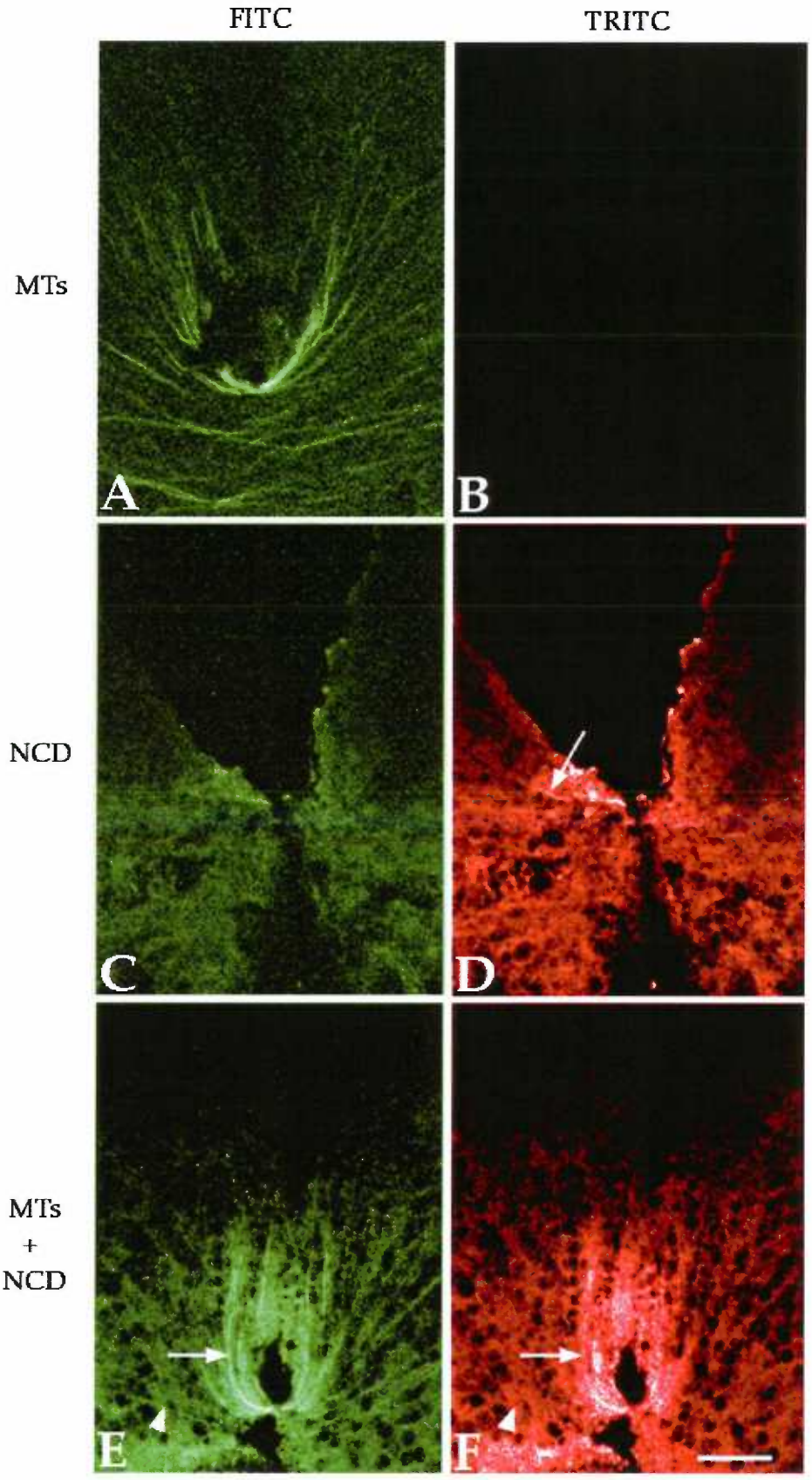
FITC
TRITC
MTs
NCD
MTs
+
NCD
A
B
C
D
E
F

Figure 3.7. ATPase inhibitors that block kinesin function prevent furrow deepening and alter MT organization. 5 mM AMP-PNP halted furrowing and membrane addition (A) and resulted in disorganized MTs (D) reminiscent of earlier timepoints (compare with Figure 1.2 C). The shallowness of the furrow is evident by the lack of large yolk platelets. 5 mM NEM blocked furrowing, but not membrane addition (B) and also resulted in disorganized short MT bundles and normal thin MT bundles (arrows, E). Water, the solvent for AMP-PNP and NEM had no effect on furrow deepening (C) or MT organization (F).

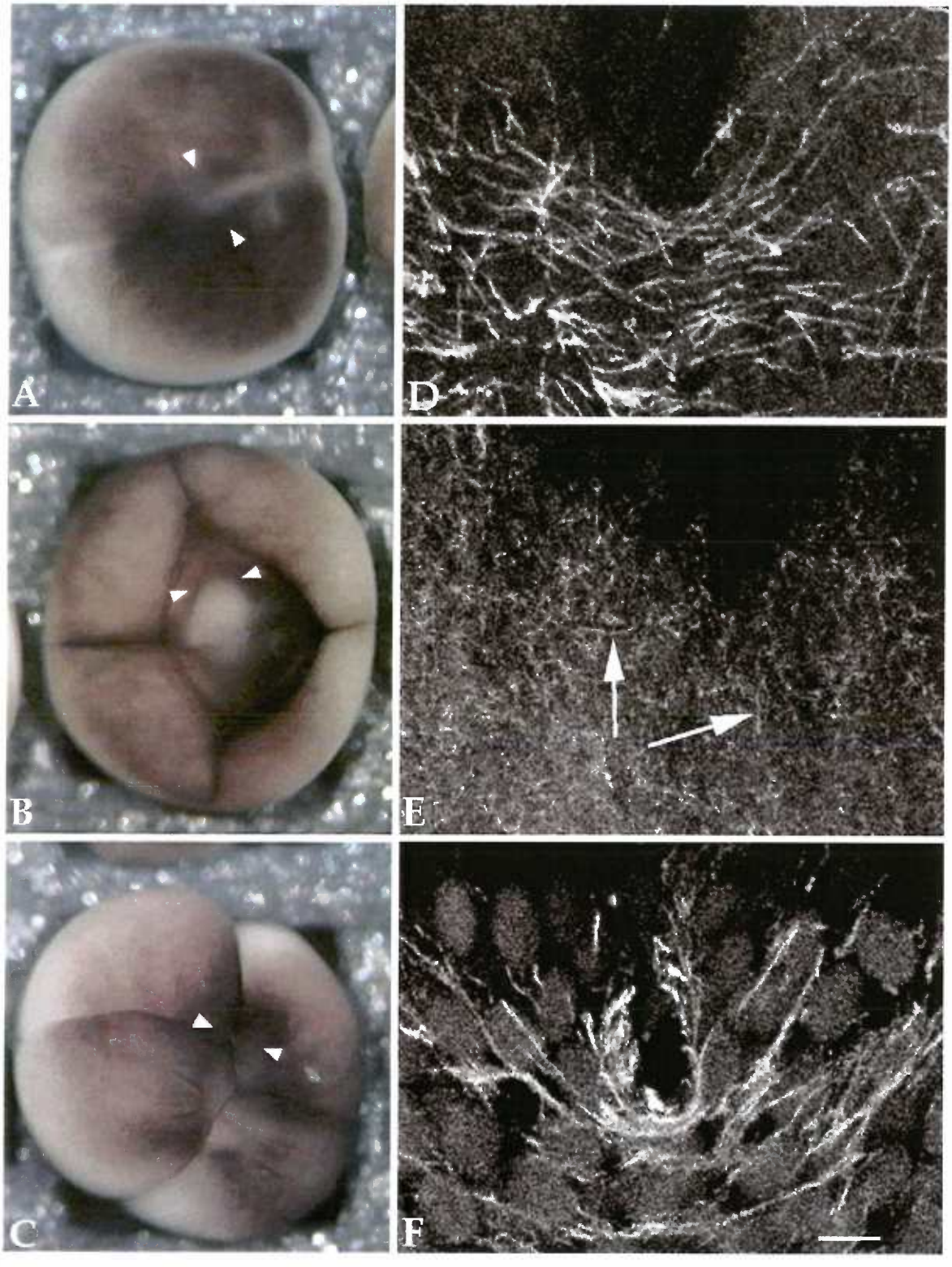
A
D
B
E
C
F

Figure 3.8. ATPase inhibitors that do not block kinesin function do not alter furrow deepening, membrane addition, or MT organization. 2 mM NEM (A, D),1 mM EHNA (B,E), and ethanol, the solvent for EHNA, (C, F) had no effect on cleavage. Injection of water, the solvent for NEM likewise, had no effect (see Figure 3.8 C and F).

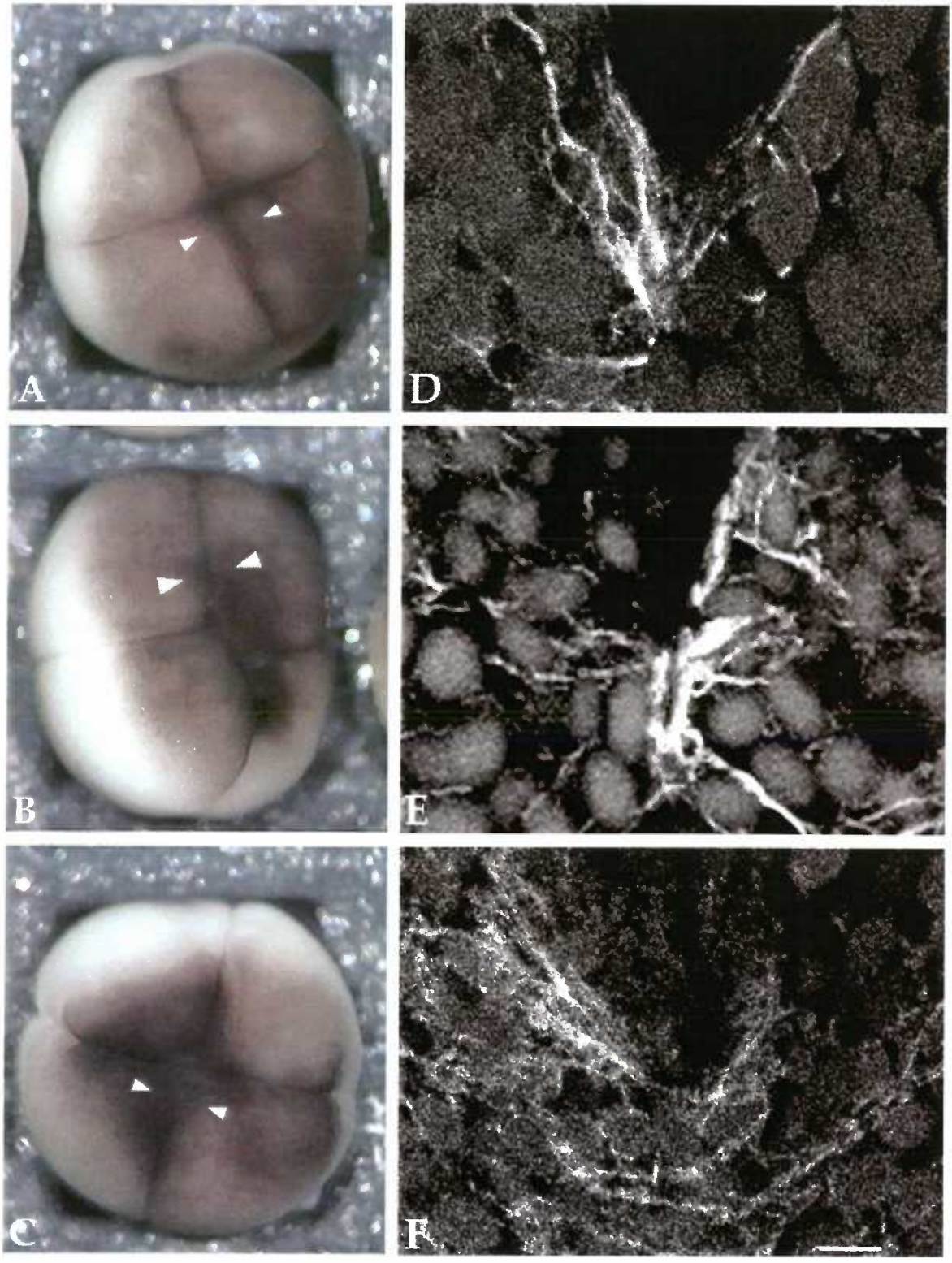
A
D
B
E
C
F

Figure 3.9. The minus end-directed kinesin is involved in furrow deepening and MT organization. Injection of anti-NCD into dividing embryos prevented furrow deepening but not membrane addition (A), whereas injection of another rabbit antibody (anti-fibronectin) had no effect on cleavage (B). MT-staining of anti-NCD-injected embryos revealed disorganized MTs at the relaxed furrow (C). MTs in anti-fibronectin injected embryos were organized as normal FMAs (D). Scale bar for C and D is 10 μm.

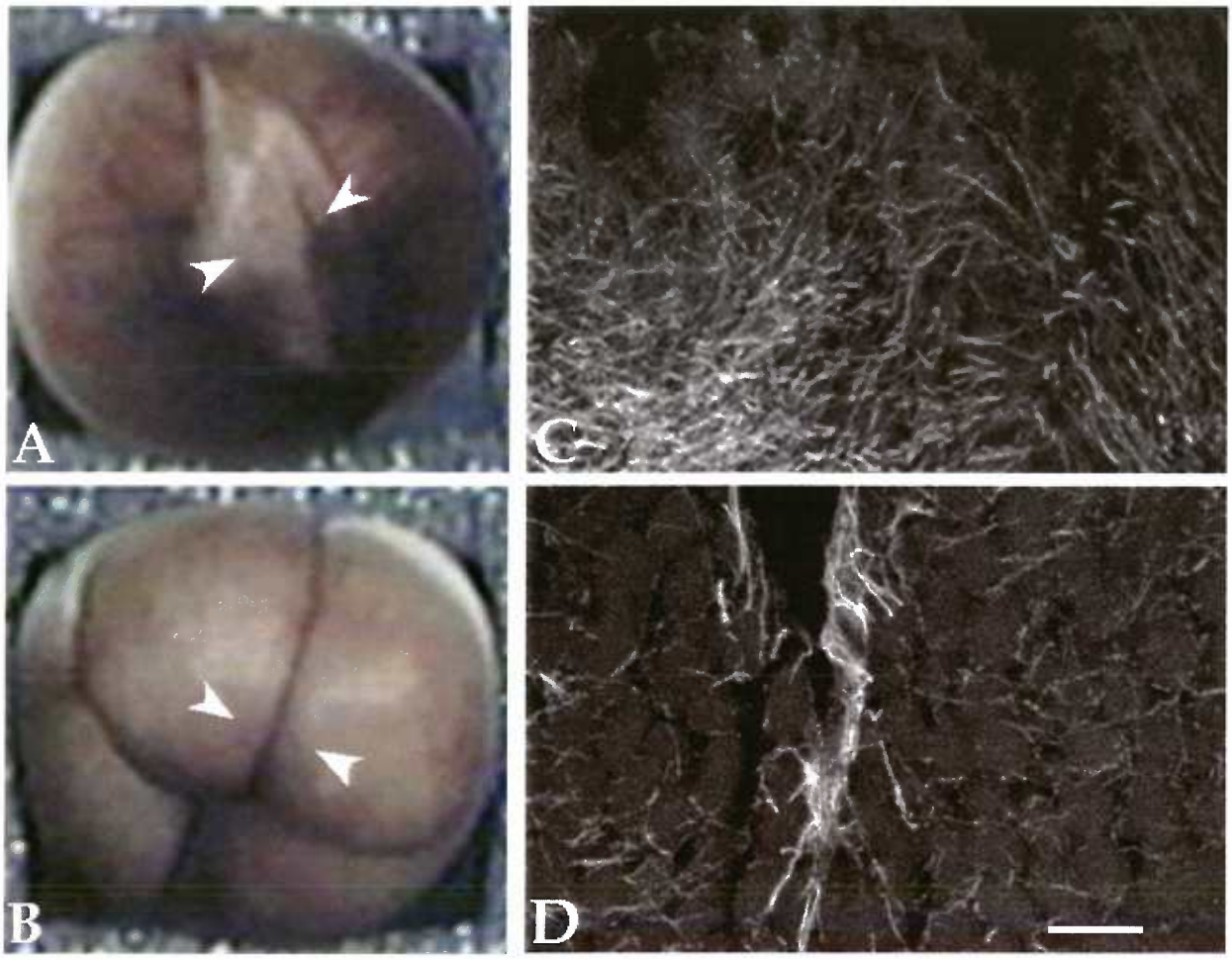
A
B
C
D

Figure 3.10. A model of cleavage in *X. laevis* embryos. In an early furrow (A) the FMA (thick dark green lines) is broad and associated with NCD (red dots). Membrane is added to the new surface (thin brown line) in the form of vesicles (yellow circles) and is dependent upon old unbundled MTs (thin green lines). (B) In later furrows that have cut into the yolk mass (yellow-orange ovals), the FMA is generally closer to the furrow sides, possibly due to association with the CR (orange crescent), and is still associated with NCD (red dots).

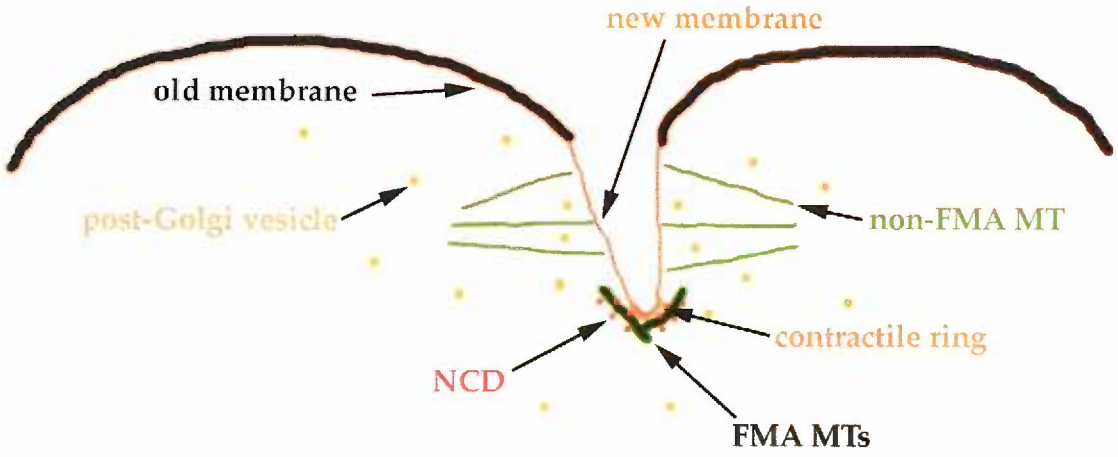
new membrane
old membrane
post-Golgi vesicle
non-FMA MT
contractile ring
NCD
FMA MTs

A

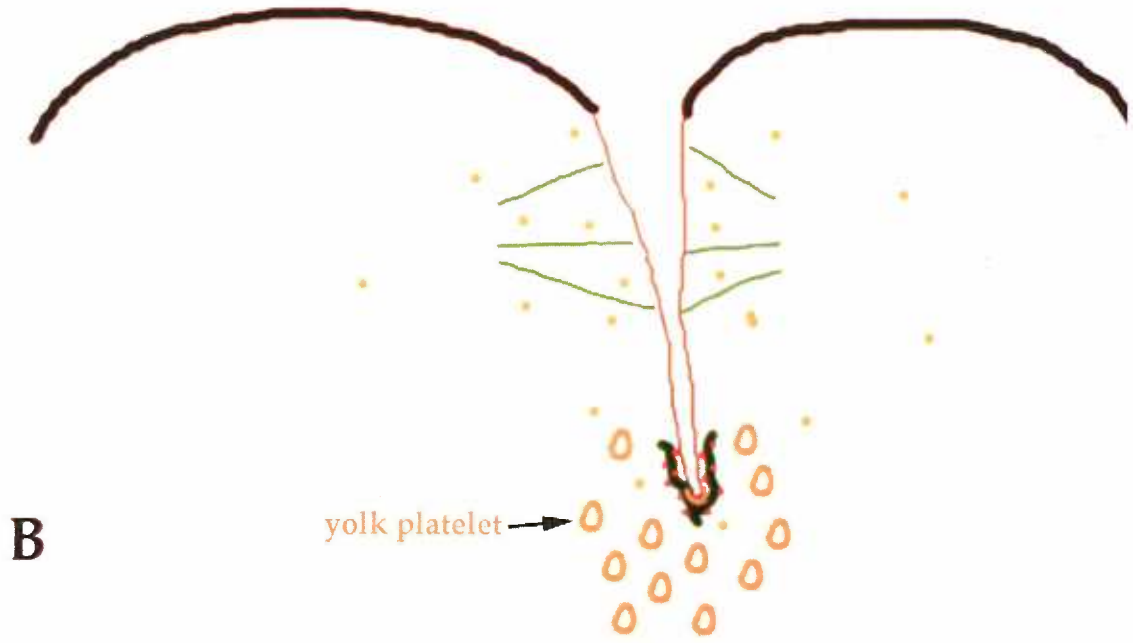
yolk platelet

B

Chapter 4

Ventral cell rearrangements contribute the anterior-posterior axis lengthening

between the neurula and tailbud stages in *Xenopus laevis*.

Abstract

Studies of morphogenesis in early *X. laevis* embryos have focused primarily on gastrulation and neurulation. Immediately following these stages is another period of intense morphogenetic activity, the neurula-to-tailbud transition. During this period the embryo is transformed from the spherical shape of early stages into the long, thin shape of the tailbud stages. While gastrulation and neurulation depend largely on active cell rearrangement and cell shape changes in dorsal tissues, we find that the neurula-to-tailbud transition depends in part on activities of ventral cells. Ventral explants of neurulae lengthen autonomously as much as the ventral sides of intact embryos, while dorsal explants lengthen less than the dorsal sides of intact embryos. Analyses of cell division, cell shapes, and of cell rearrangement by transplantation of labeled cells and by time lapse recordings in live intact embryos concur that cell rearrangements in ventral mesoderm and ectoderm contribute to the autonomous anterior-posterior axis lengthening of ventral explants between neurula and tailbud stages.

Introduction

Between the relatively calm periods of cleavage and larval growth, there is a period of intense global morphogenetic movements that consists of gastrulation (stages 10 to 12), neurulation (stages 12 to 16), and the neurula-to-tailbud transition (stages 16 to 27) (Nieuwkoop and Faber, 1994). Between neurula (stage 16) and tailbud stages (stage 27), a dramatic morphological transformation from spherical to linear body shape takes place -- *X. laevis* embryos more than double in length (Nieuwkoop and Faber, 1994). The physical mechanism of this event is unknown, but may involve cell division, as occurs during epiboly of superficial cells of the animal cap during blastula stages (Keller, 1978), cell shape change, as in bottle cell formation (Keller, 1981; Hardin and Keller, 1988), or cell rearrangement, both mediolateral and radial, as in gastrulation (Keller *et al.*, 1985a; Keller *et al.*, 1985b; Keller and Danilchik, 1988; Wilson and Keller, 1991; Keller and Shih, 1992; Keller *et al.*, 1992; Keller and Winklbauer, 1992).

Rearrangement of dorsal mesodermal cells during gastrulation nearly doubles the length of that tissue, and consequently, the dorsal side of the embryo (Keller *et al.*, 1985a; Keller *et al.*, 1985b; Keller and Danilchik, 1988; Wilson and Keller, 1991; Keller and Shih, 1992; Keller *et al.*, 1992; Keller and Winklbauer, 1992). Dorsal mesodermal cells first intercalate radially, thinning the mesodermal sheet along the dorso-ventral (D-V) axis while lengthening it in the anterior-posterior (A-P) dimension. Later, intercalation of dorsal mesodermal cells occurs in the mediolateral dimension, narrowing the mesodermal sheet along the left-right axis while continuing to lengthen it along the A-P axis (Wilson and Keller, 1991; Keller and Shih, 1992; Keller *et al.*, 1992; Shih and Keller, 1992).

Studies disrupting the notochord suggest that it is not required for A-P axis lengthening during neurula stages (Malacinski and Youn, 1981; Youn and Malacinski, 1981). Wilson *et al.* (1989) followed up those observations using notochordless dorsal explants and found that segmentation and rotation of somites was capable of lengthening the A-P axis of dorsal pieces by 45% during and after neurulation (stages 12.5 to 21). Therefore, somite rotation can account fully for the degree of lengthening observed during the stages studied.

An even more dramatic A-P lengthening occurs after neurulation, when the embryo transforms from the spherical shape of the embryo into the elongate shape of the tadpole. At these later stages, somites are still undergoing segmentation and rotation, but this is insufficient to account for the doubling in length of the embryo. Thus it seems likely that other tissues in the embryo contribute to A-P axis extension. Here we show that ventral explants double in length autonomously and that mediolateral intercalation of ventral mesodermal cells is the most likely mechanism for the lengthening observed in ventral explants during the neurula-to-tailbud transition.

Results

Ventral explants lengthen autonomously between neurula and tailbud stages.

The starting and stopping points of our experiments were carefully chosen to exclude the influences of neurulation and tailbud extension. In intact embryos the A-P axis does not lengthen significantly until stage 20; however, stage 16 was chosen as the time of separation of dorsal and ventral explants because it is an easily identifiable stage that occurs at a convenient time relative to both fertilization and the stopping point of the experiments. Stage 27 was chosen as the stopping point because this stage marks the transition between A-P lengthening and tailbud extension. The tailbud is a dorsally located region that undergoes dramatic morphogenetic activities between stages 24 and 35 (Gont *et al.*, 1993; Tucker and Slack, 1995). Although a small amount of tailbud growth occurs before stage 27, it contributes little to the lengthening of the A-P axis, and is included only in dorsal measurements (Figure 4.1 E, E'), therefore any lengthening of ventral explants is due solely to activities of ventral cells.

Intact embryos served as controls for length measurements of dorsal and ventral explants. Measurements were made from video images taken at the time of separation of experimental embryos into dorsal and ventral pieces (Figure 4.1). The ventral sides of intact embryos were measured on a video monitor by tracing the distance just posterior of the most anterior neural fold to the blastopore along the ventral surface (Figure 4.1 E, E'). Likewise, dorsal sides of intact embryos were measured from just posterior of the most anterior neural fold to the blastopore, but along the dorsal surface (Figure 4.1 E, E'). Ventral and dorsal explants were measured in the same manner as

controls, but after dissection (Figure 4.1 C, C′, D, D′). Measurements were made at stages 16 and 27 for each embryo and explant from multiple batches of embryos. Explants that curled were measured along the external contour as were uncurled explants and embryos (Figure 4.1 C′, D′).

Ventral explants lengthened as much as the ventral sides of intact embryos (Figure 4.2 B and B′ *vs.* C and C′, and Figure 4.3), suggesting that considerable autonomous morphogenetic activity resides in ventral tissue after neurulation. Dorsal explants, on the other hand, elongated less than the dorsal sides of intact controls (Figure 4.2 A and A′ *vs.* C and C′, and Figure 4.3). The lengthening observed in dorsal explants is consistent with the amount of lengthening somite rotation is reported to cause at slightly earlier stages (Wilson *et al.*, 1989). The inability of dorsal tissue to lengthen normally *in vitro* at these late stages is consistent with the findings of Tucker and Slack (1995) regarding tailbud explants which also lengthened less than tailbuds of intact embryos. Separation of only the anterior or posterior region also prevented normal dorsal lengthening without altering ventral lengthening (not shown). Sensitivity of the dorsal side to wounding confounds experiments relating to autonomous lengthening of this side. The ability of ventral explants to lengthen autonomously is unexpected, considering the relative morphogenetic inactivity of ventral cells during gastrulation and neurulation. The following experiments test the role of morphogenetic mechanisms that can cause this tissue lengthening.

Analysis of cell division rates indicates that cell proliferation cannot account for the observed A-P lengthening.

If cell proliferation were a major contributor to axial lengthening, one

would expect most cell cleavage planes to be approximately perpendicular to the A-P axis, and therefore, the mitotic spindle axis of dividing cells would be roughly parallel to the lengthening body axis. To test the importance of cell division in A-P axis lengthening, embryos of stages 21 through 24 were fixed in Dent's with 5 μg/mL propidium iodide, optically sectioned on the confocal microscope and counts of mitotic figures as well as total nuclei were made. Only cells in metaphase, anaphase, or telophase were counted as mitotic, so that spindle orientation could also be scored. Division rates in anterior, middle and tailbud regions were determined for both ectodermal and mesodermal cells of the ventral side. The regions surveyed were of constant volumes, 211 μm long by 317 μm wide, by 20 μm deep. In embryos of each stage, the anterior region extended posteriorly from the cement gland, the middle region was centered on the mid-point of the A-P axis, and the posterior region extended anteriorly from the anus (Figure 4.4 A).

The overall percentage of dividing cells of both cell types in all three regions of all four stages was 0.82%. Additionally, only 0.36% of ectodermal or mesodermal cells in any region had their spindle axes parallel to the A-P axis. When cell division rates were broken down by region, germ layer, and spindle orientation, rates were still below 1%, except for posterior mesodermal cells dividing with the cleavage plane perpendicular to the A-P axis, which reached 2.5% (Figure 4.4 B). Since this analysis relies on numbers of cells dividing at the time of fixation, the total numbers of cells in the surveyed regions were compared among stages. Compared by region and germ layer, these data hint at a slight increase in cell number with age, but differences are within one standard deviation (Figure 4.4 C). Given the low number of dividing cells observed in fixed embryos (Figure 4.4 B) and the lack

of increase in actual cell number in regions with similar position and identical dimensions (Figure 4.4 C), we conclude that cell division makes, at most, a minor contribution to the lengthening of the A-P axis.

Mesodermal cell shapes suggest cell rearrangements are involved in A-P axis extension.

Cell shapes can be diagnostic of morphogenetic events; for example, bottle cells shorten a cell sheet by constricting their apices. If cell shape change drives A-P lengthening, then cells would have to align their long axes parallel to the A-P axis. If, however, cell rearrangement drives A-P lengthening, then cells would align their long axes perpendicular to the A-P axis, as occurs in dorsal mesoderm during gastrulation (Keller, 1980). Figure 4.5 A diagrams the effects of cell shape changes and mediolateral cell rearrangements on tissue dimensions. Scanning electron microscopy was used to study the shapes of the ventro-lateral mesoderm cells of mid- to late neurulae (stages 22 through 24). Length and width measurements of ventral mesodermal cells were made on neurulae stripped of ectoderm after fixation. Embryos were viewed at low magnification and low voltage to reduce charging of specimens by the electron beam. Analysis of embryos at stages 22 through 24 revealed that the long axis of most ventral mesodermal cells was perpendicular to the A-P axis (Figure 4.5 B). Outlines of the cells in Figure 4.5 B are presented in Figure 4.5 B′ to illustrate cell shapes.

Length-width ratios for ventral mesoderm cells were determined by measuring for each cell in the field of view long and short axes that were perpendicular to each other and were approximately aligned with the A-P axis of the embryo. Anterior and posterior regions were examined and fell within the regions analyzed above for cell division, but were smaller in area (137 by

176 μm). Length-width ratios of ventral mesoderm cells were higher in anterior than posterior regions and in older embryos, *i.e.* stage 24 *vs.* stage 22 (Figure 4.6). No difference in length-width ratio was found between cells at the ventral midline and more lateral cells from embryos of the same stage and similar A-P position (not shown). Dividing cells were not evident in the embryos examined. Some rosette arrangements of cells, which might be related to radial intercalation, were found equally distributed along the A-P and left-right axes (Figure 4.5 B, arrow).

The importance of radial intercalation of cells in epiboly of the animal cap during blastula stages and early in gastrulation led us to look for evidence of radial intercalation in the form of wedge shaped cells in bisected embryos (Keller, 1980). In embryos of each stage (22 through 24) the ventro-lateral mesoderm was bilayered with the outer layer consisting of a thin layer of single cells of a squamous nature. The inner layer was approximately twice as thick, but still most commonly composed of one cell layer. In places, however, the inner layer was composed of two cell layers, and some cells were wedge shaped (Figure 4.5 C, arrowhead). A rosette is also visible in the surface just where the wedge-shaped cells are exposed (Figure 4.5 C, arrow) suggesting a correlation between the rosette arrangement and radial intercalation. Wedge-shaped cells from Figure 4.5 C are outlined in Figure 4.5 C′ with the markers in the same positions.

Because ventral mesoderm cells were found to have their long axes perpendicular to the A-P axis, it is unlikely that cell shape change drives A-P axis extension between neurula and tailbud stages. The observed cell orientations and length-width ratios do, however, support a role for cell rearrangements, primarily mediolateral intercalation, with some radial

intercalation likely taking place.

Transplants of labeled tissues reveal cell rearrangements in the mediolateral dimension.

To demonstrate cell rearrangement in ventral mesoderm, labeled mesoderm and ectoderm cells from the ventro-lateral region of neurulae were transplanted into the same region of unlabeled embryos and the positions of the cells determined at the tailbud stage (Figure 4.7 A). Transplants were strips of meso-ectoderm that were longer in the A-P than the D-V dimension to aid visualization of cell rearrangement. The site of transplantation was lateral to the ventral midline and was a region found by SEM to contain many cells that had a shape suggestive of actively rearranging cells (*i.e.* length-width ratio about 2). Labeled mesodermal cells were found closer to the ventral midline than their original position, indicative of ventrad migration (compare Figure 4.7 C and F). The bulk of the grafts stayed intact, but numerous cells became separated along the A-P axis as expected if interdigitation of host and donor cells occurs (Figure 4.7 G, arrows). Some labeled cells were separated along the D-V axis from the main mass of transplanted cells, and may have stayed at the original graft site as the bulk of the graft moved toward the ventral midline (Figure 4.7 G, arrowhead). The intermixing of labeled and unlabeled cells is suggestive of cell rearrangement, and particularly of mediolateral intercalation as has been shown in dorsal mesoderm of gastrula stages (Keller and Tibbetts, 1989).

Time-lapse recordings of vitally stained mesodermal cells demonstrate mediolateral intercalation.

In addition to the static evidence for intercalation presented above, cell rearrangements within the ventral mesoderm were viewed in live embryos stripped of ectoderm. Ectoderm was removed from mid-neurulae (stage 24) with forceps and eyelash knives in 1 X MMR. The mesoderm was then stained by adding 1% Nile blue to the medium, rinsing in fresh medium, then recording time-series on the confocal microscope. Alternatively, embryos labeled with TRITC-dex at the 4-cell stage were stripped of ectoderm and time series were recorded. Time-lapse recordings using either labeling method revealed mediolateral cell rearrangements within the ventral mesoderm. A series of frames from one of nine time-lapse recordings illustrates the intercalation behavior of ventral mesodermal cells (Figure 4.8).

Discussion

The morphogenetic events preceding and following the neurula-to-tailbud transition have been characterized in great detail in *X. laevis*. After cleavage stages, epiboly occurs in the animal region (Keller, 1978), later bottle cells form at the onset of gastrulation (Keller, 1981; Hardin and Keller, 1988), following which mediolateral intercalation of dorsal mesoderm cells drives the lengthening of the A-P axis of the dorsal side of the gastrula (Keller *et al.*, 1985a; Keller *et al.*, 1985b; Keller and Danilchik, 1988; Wilson and Keller, 1991; Keller and Shih, 1992; Keller *et al.*, 1992; Keller and Winklbauer, 1992). During neurulation, changes in cell shapes and sizes account for the bulk of neural tube formation, somite rotation (Youn and Malacinski, 1981; Wilson *et al.*, 1989), and notochordal stiffening (Mookerjee *et al.*, 1953; Youn *et al.*, 1980; Adams *et al.*, 1990; Weliky *et al.*, 1991). After the neurula-to-tailbud transition, the tailbud extends (Gont *et al.*, 1993; Tucker and Slack, 1995). There are three cellular mechanisms, contributing to various degrees, that function during these morphogenetic periods: cell division, cell shape change, and cell rearrangement.

To study the dramatic morphological change that takes place in *X. laevis* embryos following neurulation, neurulae were dissected into dorsal and ventral explants. The ventral explants were found to lengthen autonomously to a similar degree as the ventral sides of intact embryos, whereas dorsal pieces lengthened an amount similar to that found for the dorsal side at earlier stages, but less than the dorsal sides of intact embryos at these later stages. Although there appeared to be slight differences in length of ventral and dorsal sides of intact embryos and ventral and dorsal explants at stage 16, these differences were within one standard deviation. At stage 27, the

ventral side of intact embryos and ventral and dorsal explants were the same length while the dorsal side of intact embryos was much longer, *i.e.* ventral explants lengthen a normal amount autonomously while dorsal explants do not. The observed autonomous lengthening of dorsal explants can be accounted for by somite rotation but the autonomous lengthening of ventral explants is a novel finding. Therefore, we then investigated the roles of cell division, cell shape change, and cell rearrangement in ventral tissues that might account for the observed autonomous lengthening.

Very low rates of cell division (0 to 2.5%) were observed in ectoderm and mesoderm of the ventral side, and could not account for doubling the A-P axis length of ventral sides. In addition, total numbers of cells in the same-sized areas of embryos did not change significantly with age, confirming the observed division rate. The low cell division rates are not especially surprising, as after the initial burst of cleavages, the embryo begins dividing asynchronously at stage 7 and settles into a low basal rate of asynchronous division around the time of gastrulation.

Cells observed by SEM, as well as those seen in less detail with light microscopy, were oriented with the long axis perpendicular to the lengthening A-P axis. This orientation is contrary to what one would expect if shape change was driving A-P axis elongation, and is consistent with a mediolateral cell intercalation mechanism of axial lengthening. Some wedge-shaped cells were found in cross-section suggesting that radial intercalation may also contribute to lengthening, although to a minor degree.

The possibility of cell rearrangement was tested by transplanting labeled ventral mesoderm into unlabeled hosts and by time-lapse microscopy of mesodermal cells during axial extension. Transplanted labeled ventral

mesoderm cells mixed with unlabeled host cells during A-P axis lengthening, as observed in mediolateral intercalation of dorsal mesoderm cells during gastrulation (Keller and Tibbetts, 1989). Time-lapse recordings of ventral mesoderm cells shows cells squeezing between each other along the mediolateral axis like that demonstrated in dorsal mesoderm during gastrulation (Keller, 1978). These findings indicate that active medio-lateral intercalation of ventral cells takes place during the period when the A-P axis doubles in length.

Morphogenetic events prior to the neurula-to-tailbud transition have been shown to involve primarily dorsal cell rearrangements with little activity in the ventral cells. However, we find that following neurulation, ventral sides lengthen autonomously and that this lengthening is largely the result of medio-lateral cell intercalation in ventral mesoderm. These seemingly disparate observations are compatible if one considers that morphogenetic activities might alternate with organogenic activities. In this model, dorsal A-P axis extension begins dorsally during gastrulation. Then when dorsal tissues are engaged with notochord vacuolization and somite formation and rotation they contribute less to A-P extension and the ventral side lengthens its A-P axis. Later still, lengthening activity reinvigorates in the dorsal side in the form of tailbud extension as the ventral organs form.

Figures

Figure 4.1. Dissections were made through the body wall of stage 16 embryos leaving dorsal and ventral explants lined on both surfaces with an epithelial layer. Confocal cross (A) and sagittal sections (B) of stage 16 embryos with arrows indicating where cuts were made to separate embryos into dorsal and ventral explants. Video micrographs of a dorsal explant (C), a ventral explant, with the archenteron floor visible as the lightly pigmented upper surface (D), and stage 16 embryo (E). Video micrographs of the same dorsal explant (C′), ventral explant (D′), and embryo (E′) at stage 27. Arrowed, superimposed lines indicate where measurements were made. In B-E anterior is to the left and dorsal is up. Scale bar is 500 μm.

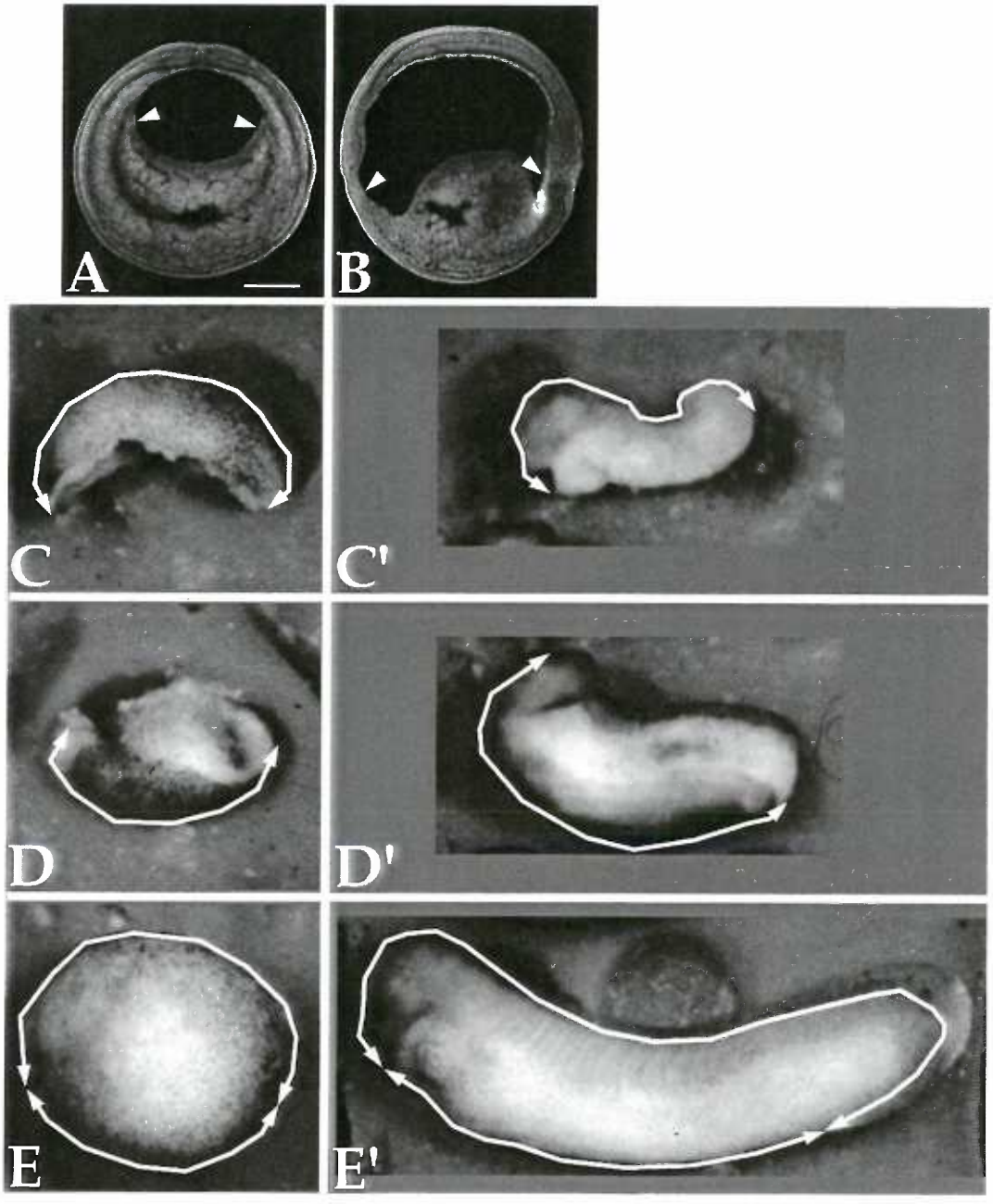
A
B
C
C'
D
D'
E
E'

Figure 4.2. Ventral explants lengthen autonomously.

Photomicrographs of the same dorsal explants (A and A′), ventral explants (B and B′), and intact embryos (C and C′) at stages 16 (A, B, and C) and 27 (A′, B′, and C′). Anterior is to the left and dorsal is up. Scale bar is 500 μm.

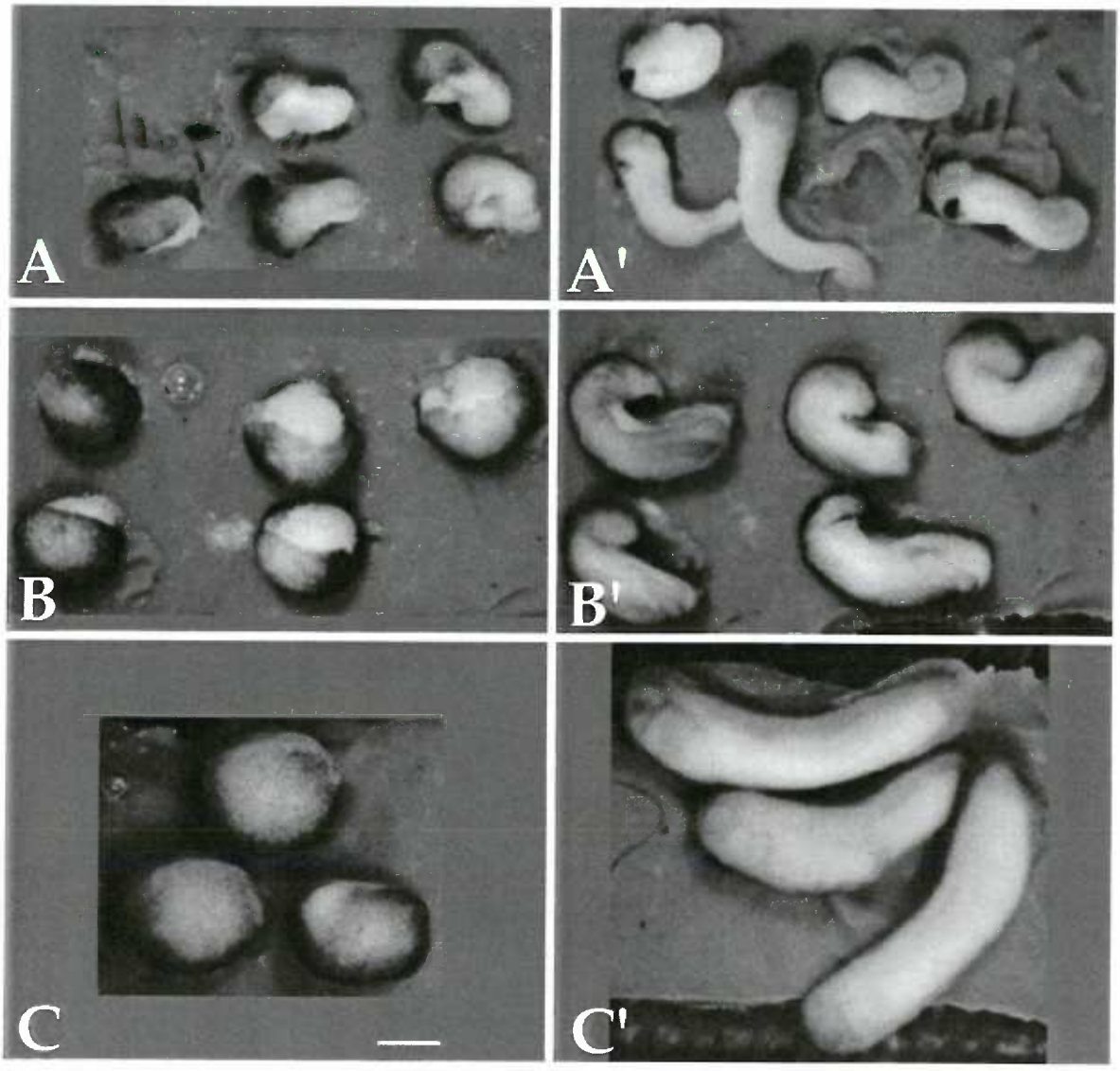
A
A'
B
B'
C
C'

Figure 4.3. Ventral explants lengthen as much as the ventral sides of intact embryos, while dorsal explants lengthen less than dorsal sides of intact embryos. Dorsal and ventral sides of 28 intact embryos, 78 ventral explants, and 77 dorsal explants were measured at stages 16 and 27. Bars represent one standard deviation.

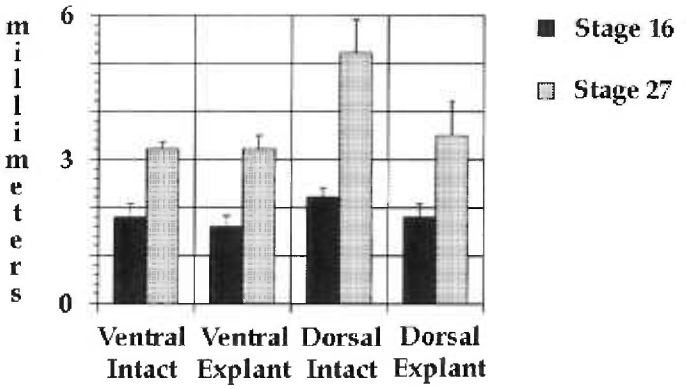
millimeters
6
3
0
Ventral Intact
Ventral Explant
Dorsal Intact
Dorsal Explant
Stage 16
Stage 27

Figure 4.4. Few mitotic cells were found at any stage and in any region, and total cell numbers did not increase significantly with age. Regions of ventral ectoderm and mesoderm of identical dimensions and locations were surveyed for mitotic figures at stages 21 through 24 (A). Each row of data refers to the embryonic stage indicated in the diagrams at left. Low percentages of division were observed in any region at any stage, many regions had no dividing cells. The labels "parallel" and "perpendicular" refer to the orientation of the division plane relative to the A-P axis (B). Cell counts averaged for six or seven embryos per stage indicate no significant change in number with age (C). A total of 31, 506 cells were scored, with 7,076, 7,400, 9,260, and 7,770 cells at stages 21 through 24, respectively.

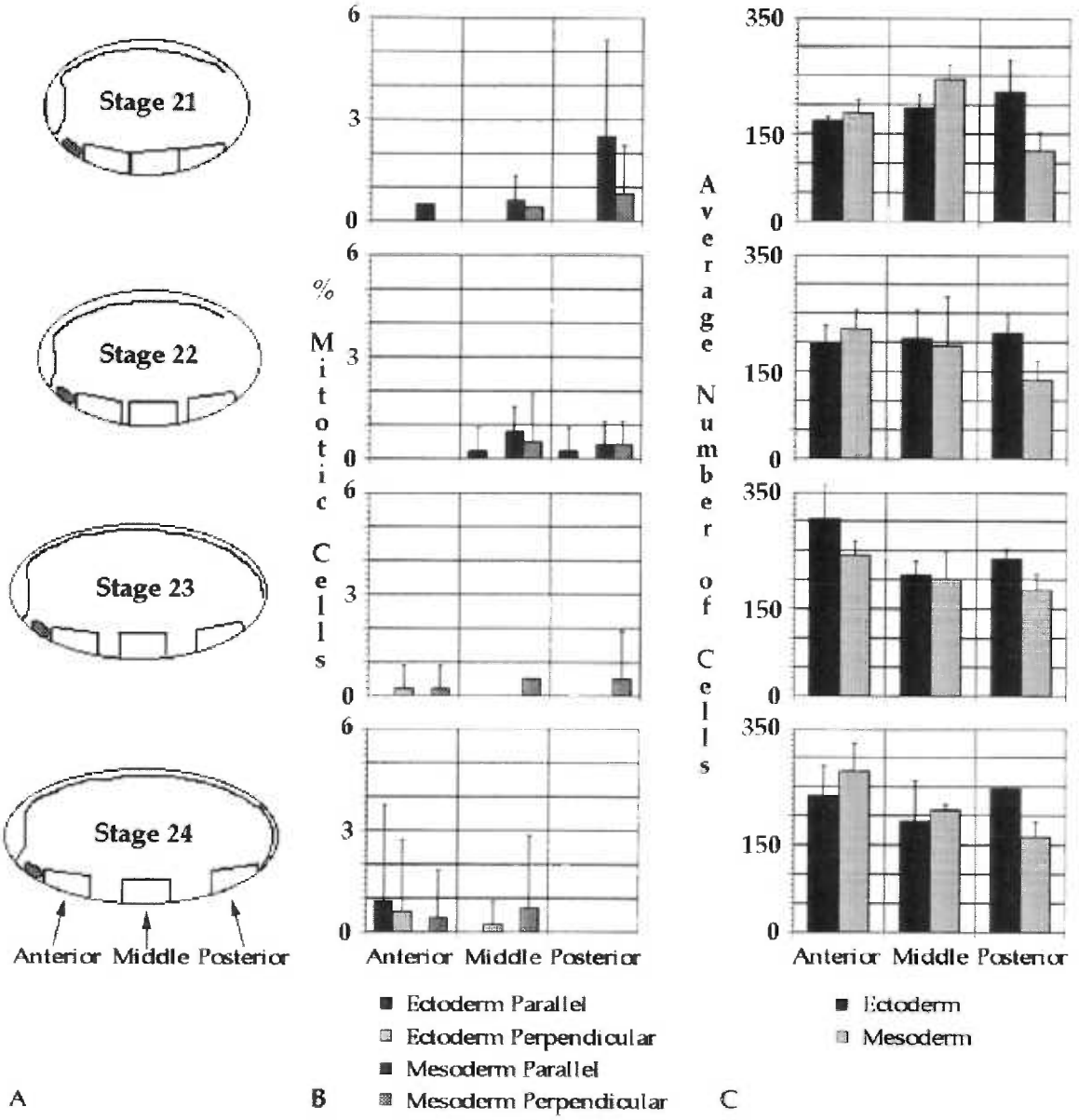
Stage 21
Stage 22
Stage 23
Stage 24
Anterior Middle Posterior
% Mitotic Cells
Average Number of Cells
6
3
0
350
150
0
Anterior Middle Posterior
Ectoderm Parallel
Ectoderm Perpendicular
Mesoderm Parallel
Mesoderm Perpendicular
Ectoderm
Mesoderm
A
B
C

Figure 4.5. Cell shapes can be indicative of morphogenetic mechanisms. If a cell sheet lengthens by cell shape change, then the cells must get longer in the dimension of sheet lengthening, whereas if lengthening occurs by cell rearrangement, intercalating cells become longer perpendicular to the direction of sheet lengthening (A). SEM of ventral mesoderm of stage 24 embryo reveals that cells have the long axis perpendicular to the A-P axis. Note the rosette arrangement at the upper right (B, arrow). Traced cell outlines of cells in B to illustrate length:width characteristics (B′) Bisected embryo with the mesodermal sheet extending beyond the ectoderm due to the fracture. Wedge-shaped cells (arrowhead) underlying a rosette (arrow) in the ventral mesoderm of a stage 24 embryo (C). Traced outlines of wedge-shaped cells and tissue layers from C (C′). Rosettes appear to be correlated with wedge-shaped cells undergoing radial intercalation. In B and B′, anterior is to the left and dorsal is up. In C and C′, dorsal is up. Scale bar is 10 μm.

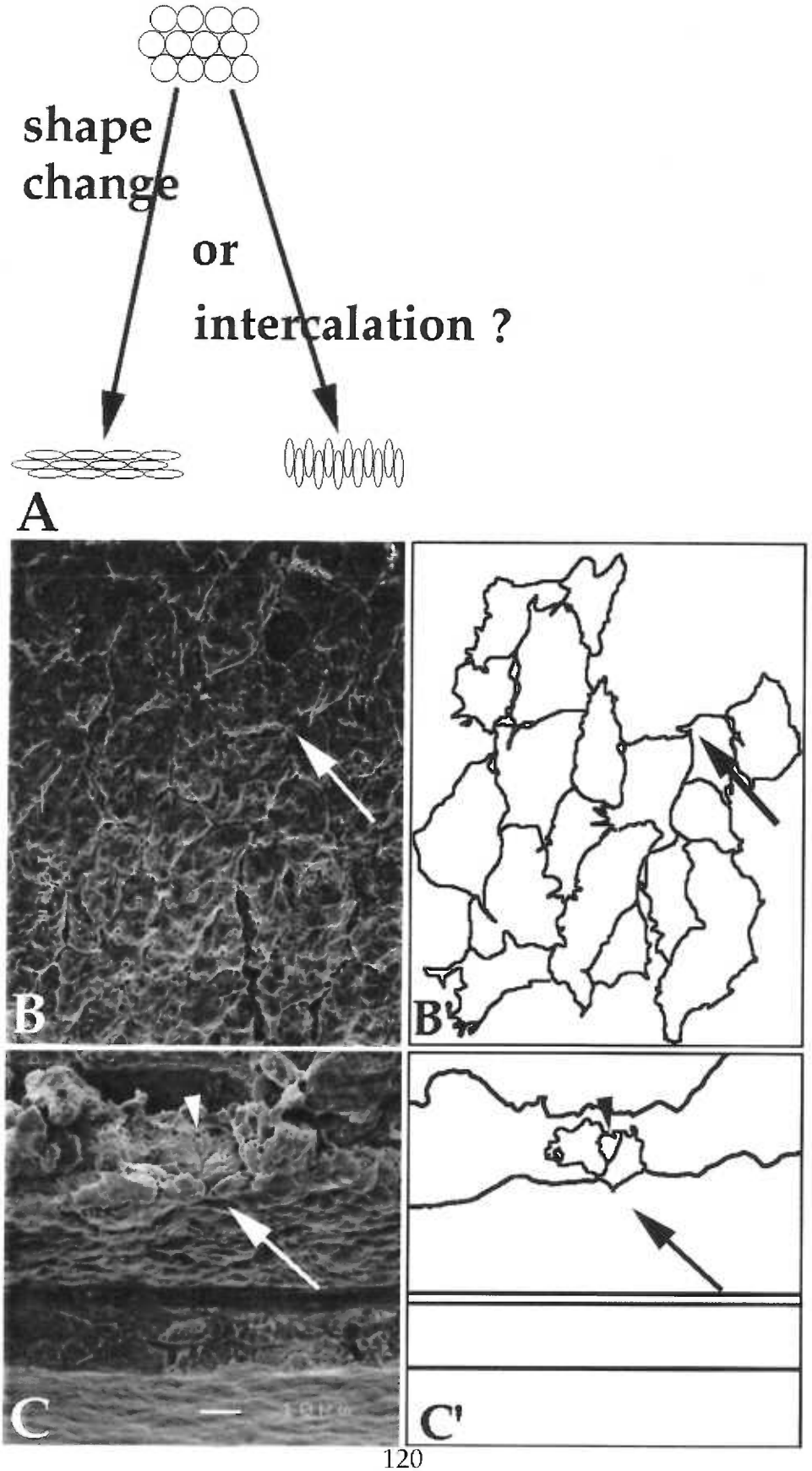
shape
change
or
intercalation ?
A
B
B'
C
C'

Figure 4.6. Length-width ratios indicate that ventral mesoderm cells are longer mediolaterally than anterioposteriorly. Length-width ratios increase posterior to anterior and in both regions with increasing age. Anterior and posterior regions at each stage are from the same embryo, numbers of cells per region ranged between 8 and 13. Error bars indicate one standard deviation. The anterior-posterior difference is likely due to the delay in development seen between those regions, similar to that seen dorsally during somite formation.

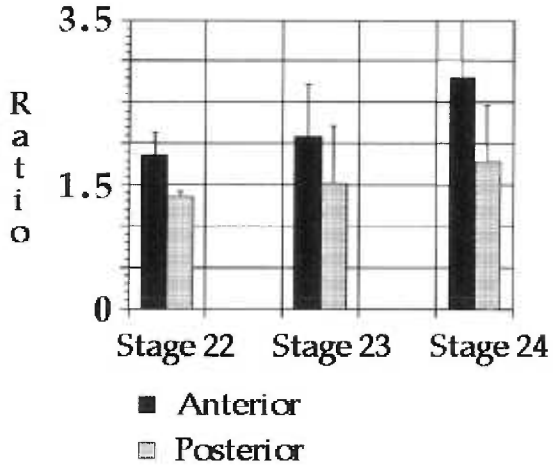
3.5
1.5
0
Ratio
Stage 22
Stage 23
Stage 24
Anterior
Posterior

Figure 4.7. Transplanted,TRITC-dex-labeled, ventral meso-ectoderm was transplanted into unlabeled hosts reveals cell mixing indicative of mediolateral intercalation. Donor embryos were injected with TRITC-dex in all cells of the 4-cell stage, at stage 16 strips of ventral meso-ectoderm were transplanted from donors to hosts, and at stage 27 hosts were fixed and labeled cells examined on a confocal microscope (A). Parasagittal (B) and cross section (C) of a neurula fixed shortly after transplantation to show the size, shape, and position of the labeled cells. Higher magnification view of the embryo in B and C to show the rectangular shape and coherence of the initial graft and position along the D-V axis (D). Confocal images of parasagittal (E) and cross section (F) of a tailbud embryo showing the more ventral location of the labeled mesodermal cells. Higher magnification view of the tailbud embryo in E and F showing labeled mesodermal cells separated from the bulk of the transplant in the A-P dimension (G, arrows) and some ectoderm cells separated from the bulk of the transplant in the D-V dimension (G, arrowhead). Host tissues are visible due to the weak autofluorescence of yolk.. Anterior is to the left and dorsal is up in B, D, E, and G. Dorsal is up in C and F. Scale bar in B applies to B, C, E, and F and is 500 μm. Scale bar in D applies to D and G and is 150 μm.

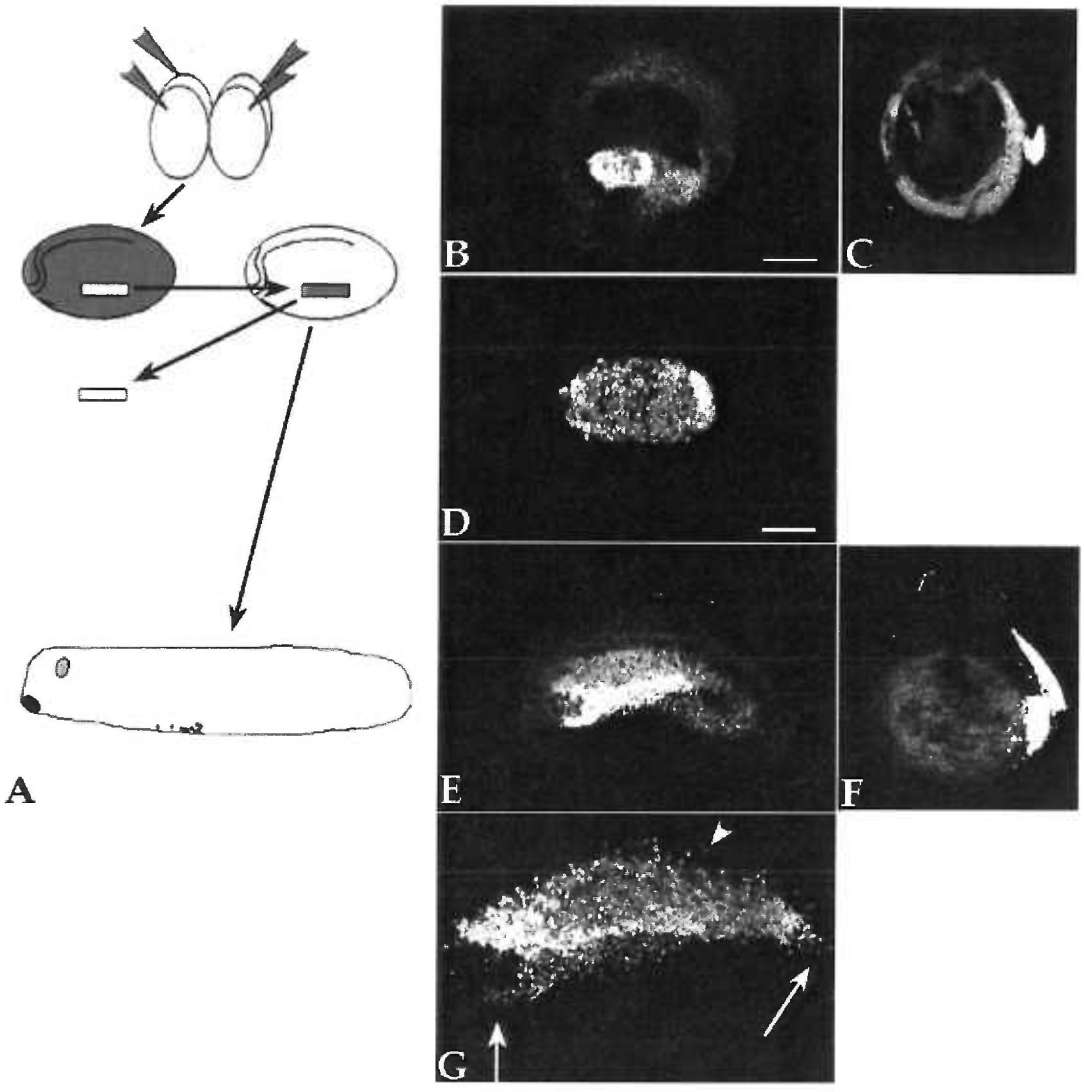
A
B
C
D
E
F
G

Figure 4.8. Active mediolateral cell intercalation of Nile blue-stained ventral mesoderm cells was recorded in time-lapse on a confocal microscope. Cells moving into alignment along the A-P axis are indicated with an * and a +. Note that the cells are longer in the mediolateral dimension. Anterior is to the lower left and dorsal is towards the top. The numbers indicate minutes elapsed after the recording began. The outlines of the marked cells were traced and placed to the side of the confocal images to illustrate cell shapes and positions. Scale bar is 10 μm.

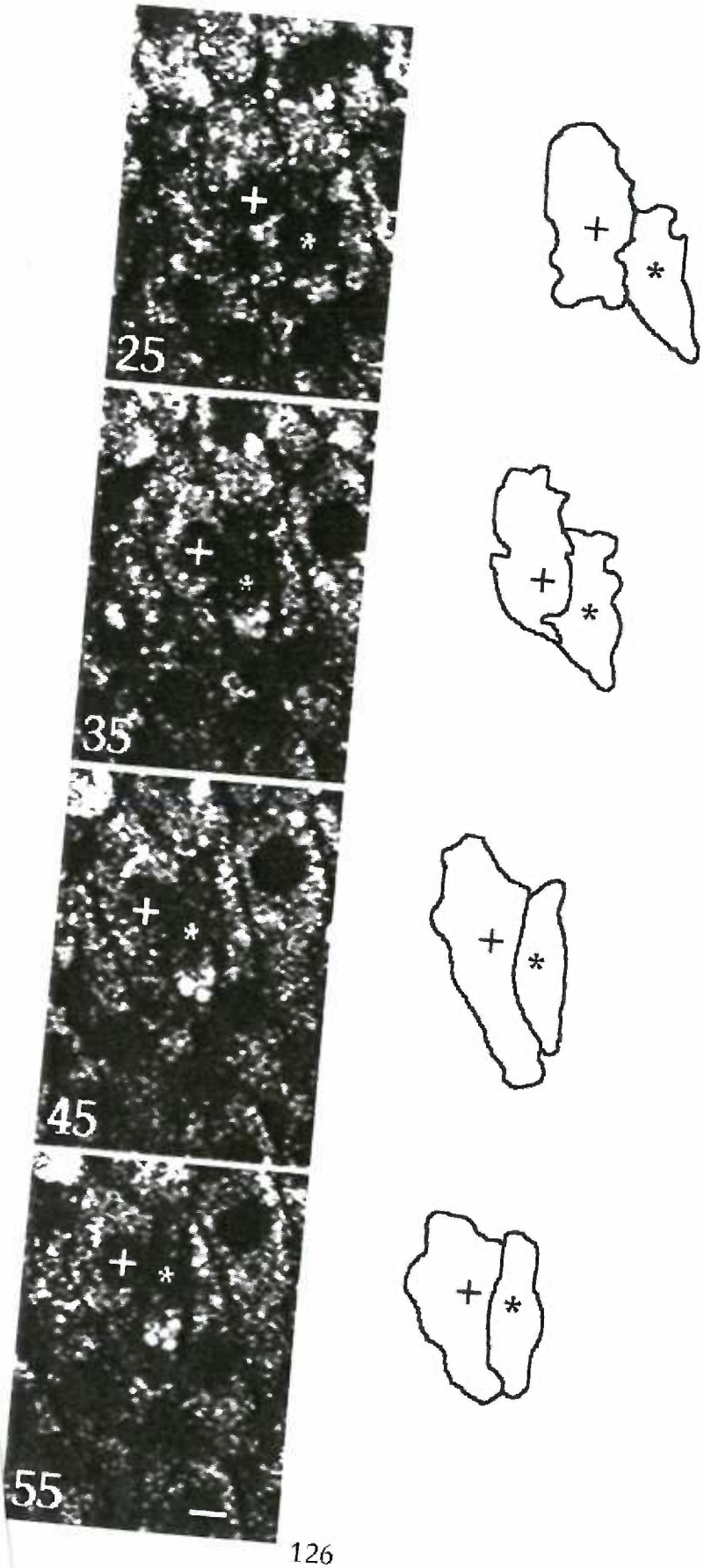
25
35
45
55

In cleavage stage frog embryos, we have shown that the FMA is necessary for furrow deepening (Chapter 3 of this thesis). This separation of the FMA from other MT structures in the dividing embryos links FMA organization to furrow deepening and disproves our earlier speculation that the FMA might be involved in membrane addition (Danilchik *et al.*, 1998). The requirement of MTs for CR function is unprecedented and opens an avenue for further research on the narrowing, or maturation, of the CR which may occur so rapidly in smaller cells as to be undetected.

The MTs required for membrane addition in frog embryos are not FMA MTs, as their disruption did not inhibit membrane addition, but their identity remains a question (Chapter 3 of this thesis). The spatially and temporally restricted addition of membrane in frog embryos may depend upon a specialization of astral MTs as these make up the majority of the non-FMA MTs in the animal hemisphere. MTs in the midzone that resemble midbody MTs could also be involved in membrane addition. It is unclear at present if membrane is added in the vegetal furrow, but if so, then involvement of astral MTs, rather than midzone MTs, is likely since the astral MTs are the most abundant MTs in the vegetal hemisphere aside from the FMA and midzone MTs are strictly in the animal hemisphere. The addition of membrane in spots associated with monastral MTs in D_2O-treated embryos supports the idea that astral MTs may be involved in normal membrane deposition in cleavage furrows (Danilchik *et al.*, 1998; Chapter 3 of this thesis).

Although cell division is the main morphological activity taking place during early stages, it plays less of a role in morphogenesis at later stages. The behaviors of dorsal cells following cleavage stages, during gastrulation and

neurulation have been well documented. The studies primarily from the Keller lab provided an excellent basis for the studies described here of the subsequent morphological event, the neurula-to-tailbud transition (Keller *et al.*, 1985a; Keller *et al.*, 1985b; Keller and Danilchik, 1988; Wilson and Keller, 1991; Keller and Shih, 1992; Keller *et al.*, 1992; Keller and Winklbauer, 1992).

Chapter three of this thesis shows that much like gastrulation, the neurula-to-tailbud transition depends little on cell division and involves primarily medio-lateral cell intercalation with some radial intercalation also contributing but unlike gastrulation, ventral cells participate in the morphogenetic movements. SEM shows protrusions on the medio-lateral tips of ventral mesodermal cells which are indicative of active intercalation and similar to those found by Keller *et al.* (1980; 1985b) on intercalating dorsal cells during gastrulation. Transplants of labeled ventral mesodermal cells into unlabeled hosts reveals cell mixing, and timelapse recordings show active medio-lateral rearrangement of ventral mesodermal cells also similar to that seen by Keller and Tibbetts (1989) in intercalating dorsal cells during gastrulation. These findings allow us to synthesize the following model of morphogenetic activity in *X. laevis* development.

After a period of rapid cell cleavages, dorsal mesodermal cells intercalate radially then medio-laterally, extending the dorsal side, although the overall size of the embryo remains unchanged. Following gastrulation, dorsal mesoderm segments into somites and notochord, while dorsal ectoderm folds creating the neural tube. During and after neurulation, ventral mesoderm cells intercalate radially and medio-laterally, helping to extend the body axis, now made rigid by the notochord, into the long, narrow shape of the tailbud stage embryo. The subsequent events involve tailbud

extension, organogenesis, and metamorphosis. Therefore, there is a transfer of morphogenetic activity from dorsal cells to ventral cells and back again. This brings us to the end of this analysis of cellular mechanisms of morphogenesis.

References

Adachi, H., Takahashi, Y., Hasebe, T., Shirouzu, M., Yokoyama, S., and Sutoh, K. (1997). *Dictyostelium* IQGAP-related protein specifically involved in the completion of cytokinesis. *Journal of Cell Biology* **137,** 891-8.

Adams, D. S., Keller, R., and Koehl, M. A. (1990). The mechanics of notochord elongation, straightening and stiffening in the embryo of *Xenopus laevis*. *Development* **110,** 115-30.

Akashi, T., Yoon, Y., and Oakley, B. R. (1997). Characterization of gamma-tubulin complexes in *Aspergillus nidulans* and detection of putative gamma-tubulin interacting proteins. *Cell Motility and the Cytoskeleton* **37,** 149-58.

Alberts, B., Bray, D., Lewis, J., Raff, M., Roberts, K., and Watson, J. (1994). "Molecular Biology of the Cell", third edition, Garland Publishing, New York.

Allan, V. (1995). Protein phosphatase 1 regulates the cytoplasmic dynein-driven formation of endoplasmic reticulum networks *in vitro*. *Journal of Cell Biology* **128,** 879-91.

Allan, V. J., and Vale, R. D. (1991). Cell cycle control of microtubule-based membrane transport and tubule formation *in vitro*. *Journal of Cell Biology* **113,** 347-59.

Aronson, J., and Inoué, S. (1970). Reversal by light of the action of n-methyl n-desacetyl colcine on mitosis. *Journal of Cell Biology* **45,** 470-7.

Ashman, R. F., Kanno, Y., and Loewenstein, W. R. (1964). Intercellular electrical coupling at a forming membrane junction in a dividing cell. *Science* **145,** 604-6.

Asnes, C. F. and Schroeder, T. E. (1979). Cell cleavage. Ultrastructural evidence against equatorial stimulation by aster microtubules. *Experimental Cell Research* **122,** 327-338.

Beams, H. W., and Evans, T. C. (1940). Some effects of colchicine upon the first cleavage in *Arbacia punctulata. Biological Bulletin* **79,** 188-198.

Bestor, T. H., and Schatten, G. (1981). Anti-tubulin immunofluorescence microscopy of microtubules present during the pronuclear movement of sea urchin fertilization. *Developmental Biology* **88,** 80-91.

Bluemink, J. G., and de Laat, S. W. (1973). New membrane formation during cytokinesis in normal and cytochalasin B-treated eggs of *Xenopus laevis*. I. Electron microscope observations. *Journal of Cell Biology* **59,** 89-108.

Bluemink, J. G., Tertoolen, L. G., Ververgaert, P. H., and Verkleij, A. J. (1976). Freeze-fracture electron microscopy of preexisting and nascent cell membrane in cleaving eggs of *Xenopus laevis. Biochimica et Biophysica Acta* **443,** 143-55.

Brady, S. (1985). A novel brain ATPase with properties expected for the fast axonal transport motor. *Nature* **317,** 73-75.

Burgess, D. R., and Schroeder, T. E. (1977). Polarized bundles of actin filaments within microvilli of fertilized sea urchin eggs. *Journal of Cell Biology* **74,** 1032-7.

Byers, T. J., and Armstrong, P. B. (1986). Membrane protein redistribution during *Xenopus* first cleavage. *Journal of Cell Biology* **102,** 2176-84.

Cameron, R. A., Fraser, S. E., Britten, R. J., and Davidson, E. H. (1989). The oral-aboral axis of a sea urchin embryo is specified by first cleavage. *Development* **106,** 641-7.

Chandra, R., Endow, S. A., and Salmon, E. D. (1993). An N-terminal truncation of the ncd motor protein supports diffusional movement of microtubules in motility assays. *Journal of Cell Science* **104,** 899-906.

Cohn, S. A., Ingold, A. L., and Scholey, J. M. (1987). Correlation between the ATPase and microtubule translocating activities of sea urchin egg kinesin. *Nature* **328,** 160-3.

Conrad, A. H., Paulsen, A. Q., and Conrad, G. W. (1992). The role of microtubules in contractile ring function. *Journal of Experimental Zoology* **262,** 154-65.

Conrad, A. H., Stephens, A. P., Paulsen, A. Q., Schwarting, S. S., and Conrad, G. W. (1994). Effects of silver ions (Ag^+) on contractile ring function and microtubule dynamics during first cleavage in *Ilyanassa obsoleta*. *Cell Motility & the Cytoskeleton* **27,** 117-32.

Dale, B., deSantis, A., Ortolani, G., Rasotto, M., and Santella, L. (1982). Electrical coupling of blastomeres in early embryos of ascidians and sea urchins. *Experimental Cell Research* **140,** 457-61.

Dan, K. (1960). Cytoembryology of echinoderms and amphibia. *International Review of Cytology* **9,** 321-67.

Danilchik, M. V., Funk, W. C., Brown, E. E., and Larkin, K. (1998). Requirement for microtubules in new membrane formation during cytokinesis of *Xenopus* embryos. *Developmental Biology* **194,** 47-60.

Drechsel, D. N., Hyman, A. A., Hall, A., and Glotzer, M. (1997). A requirement for Rho and Cdc42 during cytokinesis in *Xenopus* embryos. *Current Biology* **7,** 12-23.

Endow, S. A., Chandra, R., Komma, D. J., Yamanoto, A. H., and Salmon, E. D. (1994). Mutants of the *Drosophila* ncd microtubule motor protein

cause centrosomal and spindle pole defects in mitosis. *Journal of Cell Science* **107,** 859-867.

Endow, S. A., and Komma, D. J. (1996). Centrosome and spindle function of the *Drosophila* Ncd microtubule motor visualized in live embryos using Ncd-GFP fusion proteins. *Journal of Cell Science* **109,** 2429-42.

Endow, S. A., and Komma, D. J. (1997). Spindle dynamics during meiosis in *Drosophila* oocytes. *Journal of Cell Biology* **137,** 1321-36.

Euteneuer, U., Koonce, M. P., Pfister, K. K., and Schliwa, M. (1988). An ATPase with properties expected for the organelle motor of the giant amoeba, *Reticulomyxa*. *Nature* **332,** 176-8.

Fares, H., Peifer, M., and Pringle, J. R. (1995). Localization and possible functions of *Drosophila* septins. *Molecular Biology of the Cell* **6,** 1843-59.

Fath, K. R., Trimbur, G. M., and Burgess, D. R. (1994). Molecular motors are differentially distributed on Golgi membranes from polarized epithelial cells. *Journal of Cell Biology* **126,** 661-75.

Foster, K. A., Correia, J. J., and Gilbert, S. P. (1998). Equilibrium binding studies of non-claret disjunctional protein (Ncd) reveal cooperative interactions between the motor domains. *Journal of Biological Chemistry* **273,** 35307-18.

Gard, D. L. (1994). Gamma-tubulin is asymmetrically distributed in the cortex of *Xenopus* oocytes. *Developmental Biology* **161,** 131-140.

Gard, D. L., Affleck, D., and Error, B. M. (1995). Microtubule organization, acetylation, and nucleation in *Xenopus laevis* oocytes: II. A developmental transition in microtubule organization during early diplotene. *Developmental Biology* **168,** 189-201.

Gerhart, J., Wu, M., and Kirschner, M. (1984). Cell cycle dynamics of an M-

phase-specific cytoplasmic factor in Xenopus laevis oocytes and eggs. *Journal of Cell Biology* **98,** 1247-55.

Goldstein, B., and Freeman, G. (1996). Axis specification in animal development. *BioEssays* **19,** 105-116.

Gont, L. K., Steinbeisser, H., Blumberg, B., and de Robertis, E. M. (1993). Tail formation as a continuation of gastrulation: the multiple cell populations of the *Xenopus* tailbud derive from the late blastopore lip. *Development* **119,** 991-1004.

Goodenough, D. A., Ito, S., and Revel, J.-P. (1968). Electron microscopy of early cleavage stages in *Arbacia punctulata* . *Biological Bulletin* **135,** 420-1.

Gross, P. R., Philpott, D. E., and Nass, S. (1958). The fine-structure of the mitotic spindle in sea urchin eggs. *Journal of Ultrastructure Research* **2,** 55-72.

Hamaguchi, M. S., and Hiramoto, Y. (1980). Fertilization process in the heart-urchin, *Clypaester japonicus,* observed with a differential interference microscope. *Development Growth and Differentiation* **22,** 517-30.

Hamm-Alvarez, S. F., Kim, P. Y., and Sheetz, M. P. (1993). Regulation of vesicle transport in CV-1 cells and extracts. *Journal of Cell Science* **106,** 955-66.

Hardin, J., and Keller, R. (1988). The behaviour and function of bottle cells during gastrulation of *Xenopus laevis*. *Development* **103,** 211-30.

Harris, P. (1970). A spiral cortical fiber system in fertilized sea urchin eggs. *Developmental Biology* **68,** 525-32.

Harris, P., Osborn, M., and Weber, K. (1980a). Distribution of tubulin-containing structures in the egg of the sea urchin *Strongylocentrotus purpuratus* from fertilization through first cleavage. *Journal of Cell*

Biology **84,** 668-79.

Harris, P., Osborn, M., and Weber, K. (1980b). A spiral array of microtubules in the fertilized sea urchin egg cortex examined by indirect immunofluorescence and electron microscopy. *Experimental Cell Research* **126,** 227-36.

Hinegardner, R. T., Rao, B., and Feldman, D. E. (1964). The DNA synthetic period during early development of the sea urchin egg. *Experimental Cell Research* **36,** 53-61.

Hiramoto, Y. (1956). Cell division without mitotic apparatus in sea urchin eggs. *Experimental Cell Research* **11,** 630-636.

Hiramoto, Y. (1968). The mechanics and mechanism of cleavage in the sea urchin egg. *Symposia of the Society for Experimental Biology* **22,** 311-27.

Hiramoto, Y. (1971). Analysis of cleavage stimulus by means of micromanipulation of sea urchin eggs. *Experimental Cell Research* **68,** 291-8.

Jesuthasan, S. (1998). Furrow-associated microtubule arrays are required for the cohesion of zebrafish blastomeres following cytokinesis. *Journal of Cell Science* **111,** 3695-703.

Jin, D. Y., Spencer, F., and Jeang, K. T. (1998). Human T cell leukemia virus type 1 oncoprotein Tax targets the human mitotic checkpoint protein MAD1. *Cell* **93,** 81-91.

Julian, M., Tollon, Y., Lajoie-Mazenc, I., Moisand, A., Mazarguil, H., Puget, A., and Wright, M. (1993). gamma-Tubulin participates in the formation of the midbody during cytokinesis in mammalian cells. *Journal of Cell Science* **105,** 145-56.

Karabay, A., and Walker, R. A. (1999). Identification of microtubule binding sites in the Ncd tail domain. *Biochemistry* **38,** 1838-49.

Keller, R. E. (1978). Time-lapse cinemicrographic analysis of superficial cell behavior during and prior to gastrulation in *Xenopus laevis*. *Journal of Morphology* **157,** 223-48.

Keller, R. E. (1980). The cellular basis of epiboly: an SEM study of deep-cell rearrangement during gastrulation in *Xenopus laevis*. *Journal of Embryology and Experimental Morphology* **60,** 201-34.

Keller, R. E. (1981). An experimental analysis of the role of bottle cells and the deep marginal zone in gastrulation of *Xenopus laevis*. *Journal of Experimental Zoology* **216,** 81-101.

Keller, R. E. (1991). Early embryonic development of *Xenopus laevis*. In "*Xenopus laevis*: Practical Uses in Cell and Molecular Biology" (Kay, B. K., and Peng, H. B., Eds.), *Methods in Cell Biology* **36,** 63-113.

Keller, R. E., Danilchik, M., Gimlich, R., and Shih, J. (1985a). The function and mechanism of convergent extension during gastrulation of *Xenopus laevis*. *Journal of Embryology and Experimental Morphology* **89,** 185-209.

Keller, R. E., Danilchik, M. V., Gimlich, R. L., and Shih, J. (1985b). Convergent extension by cell intercalation during gastrulation of *Xenopus laevis*. In "Symposia on Molecular and Cellular Biology" (G. M. Edelman, Ed.), Vol. 31. Alan R. Liss, Inc, UCLA.

Keller, R., and Danilchik, M. (1988). Regional expression, pattern and timing of convergence and extension during gastrulation of *Xenopus laevis*. *Development* **103,** 193-209.

Keller, R., and Tibbetts, P. (1989). Mediolateral cell intercalation in the dorsal,

axial mesoderm of *Xenopus laevis*. *Developmental Biology* **131,** 539-49.

Keller, R. E., and Shih, J. (1992). Mediolateral Intercalation of Mesodermal Cells in the *Xenopus laevis* Gastrula. In "Formation and Differentiation of Early Embryonic Mesoderm" (R. Bellairs, E. J. Sanders, and J. W. Lash, Eds.), Vol. 231, pp. 47-61. Plennum Press, New York.

Keller, R., Shih, J., and Domingo, C. (1992). The patterning and functioning of protrusive activity during convergence and extension of the *Xenopus* organiser. *Development* - **Supplement**, 81-91.

Keller, R., and Winklbauer, R. (1992). Cellular basis of amphibian gastrulation. *Current Topics in Developmental Biology* **27,** 39-89.

Kinoshita, M., Kumar, S., Mizoguchi, A., Ide, C., Kinoshita, A., Haraguchi, T., Hiraoka, Y., and Noda, M. (1997). Nedd5, a mammalian septin, is a novel cytoskeletal component interacting with actin-based structures. *Genes & Development* **11,** 1535-47.

Kishi, K., Sasaki, T., Kuroda, S., Itoh, T., and Takai, Y. (1993). Regulation of cytoplasmic division of *Xenopus* embryo by rho p21 and its inhibitory GDP/GTP exchange protein (rho GDI). *Journal of Cell Biology* **120,** 1187-95.

Kuriyama, R., and Borisy, G. G. (1983). Cytasters induced within unfertilized sea-urchin eggs. *Journal of Cell Science* **61,** 175-89

Knecht, D. A., and Loomis, W. F. (1987). Antisense RNA inactivation of myosin heavy chain gene expression in *Dictyostelium discoideum*. *Science* **236,** 1081-6.

Lacey, M. L. and Haimo, L. T. (1994). Cytoplasmic dynein binds to phospholipid vesicles. *Cell Motility and the Cytoskeleton* **28,** 205-12.

Larkin, K. and Danilchik, M. (1999). Microtubules are required for completion of cleavage in sea urchin eggs. *Developmental Biology* in press.

Larkin, K. and Danilchik, M. (1999). Ventral cell rearrangements contribute to anterior-posterior axis lengthening between the neurula and tailbud stages in *Xenopus laevis*. *Developmental Biology* in press.

Longo, F. J. (1972). An ultrastructural analysis of mitosis and cytokinesis in the zygote of the sea urchin, *Arbacia punctulata*. *Journal of Morphology* **138,** 207-38.

Mabuchi, I. (1990). Cleavage furrow formation and actin-modulating proteins. *Annals of the New York Academy of Sciences* **582,** 131-46.

Mabuchi, I., Hamaguchi, Y., Fujimoto, H., Morii, N., Mishima, M., and Narumiya, S. (1993). A rho-like protein is involved in the organisation of the contractile ring in dividing sand dollar eggs. *Zygote* **1,** 325-31.

Mackay, A. M., Ainsztein, A. M., Eckley, D. M., and Earnshaw, W. C. (1998). A dominant mutant of inner centromere protein (INCENP), a chromosomal protein, disrupts prometaphase congression and cytokinesis. *Journal of Cell Biology* **140,** 991-1002.

Madaule, P., Eda, M., Watanabe, N., Fujisawa, K., Matsuoka, T., Bito, H., Ishizaki, T., and Narumiya, S. (1998). Role of citron kinase as a target of the small GTPase Rho in cytokinesis. *Nature* **394,** 491-4.

Malacinski, G. M., and Youn, B. W. (1981). Neural plate morphogenesis and axial stretching in "notochord-defective" *Xenopus laevis* embryos. *Developmental Biology* **88,** 352-7.

Matthies, H. J., McDonald, H. B., Goldstein, L. S., and Theurkauf, W. E. (1996). Anastral meiotic spindle morphogenesis: role of the non-claret disjunctional kinesin-like protein. *Journal of Cell Biology* **134,** 455-64.

McCain, E. R., and McClay, D. R. (1996). The establishment of bilateral asymmetry in sea urchin embryos. *Development* **120,** 395-404.

McDonald, H. B., and Goldstein, L. S. (1990). Identification and characterization of a gene encoding a kinesin-like protein in *Drosophila*. *Cell* **61,** 991-1000.

McDonald, H. B., Stewart, R. J., and Goldstein, L. S. (1990). The kinesin-like ncd protein of *Drosophila* is a minus end-directed microtubule motor. *Cell* **63,** 1159-65.

Meyerhof, P. G., and Masui, Y. (1977). Ca and Mg control of cytostatic factors from *Rana pipiens* oocytes which cause metaphase and cleavage arrest. *Developmental Biology* **61,** 214-29.

Mookerjee, S. (1953). An experimental study of the development of the notochordal sheath. *Journal Experimental Embryology and Morphology* **1,** 411-6.

Mookerjee, S., Deuchar, E. M., and Waddington, C. H. (1953). The morphogenesis of the notochord in amphibia. *Journal of Embryology and Experimental Morphology* **1,** 399-409.

Moore, A. R. (1930). Fertilization and development without membrane formation in the egg of the sea urchin, *Strongylocentrotus purpuratus*. *Protoplasma* **9,** 9-17.

Morgan, A. (1995). Exocytosis. *Essays in Biochemistry* **30,** 77-95.

Mountain, V., and Compton, D. A. (1998). The kinesin-related protein, HSET, exists in multiple isoforms in various cell types and is involved in focussing microtubule minus ends at spindle poles. *Molecular Biology of The Cell* **9 Supplement,** 43.

Newport, J. W. and Kirschner, M. W. (1982). A major developmental

transition in early *Xenopus* embryos: I. characterization and timing of cellular changes at midblastula stage. *Cell* **30,** 675-86.

Niclas, J., Allan, V. J., and Vale, R. D. (1996). Cell cycle regulation of dynein association with membranes modulates microtubule-based organelle transport. *Journal of Cell Biology* **133,** 585-93.

Nieuwkoop, P. D., and Faber, J. (1994). "Normal Table of *Xenopus laevis* (Daudin)." Garland Publishing, Inc., New York.

Oakley, B. R., Oakley, C. E., Yoon, Y., and Jung, M. K. (1990). Gamma-tubulin is a component of the spindle pole body that is essential for microtubule function in *Aspergillus nidulans*. *Cell* **61,** 1289-301.

Oakley, C. E., and Oakley, B. R. (1989). Identification of gamma-tubulin, a new member of the tubulin superfamily encoded by mipA gene of *Aspergillus nidulans*. *Nature* **338,** 662-4.

Otto, J.J. and Schroeder, T. E. (1984). Microtubule arrays in the cortex and near the germinal vesicle of immature starfish oocytes. *Developmental Biology* **101,** 274-81.

Pennigroth, S. M. (1972). Erythro-9-[3-(2-hydroxynonyl)]adenine and vanadate as probes for microtubule-based cytoskeletal mechanochemistry. *Methods in Enzymology* **134,** 477-487.

Piperno, G. (1984). Monoclonal antibodies to dynein subunits reveal the existence of cytoplasmic antigens in sea urchin egg. *Journal of Cell Biology* **98,** 1842-50.

Pochapin, M. B., Sanger, J. M., and Sanger, J. W. (1983). Microinjection of Lucifer yellow CH into sea urchin eggs and embryos. *Cell Tissue Research* **234,** 309-18.

Pratt, M. M., Otter, T., and Salmon, E. D. (1980). Dynein-like Mg^{2+}-ATPase in

mitotic spindles isolated from sea urchin embryos (*Strongylocentrotus droebachiensis*). *Journal of Cell Biology* **86,** 738-45.

Rappaport, R. (1961). Experiments concerning the cleavage stimulus in sand dollar eggs. *Journal of Experimental Zoology* **148,** 81-9.

Rappaport, R. (1969). Aster-equatorial surface relations and furrow establishment. *Journal of Experimental Zoology* **171,** 59-68.

Rappaport, R. (1996). "Cytokinesis in Animal Cells." Cambridge University Press, Cambridge, U.K.

Rappaport, R., and Rappaport, B. N. (1974). Establishment of cleavage furrows by the mitotic spindle. *Journal of Experimental Zoology* **189,** 189-96.

Rappaport, R., and Rappaport, B. N. (1993). Duration of division-related events in cleaving sand dollar eggs. *Developmental Biology* **158,** 265-73.

Rappaport, R., and Rappaport, B. N. (1994). Cleavage in conical sand dollar eggs. *Developmental Biology* **164,** 258-66.

Rebhun, L. I., and Sander, G. (1967). Ultrastructure and birefringence of the isolated mitotic apparatus of marine eggs. *Journal of Cell Biology* **34,** 859-883.

Rothman, J. E. (1996). Felix Hoppe-Seyler Lecture 1996. Mechanisms of intracellular protein transport. *Biological Chemistry* **377,** 407-410.

Rowning, B. A., Wells, J., Wu, M., Gerhart, J. C., Moon, R. T., and Larabell, C. A. (1997). Microtubule-mediated transport of organelles and localization of beta-catenin to the future dorsal side of *Xenopus* eggs. *Proceedings of the National Academy of Sciences of the United States of America* **94,** 1224-9.

Sanger, J. M., Pochapin, M. B., and Sanger, J. W. (1985). Midbody sealing after cytokinesis in embryos of the sea urchin *Arbacia punctulata*. *Cell*

Tissue Research **240,** 287-92.

Sato, H., Ellis, G. W., and Inoué, S. (1975). Microtubular origin of mitotic spindle form birefringence. Demonstration of the applicability of Wiener's equation. *Journal of Cell Biology* **67,** 501-17.

Sawai, T. (1987). Surface movement in the region of the cleavage furrow of amphibian eggs. *Zool. Sci.* **4,** 825-32.

Sawai, T. (1992). Effect of microtubular poisons on cleavage furrow formation and induction of furrow-like dent in amphibian eggs. *Development Growth and Differentiation* **34,** 669-75.

Savoian, M. S., Earnshaw, W. C., Khodjakov, A., and Rieder, C. L. (1999). Cleavage furrows formed between centrosomes lacking an intervening spindle and chromosomes contain microtubule bundles, INCENP, and CHO1 but not CENP-E. *Molecular Biology of the Cell* **10,** 297-311.

Schmekel, L. (1975). Egg and embryo ultrastructure. *In* "The Sea Urchin Embryo: Biochemistry and Morphogenesis" (G. Czihak, Ed.). Springer-Verlag.

Schnapp, B. J., Vale, R. D., Sheetz, M. P., and Reese, T. S. (1985). Single microtubules from squid axoplasm support bidirectional movement of organelles. *Cell* **40,** 455-62.

Schnapp, B. J., Reese, T. S., and Bechtold, R. (1992). Kinesin is bound with high affinity to squid axon organelles that move to the plus-end of microtubules. *Journal of Cell Biology* **119,** 389-99.

Scholey, J. M., Neighbors, B., McIntosh, J. R., and Salmon, E. D. (1984). Isolation of microtubules and a dynein-like MgATPase from unfertilized sea urchin eggs. *Journal of Biological Chemistry* **259,** 6516-25.

Scholey, J. M., Porter, M. E., Grissom, P. M., and McIntosh, J. R. (1985). Identification of kinesin in sea urchin eggs, and evidence for its localization in the mitotic spindle. *Nature* **318,** 483-486.

Schroeder, T. E. (1968). Cytokinesis: filaments in the cleavage furrow. *Experimental Cell Research* **53,** 272-6.

Schroeder, T. E. (1969). The role of 'contractile ring' filaments in dividing *Arbacia* egg. *Biological Bulletin* **137,** 413-4.

Schroeder, T. E. (1972). The contractile ring. II. Determining its brief existence, volumetric changes, and vital role in cleaving *Arbacia* eggs. *Journal of Cell Biology* **53,** 419-34.

Schroeder, T. E. (1973). Actin in dividing cells: contractile ring filaments bind heavy meromyosin. *Proceedings of the National Academy of Sciences of the United States of America* **70,** 1688-92.

Schroeder, T. E. (1975). Dynamics of the contractile ring. *Society of General Physiologists Series* **30,** 305-34.

Schroeder, T. E. (1978). Microvilli on sea urchin eggs: a second burst of elongation. *Developmental Biology* **64,** 342-6.

Schroeder, T. E. (1979). Surface area change at fertilization: resorption of the mosaic membrane. *Developmental Biology* **70,** 306-26.

Schroeder, T. E. (1981). The origin of cleavage forces in dividing eggs. A mechanism in two steps. *Experimental Cell Research* **134,** 231-40.

Schroeder, T. E. (1987). Fourth cleavage of sea urchin blastomeres: microtubule patterns and myosin localization in equal and unequal cell divisions. *Developmental Biology* **124,** 9-22.

Schroeder, T. E. (1990). The contractile ring and furrowing in dividing cells. *Annals of the New York Academy of Sciences* **582,** 78-87.

Schroeder, T. E., and Battaglia, D. E. (1985). "Spiral asters" and cytoplasmic rotation in sea urchin eggs: induction in *Strongylocentrotus purpuratus* eggs by elevated temperature. *Journal of Cell Biology* **100,** 1056-62.

Scott, A. (1946). The effect of low temperature and of hypotonicity on the morphology of the cleavage furrow in *Arbacia* eggs. *Biological Bulletin* **91,** 272-287.

Selman, G. G., and Perry, M. M. (1970). Ultrastructural changes in the surface layer of the newt's egg in relation to the mechanism of its cleavage. *Journal of Cell Science* **6,** 207-27.

Séron, K., Tieaho, V., Prescianotto-Baschong, C., Aust, T., Blondel, M. O., Guillaud, P., Devilliers, G., Rossanese, O. W., Glick, B. S., Riezman, H., Keranen, S., and Haguenauer-Tsapis, R. (1998). A yeast t-SNARE involved in endocytosis. *Molecular Biology of the Cell* **9,** 2873-2889.

Shih, J., and Keller, R. (1992). Cell motility driving mediolateral intercalation in explants of *Xenopus laevis*. *Development* **116,** 901-914.

Shu, H. B., Li, Z., Palacios, M. J., Li, Q., and Joshi, H. C. (1995). A transient association of gamma-tubulin at the midbody is required for the completion of cytokinesis during the mammalian cell division. *Journal of Cell Science* **108,** 2955-62.

Sluder, G. (1976). Experimental manipulation of the amount of tubulin available for assembly into the spindle of dividing sea urchin eggs. *Journal of Cell Biology* **70,** 75-85.

Sluder, G. (1979). Role of spindle microtubules in the control of cell cycle timing. *Journal of Cell Biology* **80,** 674-91.

Sluder, G., Miller, F. J., and Spanjian, K. (1986). The role of spindle

microtubules in the timing of the cell cycle in echinoderm eggs. *Journal of Experimental Zoology* **238,** 325-336.

Steuer, E. R., Wordeman, L., Schroer, T. A., and Sheetz, M. P. (1990). Localization of cytoplasmic dynein to mitotic spindles and kinetochores. *Nature* **345,** 266-8.

Strathmann, M. F. (1992). "Reproduction and Development of Marine Invertebrates of the Northern Pacific Coast: Data and Methods for the Study of Eggs, Embryos, and Larvae." University of Washington Press, Seattle.

Summers, R. G., Piston, D. W., Harris, K. M., and Morrill, J. B. (1996). The orientation of first cleavage in the sea urchin embryo, *Lytechinus variegatus*, does not specify the axes of bilateral symmetry. *Developmental Biology* **175,** 177-83.

Swan, K. A., Severson, A. F., Carter, J. C., Martin, P. R., Schnabel, H., Schnabel, R., and Bowerman, B. (1998). cyk1: a *C. elegans* FH gene required for a late step in embryonic cytokinesis. *Journal of Cell Science* **111,** 2017-27.

Swann, M. M., and Mitchison, J. M. (1953). Cleavage of sea urchin eggs in colchicine. *Journal of Experimental Biology* **30,** 506-514.

Sze, L. C. (1953). Changes in the amount of deoxyribonucleic acid in the development of *Rana pipiens*. *Journal of Experimental Zoology* **122,** 577-601.

Terada, Y., Tatsuka, M., Suzuki, F., Yasuda, Y., Fujita, S., and Otsu, M. (1998). AIM-1: a mammalian midbody-associated protein required for cytokinesis. *EMBO Journal* **17,** 667-76.

Tilney, L. G., and Marsland, D. (1969). A fine structural analysis of cleavage induction and furrowing in the eggs of *Arbacia punctulata*. *Journal of Cell Biology* **42,** 170-84.

Tucker, A. S., and Slack, J. M. W. (1995). The *Xenopus laevis* tail-forming region. *Development* **121,** 249-6.

Tupper, J., Saunders, J. W. J., and Edwards, C. (1970). The onset of electrical communication between cells in the developing starfish embryo. *Journal of Cell Biology* **46,** 187-91.

Vacquier, V. D. (1968). The connection of blastomeres of sea urchin embryos by filopodia. *Experimental Cell Research* **52,** 571-81.

Vale, R. D., Reese, T. S., and Sheetz, M. P. (1985a). Identification of a novel force-generating protein, kinesin, involved in microtubule-based motility. *Cell* **42,** 39-50.

Vale, R. D., Schnapp, B. J., Reese, T. S., and Sheetz, M. P. (1985b). Movement of organelles along filaments dissociated from the axoplasm of the squid giant axon. *Cell* **40,** 449-54.

Vale, R. D., Schnapp, B. J., Reese, T. S., and Sheetz, M. P. (1985c). Organelle, bead, and microtubule translocations promoted by soluble factors from the squid giant axon. *Cell* **40,** 559-569.

Vale, R. D., Funatsu, T., Pierce, D. W., Romberg, L., Harada, Y., and Yanagida, T. (1996). Direct observation of single kinesin molecules moving along microtubules. *Nature* **380,** 451-3.

Wang, Y.-l., and Wheatley, S. P. (1997). Functional role of interzonal microtubules in cytokinesis. *Molecular Biology of the Cell* **8S,** 352a.

Waterman-Storer, C. M., Sanger, J. W., and Sanger, J. M. (1993). , Dynamics of organelles in the mitotic spindles of living cells: membrane and microtubule interactions. *Cell Motility and the Cytoskeleton* **26,** 19-39.

Weliky, M., Minsuk, S., Keller, R., and Oster, G. (1991). Notochord morphogenesis in *Xenopus laevis*: simulation of cell behavior

underlying tissue convergence and extension. *Development* **113,** 1231-44.

Wheatley, S. P., and Wang, Y.-l. (1996). Midzone microtubule bundles are continuously required for cytokinesis in cultured epithelial cells. *Journal of Cell Biology* **135,** 981-9.

Wilson, E. B. (1896). "The Cell in Development and Inheritance." New York.

Wilson, P., and Keller, R. (1991). Cell rearrangement during gastrulation of *Xenopus*: direct observation of cultured explants. *Development* **112,** 289-300.

Wilson, P. A., Oster, G., and Keller, R. (1989). Cell rearrangement and segmentation in *Xenopus*: direct observation of cultured explants. *Development* **105,** 155-66.

Yamin, M. A., and Tamm, S. L. (1982). ATP reactivation of the rotary axostyle in termite flagellates: effects of dynein ATPase inhibitors. *Journal of Cell Biology* **95,** 589-97.

Youn, B. W., Keller, R. E., and Malacinski, G. M. (1980). An atlas of notochord and somite morphogenesis in several anuran and urodelean amphibians. *Journal of Embryology & Experimental Morphology* **59,** 223-47.

Youn, B. W., and Malacinski, G. M. (1981). Somitogenesis in the amphibian *Xenopus laevis*: scanning electron microscopic analysis of intrasomitic cellular arrangements during somite rotation. *Journal of Embryology & Experimental Morphology* **64,** 23-43.

Zhang, D., and Nicklas, R. B. (1996). 'Anaphase' and cytokinesis in the absence of chromosomes. *Nature* **382,** 466-8.

Zheng, Y., Wong, M. L., Alberts, B., and Mitchison, T. (1995). Nucleation of

microtubule assembly by a gamma-tubulin-containing ring complex. *Nature* **378,** 578-83.